Electronic Supplementary Material (ESI) for Dalton Transactions.

Supporting Information for

Homogeneous versus MOF-supported catalysis: A direct comparison of catalytic hydroboration at Ni tripodal P_3E (E = Si, Ge) complexes

Luz J. Barrios-Vargas,[a,†] Niroshani S. Abeynayake,[a,†] Carlee Secrist,[a] Nghia Le,[a,†] Charles Edwin Webster,[a] Bruno Donnadieu,[a] David Kaphan,[b] Amitava D. Roy,[c] Ilich A. Ibarra,[d] and Virginia Montiel-Palma*[a]

[a] Department of Chemistry, Mississippi State University, Box 9573, Mississippi, 39762, United States. E-mail: vmontiel@chemistry.msstate.edu

[b] Chemical Sciences and Engineering Division, Argonne National Laboratory, Lemont, Illinois 60439, United States

[c] Center for Advanced Microstructures and Devices (CAMD), Louisiana State University, Baton Rouge, Louisiana 70806, United States

[d] Laboratorio de Fisicoquímica y Reactividad de Superficies (LaFReS), Instituto de Investigaciones en Materiales, Universidad Nacional Autónoma de México, Circuito Exterior s/n, CU, Coyoacán, 04510, Ciudad de México, México.

Contents

1. General experimental details

The syntheses of ligands, metal precursors, and MOF materials were performed under an argon atmosphere using standard Schlenk methods or in an MBraun glove box. Laboratory solvents including hexane, THF, and toluene were dried and purified over MBraun column systems. $CDCl_3$ was passed through a Pasteur pipette containing molecular sieves and basic alumina and then degassed via three cycles of freeze-pump-thaw and stored over molecular sieves. Benzene-d_6 and other deuterated solvents were stored over molecular sieves and degassed via three freeze–pump–thaw cycles. Commercial reagents were purchased from Fisher Scientific, Sigma Aldrich, and Oakwood Chemicals and used as received. Nuclear magnetic resonance (NMR) experiments were performed on either Bruker Avance III 300 MHz, 500 MHz, or 600 MHz spectrometers operating with frequency, deuterated solvent, and temperature indicated. Chemical shifts (δ) are reported in parts per million (ppm). ^1H NMR spectra for integration were acquired with long delays (30 s). Infra-red spectra were recorded on a Bruker Alpha II ATR-FTIR instrument under nitrogen and are reported in cm^{-1}. Elemental Analysis (C, H) were carried out in an Elementar Unicube analyzer. For ICP-MS determinations, a Perkin Elmer ELAN DRC II ICP-MS instrument was used. X-ray single crystal diffractions were performed on a Bruker D8 Venture instrument with Co/Mo source. Powder X-ray diffraction measurements were done using an AXRD Benchtop from PROTO Manufacturing. X-ray absorption fine structure (XAFS) spectra were measured at the Ni K edge on the Ni-1@NU-1000 and Ni-2@NU-1000 materials at the Materials Research Collaborative Access Team (MR-CAT) beamline 10-ID at Argonne National Laboratory's Advanced Photon Source. Samples were prepared in an air-free glovebox as self-supported pressed pellets and were measured in transmission mode in a triple-sealed sample holder to minimize leakage of air. High purity Zr was used to prepare the NU-1000. Scanning electron micrographs (SEM) images were taken using a JEOL 6500F Field Emission SEM at the Institute for Imaging and Analytical Technologies (I^2AT Mississippi State University). EDS line scans were also obtained on the same instrument.

2. Synthesis of ligand [HSi(*o*-$C_6H_4CH_2P(C_6H_5)_2)_3$] (**L1**)

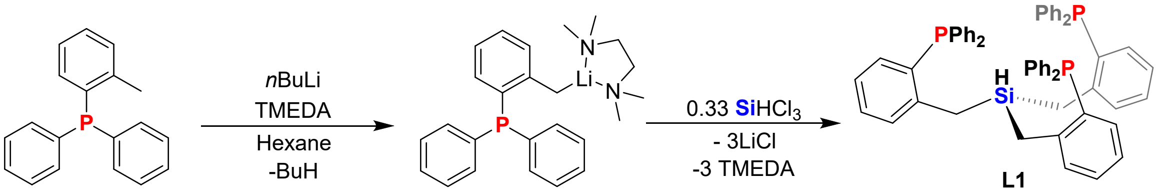

The synthesis of tripodal ligand HSi(*o*-$C_6H_4CH_2P(C_6H_5)_2)_3$, **L1**, was previously reported by Stobart and coworkers but not all the spectroscopic features were given in the original publication.[1] We implemented a few modifications detailed below, which resulted in the obtention of a crystalline solid. In a Schlenk flask, 1.0 g (3.6 mmol) of diphenyl(*o*-tolyl)phosphine was dissolved in 100 mL of hexane with vigorous stirring for at least 10 minutes. Then, at –78 °C, 0.6 mL (3.9 mmol) of TMEDA, followed by 1.5 mL (3.9 mmol) of *n*BuLi were added to the phosphine solution and the mixture was left to reach room temperature and continued to be stirred for a total of 18 hours. Afterward, a dropwise addition of 0.12 mL of trichlorosilane (1.3 mmol) to the slurry solution and subsequent stirring for 18 hours produced a white-colored mixture which was then purified by silica/celite flash chromatography column using THF (30 mL) as eluent. After the removal of the volatiles using reduced pressure, the compound was obtained as a crystalline solid (0.70 g, 62 % yield). With small deviations, in general, the spectroscopic data agree with the reported values.[1] Since in the original publications, not all features were listed, we provide all the details below. **^{1}H NMR (500 MHz, CDCl$_3$, 298 K):** δ 7.32-7.27 (m, 8H, CH$_{arom}$), 7.25-7.23 (m, 10H, CH$_{arom}$), 7.14 (t, J_{HH} = 7.2 Hz, 12H, CH$_{arom}$), 7.10 (t, J_{HH} = 7.7 Hz, 3H, CH$_{arom}$), 6.97 (t, J_{HH} = 7.5 Hz, 3H, CH$_{arom}$), 6.90 (dd, J_{HH} = 7.6, J_{HP} = 4.9 Hz, 3H, CH$_{arom}$), 6.78 (dd, J_{HH} = 7.7 Hz, , J_{HP} = 3.9 Hz 3H, CH$_{arom}$), 4.22 (br, 1H, H-Si), 2.49 (d, J_{HH} = 3.2 Hz, 6H, CH$_2$) ppm. **^{13}C{^{1}H} NMR (125.76 MHz, CDCl$_3$, 298 K):** 144.95 (d, J_{CP} 27.5 Hz, C$_{ipso}$), 137.08 (d, J_{CP} = 12.0 Hz, C$_{ipso}$), 134.80 (d, J_{CP} = 11.4 Hz, C$_{ipso}$), 134.06 (d, J_{CP} = 19.6 Hz, CH$_{arom}$), 129.51 (d, J_{CP} = 5.5 Hz, CH$_{arom}$), 128.99 (s, CH$_{arom}$), 128.49 (d, J_{CP} = 7.0 Hz, CH$_{arom}$), 124.94 (s, CH_{arom}), 20.93 (dt, J_{CP} = 21.1, 2.4 Hz, CH_2) ppm. **$^{31}P\{^1H\}$ NMR (202.5 MHz, $CDCl_3$, 298 K):** -14.28 (s) ppm. **DEPT $^{29}Si\{^1H\}$ NMR (99.4 MHz, $CDCl_3$, 298 K):** -4.53 (m) ppm. **IR**: 2160 cm^{-1} (*s*, Si-H). Elemental analyses agree with reported values for the formula $C_{57}H_{49}P_3Si$.

3. Synthesis of [HGe(*o*-$C_6H_4CH_2P(C_6H_5)_2)_3$] (**L2**)

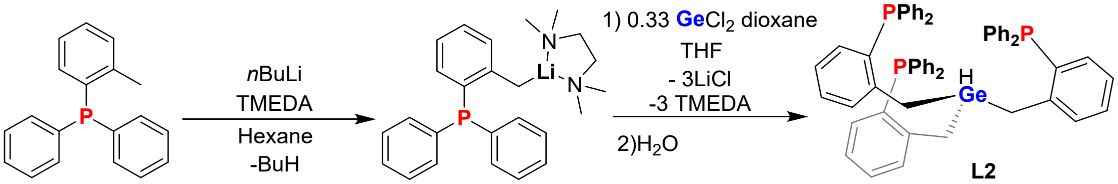

In a Schlenk flask, 1.0 g (3.6 mmol) of diphenyl(*o*-tolyl)phosphine was dissolved in 100 mL of hexane with vigorous stirring for 10 minutes. Then, at –80 °C, 0.6 mL (3.9 mmol) of TMEDA, followed by 1.6 mL (3.9 mmol) of *n*BuLi were added to the phosphine solution, and the mixture was left to reach room temperature and continued to be stirred for a total of 18 hours. The resulting suspension was dried under the vacuum to afford an orange-red color solid that was redissolved in THF (30 mL). Afterward, 0.31 g of germanium (II) chloride dioxane (1.3 mmol) in THF (30 mL) was added to the slurry solution at -80 °C. The red colored mixture was stirred for 18 hours at room temperature. Excess water (0.2 mL) was added to the solution producing a clear solution and the mixture was stirred for 1 hour at room temperature. The mixture was then purified by a silica/celite flash chromatography column using toluene (30 mL) as eluent. After the removal of the volatiles using reduced pressure, the compound was obtained as a crystalline solid (0.72 g, 60 % yield). **^1H NMR (500 MHz, C_6D_6, 298 K):** δ 7.37-7.26 (m, 12H, CH_{arom}), 7.03-6.92 (m, 27H, CH_{arom}), 6.83 (t, J_{HH} = 7.3 Hz, 3H, CH_{arom}), 4.75 (m, 1H, H-Ge), 2.92 (d, J_{HH} = 2.4 Hz, 6H, CH_2) ppm. **$^{13}C\{^1H\}$ NMR (150.92 MHz, C_6D_6, 298 K):** 146.6 (d, J_{CP} 27.4 Hz, C_{ipso}), 137.6 (d, J_{CP} = 11.5 Hz,

C_{ipso}), 134.8 (d, J_{CP} = 11.4 Hz, C_{ipso}), 134.4 (d, J_{CP} = 19.9 Hz, CH_{arom}), 134.2 (s, CH_{arom}), 129.8 (d, J_{CP} = 4.9 Hz, CH_{arom}), 129.4 (s, CH_{arom}), 128.8 (d, J_{CP} = 7.0 Hz, CH_{arom}), 128.7 (s, CH_{arom}), 128.6 (s, CH_{arom}), 128.4 (s, CH_{arom}), 125.3 (s, CH_{arom}), 22.9 (dt, J_{CP} = 22.7, 2.9 Hz, CH_2) ppm. **$^{31}P\{^1H\}$ NMR (202.5 MHz, C_6D_6, 298 K):** –14.2 (s) ppm. **IR**: 2065 cm^{-1} (*s*, νGe-H). **Anal. Calc.** for $C_{57}H_{49}P_3Ge$: C: 76.10%, H: 5.49%; Found: C: 75.99%, H: 6.05%.

4. Synthesis of [{((C$_6$H$_5$)$_2$PCH$_2$C$_6$H$_4$)$_3$Si}NiH] (**Ni-1**)

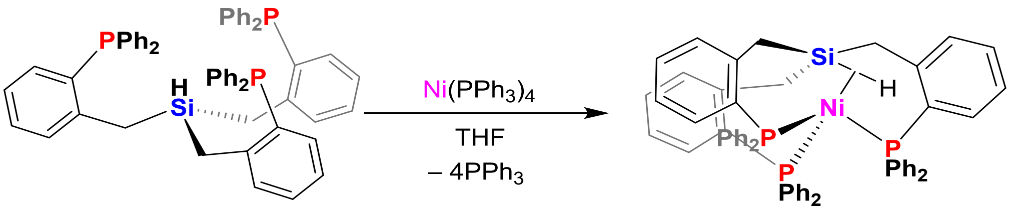

Ni-1

In a Schlenk flask, 100 mg (0.12 mmol) of **L1** was dissolved in 4.5 mL of dry THF under stirring. A solution of 130 mg (0.12 mmol) of $Ni(PPh_3)_4$ in 4.5 mL of dry THF was added dropwisely and the resulting solution was further stirred at room temperature for 12 h. The reaction mixture changes its color to red, and a yellow precipitate starts to form. After removal of the volatiles under reduced pressure, the residue was washed three times with portions of 4 mL of cold THF and dried under vacuum for 6 hours. Pure compound **Ni-1** was isolated as a yellow solid in 53% yield (57 mg, 0.061 mmol). Yellow crystals suitable for X-ray analysis were obtained by slow evaporation of a benzene-d$_6$ solution at room temperature. **^1H NMR (500 MHz, C_6D_6, 298 K):** δ 7.93 – 7.65 (m, 10H, CH_{arom}), 6.99 (d, $^2J_{HH}$= 7.7 Hz, 4H, CH_{arom}), 6.93 (td, $^2J_{HH}$= 7.4, $^3J_{HP}$= 1.4 Hz, 4H, CH_{arom}), 6.91 – 6.82 (m, 18H, CH_{arom}), 6.81 – 6.72 (m, 3H, CH_{arom}), 6.65 (t, $^2J_{HH}$= 7.4 Hz, 3H, CH_{arom}), 2.08 (s, 6H, CH_2), –6.69 (q, $^2J_{HP}$ = 37.2 Hz, $J_{H\text{-}Si}$ = 52.0 Hz, 1H, Ni-H) ppm. **$^{13}C\{^1H\}$ NMR (150.9 MHz,**

C_6D_6, 298 K): 191.3 (s, C_{ipso}), 146.3 (dd, J_{CP} = 9.3, 4.8 Hz, C_{ipso}), 138.26 (m, C_{ipso}), 134.7 (s, CH_{arom}), 132.5 (d, J_{CP} = 8.8 Hz, C_{ipso}), 132.0 (s, CH_{arom}), 131.6 (s, CH_{arom}), 130.4 (s, CH_{arom}), 129.2 (s, CH_{arom}), 128.8 (s, CH_{arom}), 128.7 (d, J_{CP} = 6.8Hz, CH_{arom}), 124.3 (s, CH_{arom}), 27.9 (m, CH_2) ppm. **$^{31}P\{^1H\}$ NMR (202.46 MHz, C_6D_6, 298 K):** 36.9 (s, J_{PSi} = 29.4 Hz) ppm. **DEPT $^{29}Si\{^1H\}$ NMR (99.36 MHz, C_6D_6, 298 K):** 66.1 (q, J_{SiP} =29.4 Hz) ppm. **IR**: 1885 cm^{-1} (*s*, Ni-H). **Anal. Calc.** for $C_{57}H_{49}NiP_3Si$: C: 74.93%, H: 5.41%; found: C: 74.77%, H: 5.91%.

5. Synthesis of $[\{((C_6H_5)_2PCH_2C_6H_4)_3Ge\}NiH]$ (**Ni-2**)

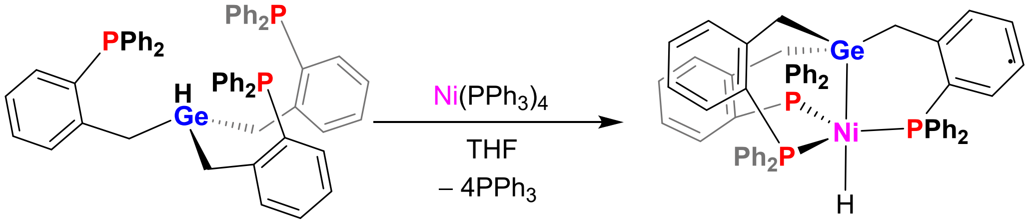

Ni-2

In a Schlenk flask, 24 mg (0.027 mmol) of **L2** was dissolved in 1 mL of dry THF with stirring. A solution of 30 mg (0.027 mmol) of $Ni(PPh_3)_4$ in 1 mL of dry THF was added dropwisely and the resulting solution was stirred at room temperature for 12 h. The reaction mixture changes its color to red and small amounts of a yellow precipitate form. After removal of the volatiles under reduced pressure, the residue was washed three times with portions of 1 mL of cold THF and dried in vacuum for 6 hours. Compound **Ni-2** was isolated as a yellow solid (23 mg, 89% yield). Yellow crystals suitable for X-ray analysis were obtained by slow evaporation of a benzene-d_6 solution at room temperature. **^1H NMR (500 MHz, C_6D_6, 298 K):** δ 8.03 – 7.67 (m, 10H, CH_{arom}), 7.05 – 7.00 (m, 4H, CH_{arom}), 6.93 (td, $^2J_{HH}$= 7.4, $^3J_{HP}$= 1.3 Hz, 4H, CH_{arom}), 7.00 – 6.81 (m, 18H, CH_{arom}), 6.80 – 6.76 (m, 3H, CH_{arom}), 6.63 (t, $^2J_{HH}$= 7.2 Hz, 3H, CH_{arom}), 2.16 (s, 6H, CH_2), -8.15 (q, $^2J_{HP}$ = 35.0 Hz, 1H, Ni-H) ppm. **$^{13}C\{^1H\}$ NMR (150.9 MHz, C_6D_6, 298 K):** 147.4 (dd, J_{CP} = 10.8, 5.3 Hz, C_{ipso}), 135.4 (q, J_{CP} = 5.1 Hz, CH_{arom}), 134.2 (d, J_{CP} = 19.7 Hz, C_{ipso}), 133.8 (s, CH_{arom}), 133.3 (dd, J_{CP} = 20.4, 8.5 Hz, C_{ipso}), 130.3 (s, CH_{arom}), 130.0 (s, CH_{arom}), 129.7 (s, CH_{arom}), 124.9 (s, CH_{arom}), 25.5 (m, CH_2) ppm. **$^{31}P\{^1H\}$ NMR (202.46 MHz, C_6D_6, 298 K):** 36.4 (s) ppm. **Anal. Calc.** for $C_{57}H_{49}NiSP_{3Co}Ge.C_6H_6$: C: 73.01%, H: 5.35%; found: C: 73.09%, H: 5.31%.

6. Chart S1. Comparison of silicon related parameters of **Ni-1** with reported related complexes

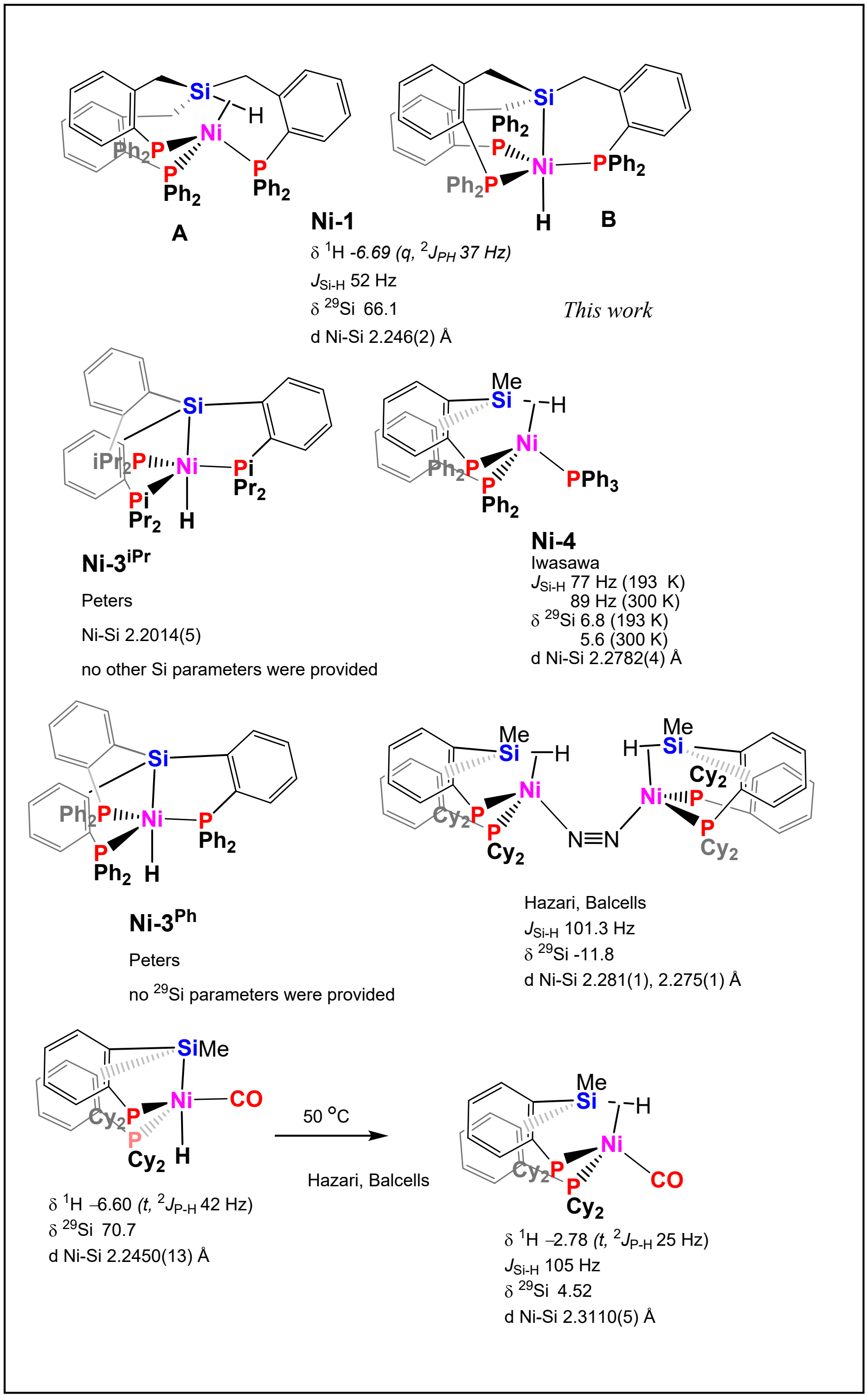

A

Ni-1

δ ^{1}H *-6.69 (q, $^2J_{PH}$ 37 Hz)*

$J_{Si\text{-}H}$ 52 Hz

δ ^{29}Si 66.1

d Ni-Si 2.246(2) Å

B

This work

Ni-3^{iPr}

Peters

Ni-Si 2.2014(5)

no other Si parameters were provided

Ni-4

Iwasawa

$J_{Si\text{-}H}$ 77 Hz (193 K)
89 Hz (300 K)

δ ^{29}Si 6.8 (193 K)
5.6 (300 K)

d Ni-Si 2.2782(4) Å

Ni-3^{Ph}

Peters

no ^{29}Si parameters were provided

Hazari, Balcells

$J_{Si\text{-}H}$ 101.3 Hz

δ ^{29}Si -11.8

d Ni-Si 2.281(1), 2.275(1) Å

δ ^{1}H –6.60 *(t,* $^2J_{P\text{-}H}$ 42 Hz)

δ ^{29}Si 70.7

d Ni-Si 2.2450(13) Å

Hazari, Balcells

δ ^{1}H –2.78 *(t,* $^2J_{P\text{-}H}$ 25 Hz)

$J_{Si\text{-}H}$ 105 Hz

δ ^{29}Si 4.52

d Ni-Si 2.3110(5) Å

Chart S1. Some spectroscopic and X-ray diffraction parameters of the complexes of this work and literature precedents when provided.[2-6]

7. DFT computations on the hydride nature in **Ni-1** and **Ni-2**

To support the structural characterization, DFT (density functional theory) computations were performed to simulate the hydride signal in the ^{1}H NMR spectra, allowing to distinguish between a classical hydride and a non-classical σ-silane or germane using the Gaussian 16 software.[7] The geometries, first, were optimized using the PBE1PBE functional with the damping dispersion correction[11] at the BS1 level of theory. In BS1, 6-31(d')[8-10] basis set is used for C and H atoms and modified LanL2DZ+ECP[11-13] is used for Ni, Si, P, and Ge atoms. Single-point calculations associated with Gauge-Independent Atomic Orbital (GIAO)[14] with the same functional at BS2 basis set were carried out on the gas phase geometries to obtain chemical shifts. At basis set BS2, 6-311+G(d,p)[15, 16] is used for C and H atoms and modified LanL2DZ is used for Ni, Si, P, and Ge atoms. In the single point calculations, solvent effect of benzene were also included with Solvation Model Based on Density (SMD)[17] calculations. The final results reported at SMD(benzene)-PBE1PBE-D3/BS2//PBE1PBE-D3/BS1 level theory are shown in **Figures S1** and **S2**.

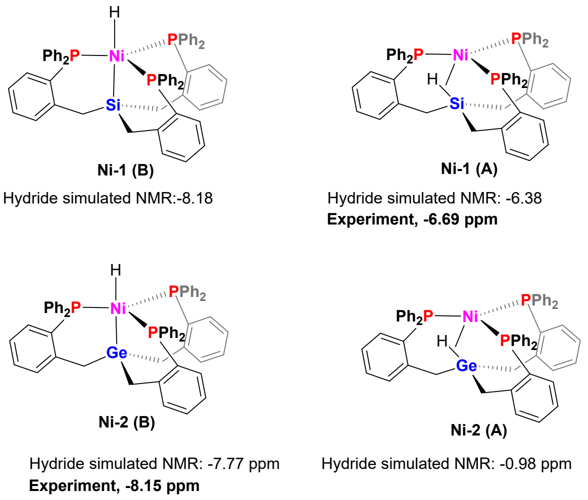

Ni-1 (B)
Hydride simulated NMR:-8.18

Ni-1 (A)
Hydride simulated NMR: -6.38
Experiment, -6.69 ppm

Ni-2 (B)
Hydride simulated NMR: -7.77 ppm
Experiment, -8.15 ppm

Ni-2 (A)
Hydride simulated NMR: -0.98 ppm

Figure S1. Simulated and experimental NMR chemical shifts of the hydride in nickel complexes **Ni-1** and **Ni-2**.

The computed values allow to differentiate between the nonclassical and classical hydride complexes, with the calculated hydride shifts significantly more upfield than the corresponding non-classical silane or germane. Comparison with the experimental data allows to conclude that complex **Ni-1** is closer to the σ-silane coordination mode while the experimental values for the complex **Ni-2** are consistent with a hydride germyl Ni(II) formulation. The simulated data in both complexes are in close agreement with the experimental values, if only slightly more downfield (0.31 and 0.38 ppm), indicating that the computed structures are good references for structural assignment.

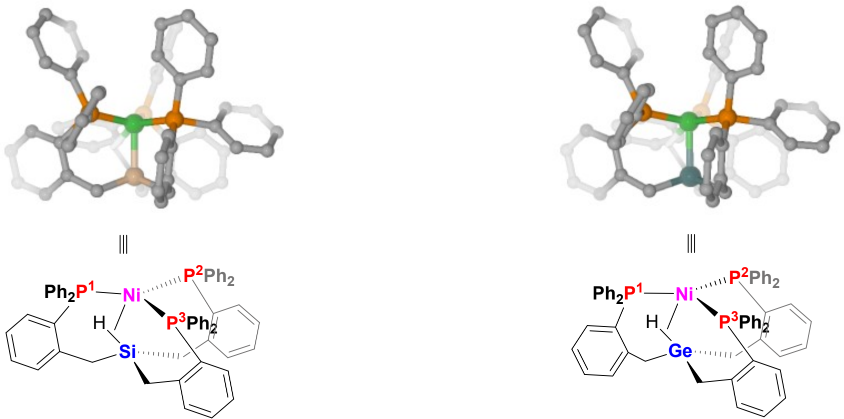

Ni-1 (A)

∠P^1NiP^2 =115.8
∠P^2NiP^3 =109.8
∠P^1NiP^3 =127.0
∠P^1NiSi =100.4
∠P^2NiSi =94.5
∠P^3NiSi =101.3
d(Ni-Si) =2.23 Å
d(Ni-H) =1.51 Å

Ni-2 (A)

∠P^1NiP^2 =115.9
∠P^2NiP^3 =109.3
∠P^1NiP^3 =127.6
∠P^1NiGe =100.3
∠P^2NiGe =93.4
∠P^3NiGe =101.7
d(Ni-Ge) =2.30 Å
d(Ni-H) =1.51 Å

Figure S2. Optimized geometries of **Ni-1 (A)** and **Ni-2 (A)** complexes with selected structural details. Hydrogen atoms of C–H bond are omitted for clarity.

8. Synthesis and characterization of grafted material **Ni-1@NU-1000**

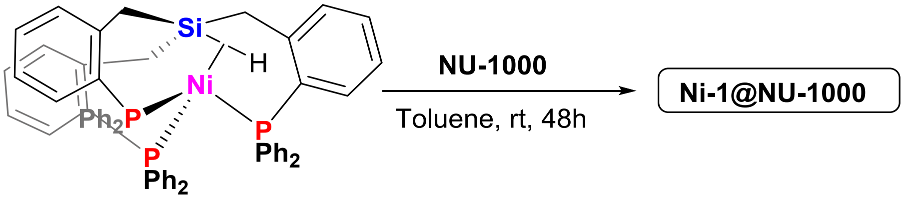

Ni-1

Microcrystalline NU-1000 (56.1 mg, 0.03 mmol) was added to a 5 mL toluene solution of **Ni-1** (60.6 mg, 0.07 mmol) at room temperature. After stirring for 48 h, the resultant yellow solid was centrifuged out of the suspension and washed with toluene and pentane 4-5 times. The solid was soaked overnight in 3 mL toluene and finally dried under dynamic vacuum for 12 h. The characterization of the material is given below.

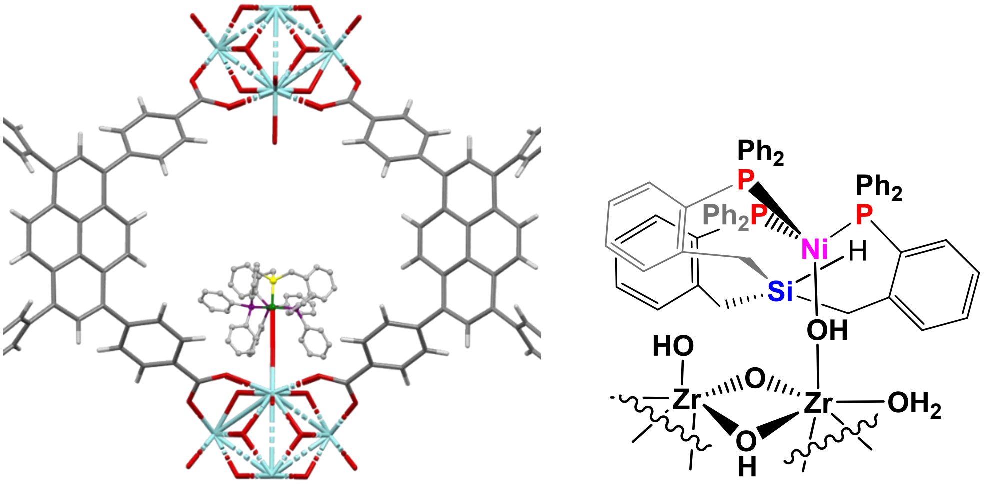

Figure S3. A proposed structure for material **Ni-1@NU-1000** resulting from the grafting of the **Ni-1** complex onto NU-1000. The structure on the right is suggested on the basis of the preliminary mechanistic findings.

8.1 Determination of Ni and Zr content by ICP-MS

The Ni and Zr metal contents in the **Ni-1@NU-1000** material were measured in an inductively coupled plasma-mass spectrometer (ICP-MS). The ICP-MS calibration curves were obtained with a series of standardized nickel and zirconium solutions, where nickel(II) nitrate and zirconium tetrachloride (CRM standards from Sigma Aldrich) were treated with a mixture of concentrated HNO_3 (5 mL), HCl (5 mL), H_2SO_4 (2 mL) and distilled water (13 mL). The desired standardized solutions were prepared by diluting an aliquot of the stock solution to a final volume of 10 mL of the same matrix. To perform the metal content determination of Ni-1@NU-1000, a sample was dissolved in a mixture of conc. HNO_3 (5 mL), HCl (5 mL), H_2SO_4 (2 mL), and distilled water (13 mL), then an aliquot (1.5 mL) of this solution was diluted to 10 mL with the acid matrix. The technique gave the values of weight percent content of each of the metals as given below.

Conversion of weight percent to mol gave an approximate molar ratio of one Ni atom per Zr_6 unit.

	Ni	**Zr**
Found w%	0.560	5.41
n/100 g sample	0.0000950 mol	0.000593 mol
Molar ratio	0.960	6.00
Approximate molar ratio	1	6

8.2 XAFS analysis of Ni-1@NU-1000

Figure S2 shows the XANES spectra of a sample of Ni-1@NU-1000. The comparison of the energies of the pre-edge peas of Ni(II) and reference compounds is consistent with an oxidation state of +2. Furthermore, comparison with Ni oxide indicates that the MOF material is not bulk NiO. There is no evidence of metallic Ni either. Thus, this study is in agreement with a grafted Ni(II) species on the material.

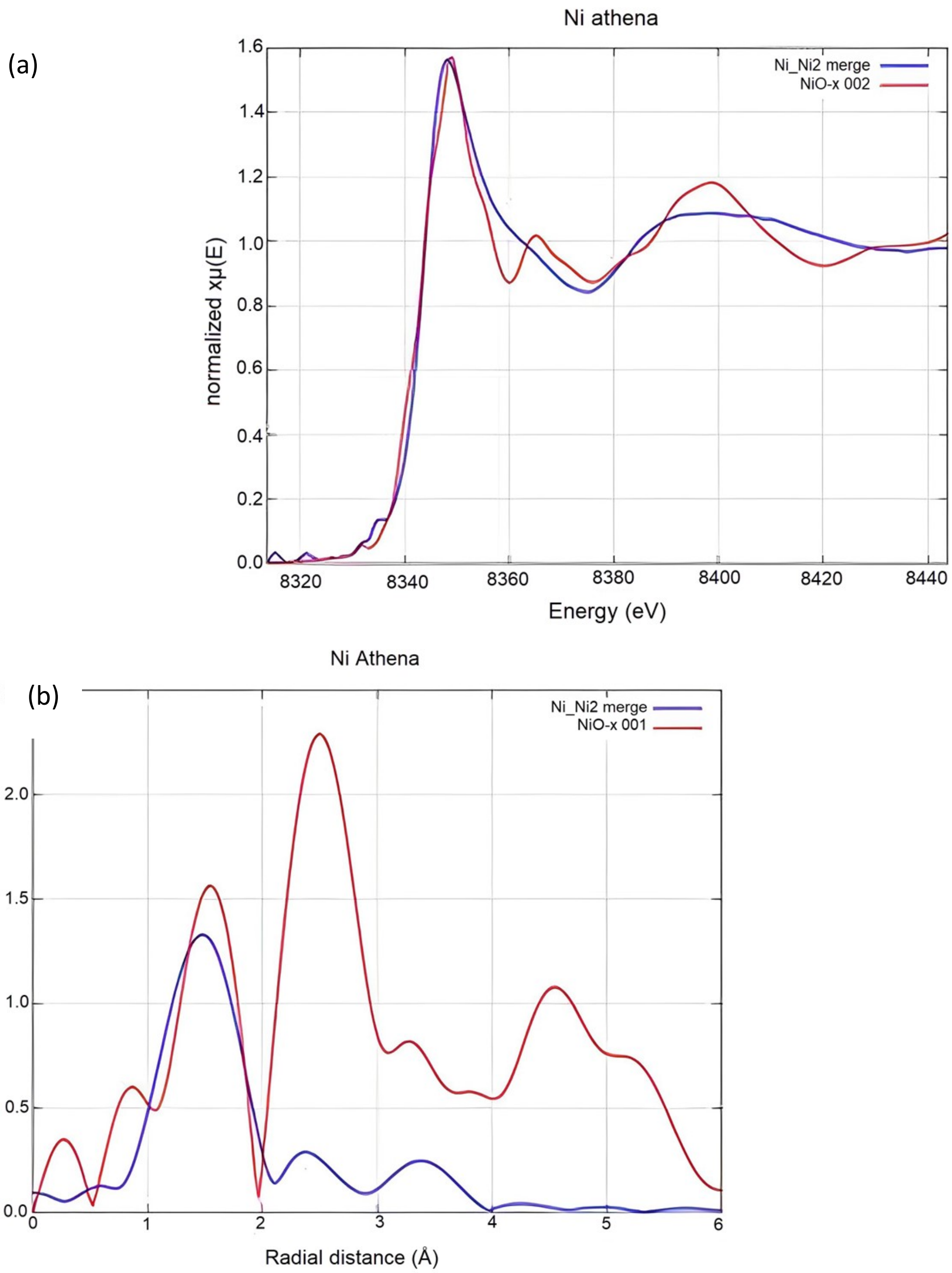

Figure S4. (a) Transmission XANES of Ni K edge of a sample of Ni-1@NU-1000 (blue trace) and comparison with Ni(II) oxide. (b) k^3-weighted Fourier transformed EXAFS (k range = 2.8-11.5 Å^{-1}), magnitude and real components showing comparisons with Ni oxide (feff v6*) scaled arbitrarily). Note that some of the pre-edge noise are artifacts but not peaks.

While it was not possible to resolve the contributions of the expected Ni-O and Ni-P/Si scattering paths to generate a uniquely-good fit due to limited data, qualitatively, the preliminary data are consistent with the proposed structure of the chemisorbed **Ni-1@NU-1000** material proposed in **Figure S3.**

8.3 SEM-EDX Analysis of Ni-1@NU-1000

Analysis by SEM (Scanning Electron Microscopy) was performed on **Ni-1@NU-1000**. This analysis is in agreement with a homogenous distribution of Ni throughout the particles.

Electron images of Ni-1@NU1000

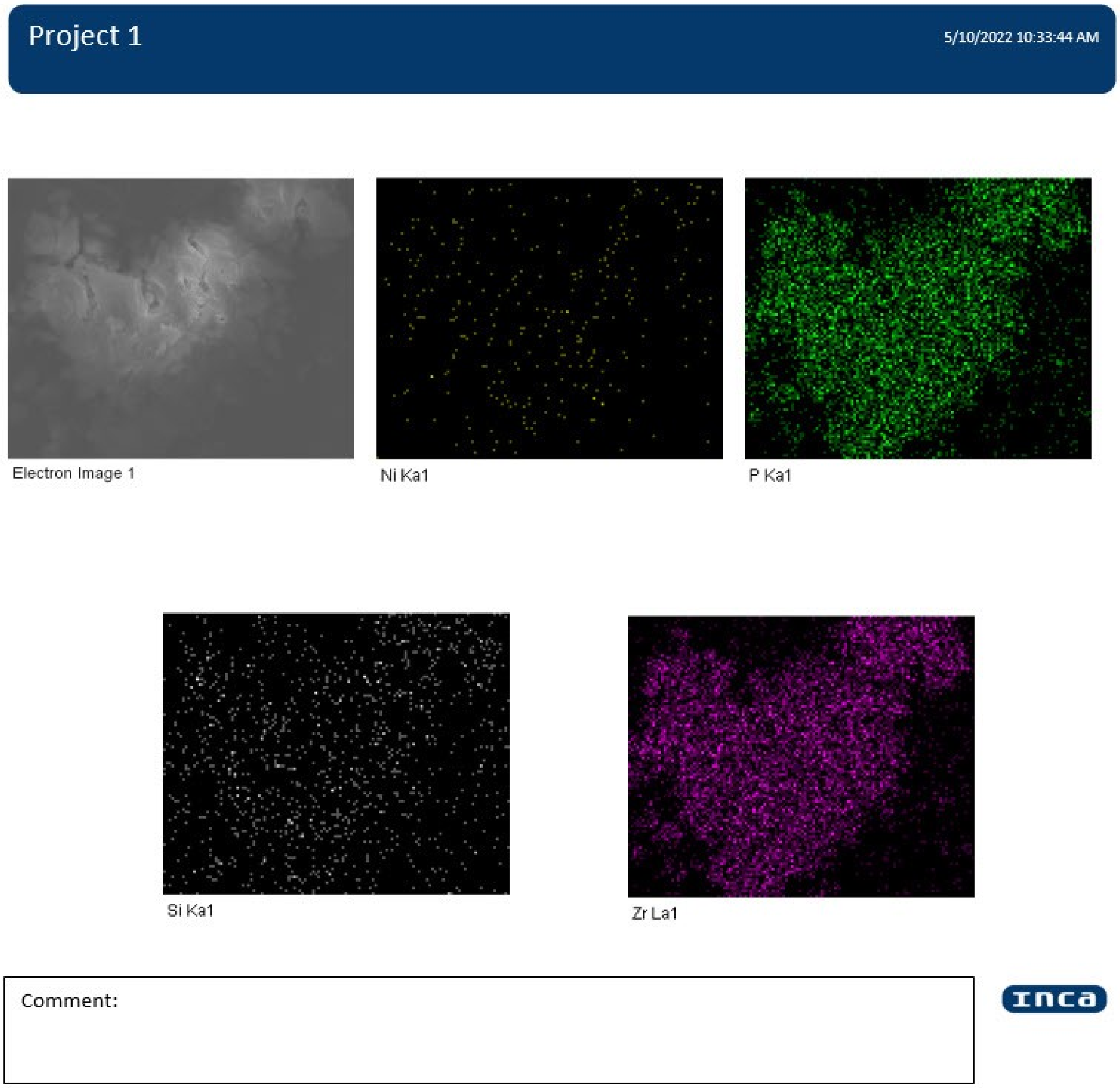

Project 1

5/10/2022 10:33:44 AM

Comment:

9. Synthesis of grafted material **Ni-2@NU-1000**

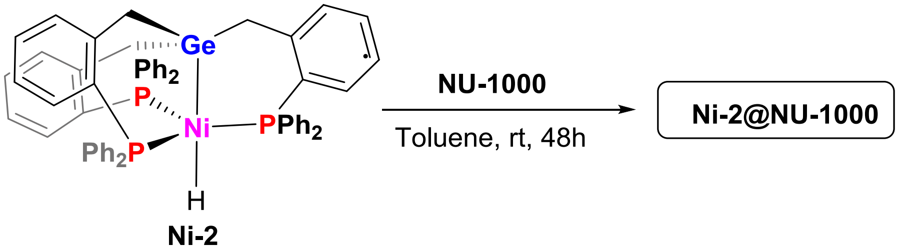

Microcrystalline NU-1000 (77.7 mg, 0.037 mmol) was added to a 5 mL toluene solution of **Ni-2** (87.8 mg, 0.092 mmol) at room temperature. After stirring for 48 h, the resultant yellow solid was centrifuged out of the suspension and washed with toluene and pentane 4-5 times. The solids were soaked overnight in 3 mL toluene and finally dried under dynamic vacuum for 12 h.

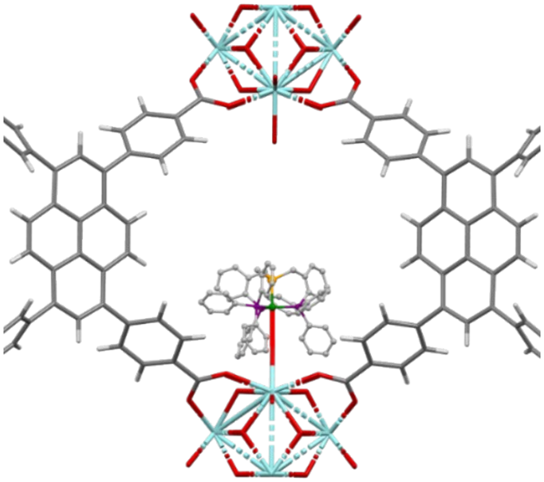

Figure S5. A proposed structure of **Ni-2@NU-1000** resulting from the grafting of the **Ni-2** complex into NU-1000.

9.1 Ni and Zr determination by ICP-MS

As in section 8.1, the metal content in **Ni-2@NU-1000** material was determined in an inductively coupled plasma-mass spectrometer (ICP-MS). A sample of **Ni-2@NU-1000**, was dissolved in a mixture of conc. HNO_3 (5 mL), HCl (5 mL), H_2SO_4 (2 mL) and distilled water (13 mL), then diluted this solution, aliquot 1.5 mL in 10 mL. The technique gave the values of weight percent content of each of the metals given below. Conversion to mol gave an approximate molar ratio of 1.5 Ni atoms per Zr_6 unit.

	Ni	**Zr**
Found w%	1.02	6.11
n/100g sample:	0.000174 mol	0.000670 mol
Molar ratio	1.56	6.00
Approximate molar ratio	3	12

9.2 SEM-EDX Analysis of **Ni-2@NU-1000**

Once again, the SEM analysis of **Ni-2@NU-1000** surface is consistent with a homogenous distribution of Ni in the sample.

Electron images of **Ni-2@NU1000**

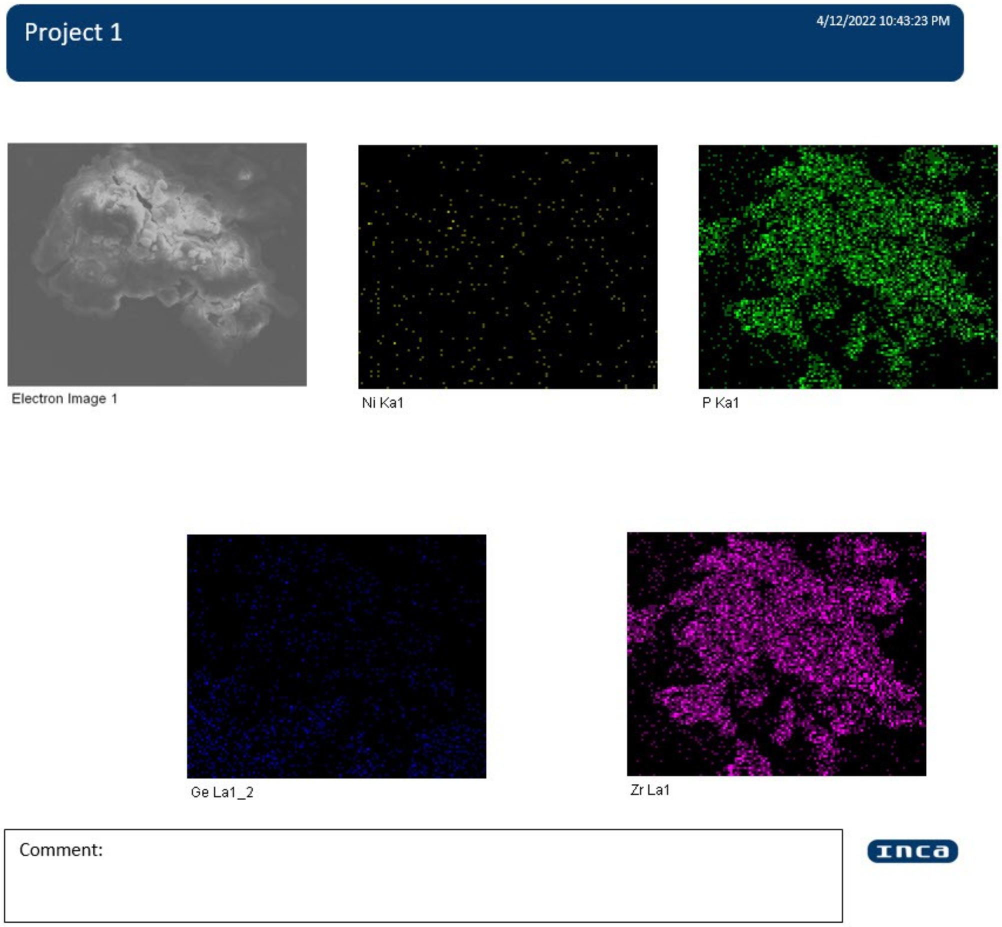

Project 1

4/12/2022 10:43:23 PM

Comment:

10. Powder X-ray Diffraction

Powder X-Ray Diffraction Patterns (PXRD) were collected on a PROTO Diffractometer, AXRD Benchtop with a Cu-Kα1 radiation (λ = 1.5406 Å) using a nickel filter. Patterns were recorded in the 2-50° 2θ range with a step scan of 0.02° and 2 seconds per step.

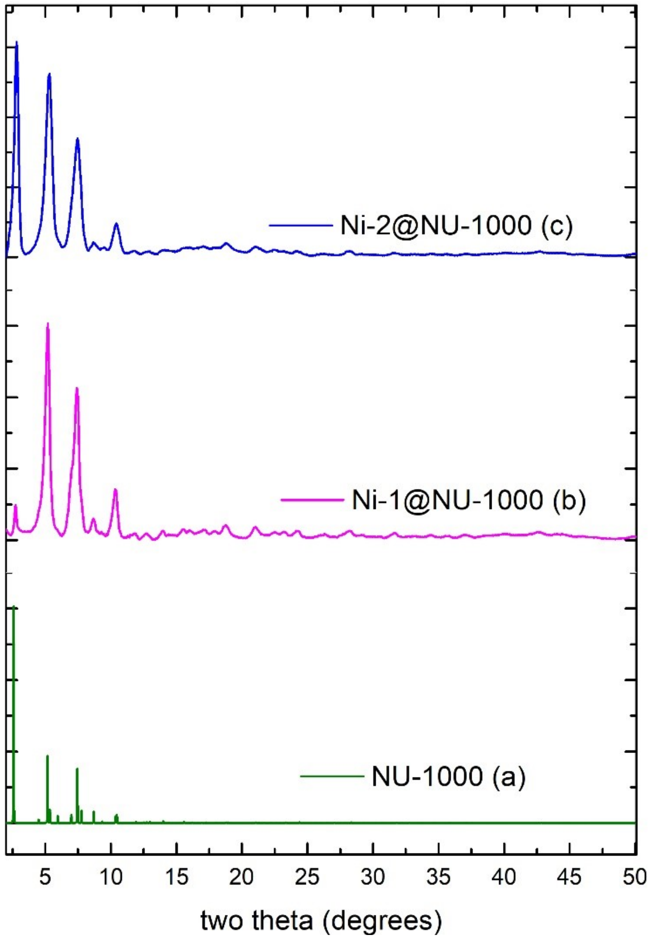

Figure S6. PXRD patterns of (a) simulated NU-1000, (b) Ni-1@NU-1000, and (c) Ni-2@NU-1000.

11. Nuclear Magnetic Resonance, ^{1}H NMR,

Nuclear magnetic resonance (NMR) experiment was performed on Bruker Avance III 300 MHz spectrometer operating with frequency, deuterated solvent (DMSO-d_6), and temperature indicated. The preparation of the samples for ^{1}H NMR followed the procedure of *Nat. Protoc. 2016, 11, 149-162*. The samples were digested using 5 drops of D_2SO_4 and sonicated to form a brown slurry. Then, 0.5mL of DMSO-d_6 was added to dissolve the slurry and solutions became clear. In these conditions, we found no significant differences from the reported spectrum. Nor did we find any difference between the ungrafted NU-1000 MOF material and the grafted Ni-1@NU-1000 and Ni-2@NU-1000 samples. This is unsurprising given the low concentration of the Ni complexes in the MOF and the relative low sensitivity of NMR spectroscopy. However, the presence of the pyrene linkers is ascertained as anticipated.

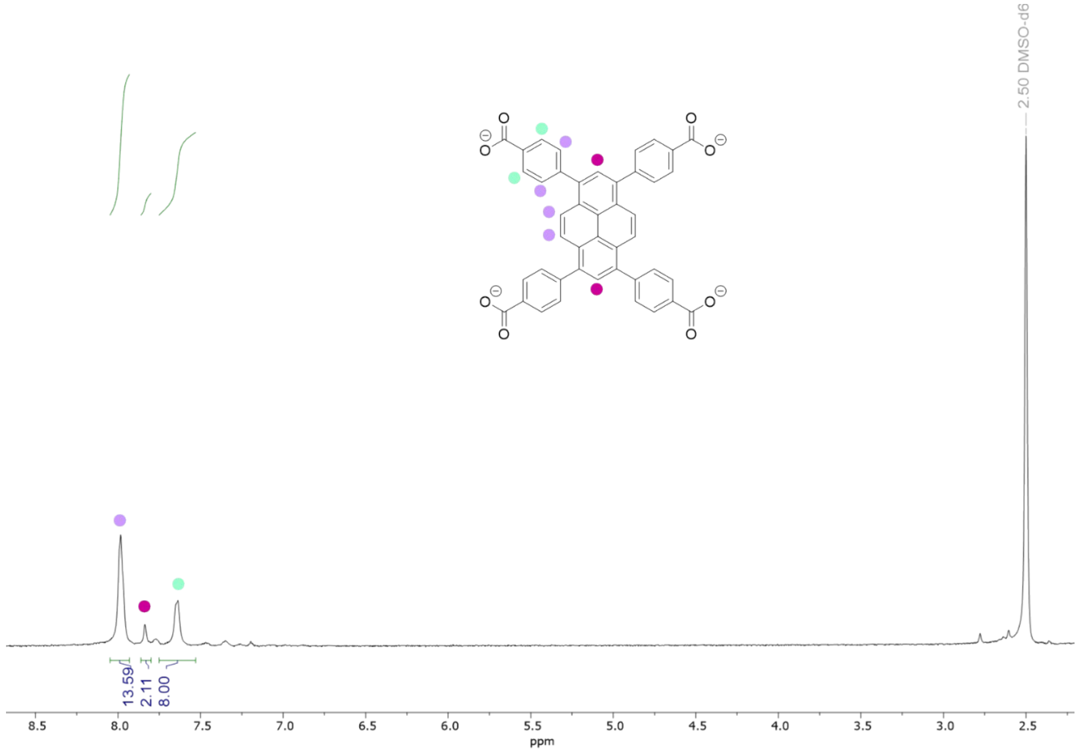

Figure S7. ^{1}H NMR spectrum (300 MHz, DMSO-d_6, 298 K) of digested **Ni-1@NU-1000.** The spectrum corresponds to that reported for digested NU-1000 and is very similar to that of digested **Ni-2@NU-1000.**

12. IR Spectroscopy

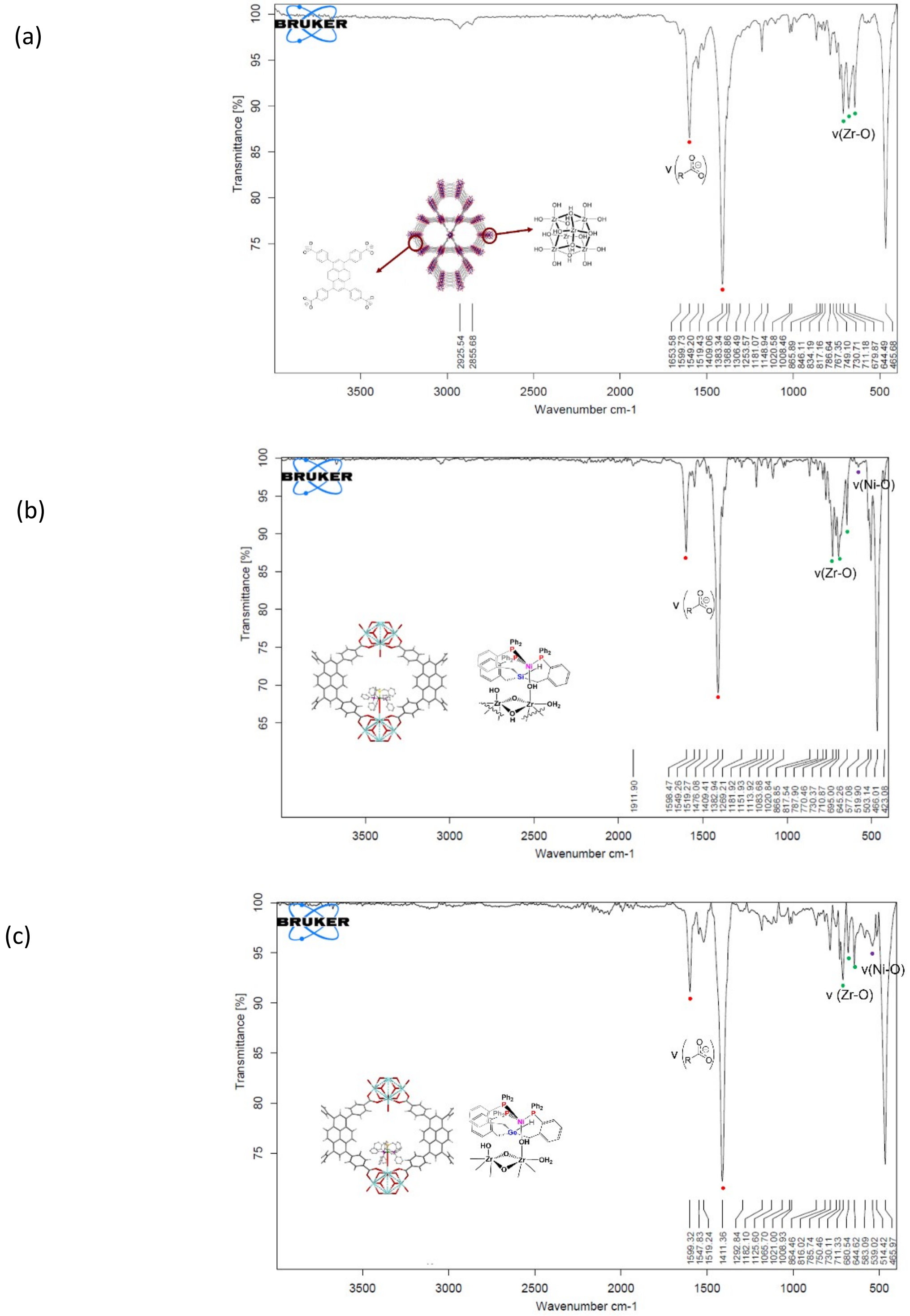

Figure S8. ATR-IR spectra of (a)NU-1000, (b) **Ni-1@NU-1000**, and (c) **Ni-2@NU-1000.**

13. Catalytic study of hydroboration of aldehydes and ketones

13.1 Homogeneous catalysis

13.1.1 General procedure for the homogenous catalysis of aldehydes

A 4 mL screw-capped vial equipped with a magnetic stir bar was charged with the catalyst (**Ni-1** or **Ni-2**, 2 mol%), freshly distilled aldehyde or ketone (0.2 mmol), and HBpin (0.3 mmol) in the glovebox under an argon atmosphere in C_6D_6 (400 µL). After optimization in homogeneous conditions, the reactions were carried under at 50 °C under stirring. After completion of the reaction, 1,3,5-trimethoxybenzene (0.2mmol) was used as an internal standard to calculate the NMR yield.

13.1.2 Optimization of the reaction conditions for homogenous hydroboration of 4-CF_3-benzaldehyde

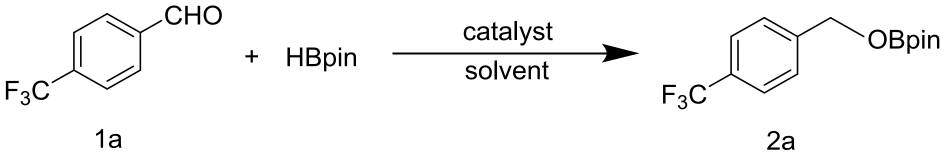

Table S1. Optimization of Ni-1 catalyzed hydroboration of 4-CF_3- benzaldehyde[a]

Entry	Catalyst	Solvent	cat. mol%	T (°C)	t(h)	NMR Yield (%)^b
1	**None**	Benzene-d_6	n/a	25	4	0
2	**Ni-1**	Toluene-d_8	2.0	50	4	78
3	**Ni-1**	Chloroform-d	2.0	50	4	42
4	**Ni-1**	Acetonitrile-d_3	2.0	50	4	55
5	**Ni-1**	Benzene-d_6	2.0	50	4	>99
6	**Ni-1**	Benzene-d_6	2.0	25	4	58
7	**Ni-1**	Benzene-d_6	0.3	50	4	41
8	**Ni-1**	Benzene-d_6	0.3	25	4	24
9	**Ni-1@NU-1000**	Benzene-d_6	0.3	25	4	>99
10	**Ni-1**	Benzene-d_6	0.1	50	4	36
11	**NU-1000**	Benzene-d_6	n/a^c	50	4	0

[a] Reaction conditions: freshly distilled 4CF_3-benzaldehyde (0.2 mmol), HBpin (0.3 mmol), catalyst (varying mol%), solvent (0.4 mL). [b] The conversion and yields were determined by NMR in the presence of 1,3,5-methoxybenzene (0.2 mmol) as the internal standard. n/a = not applicable. [c] 6 mg of unmodified NU-1000 were used.

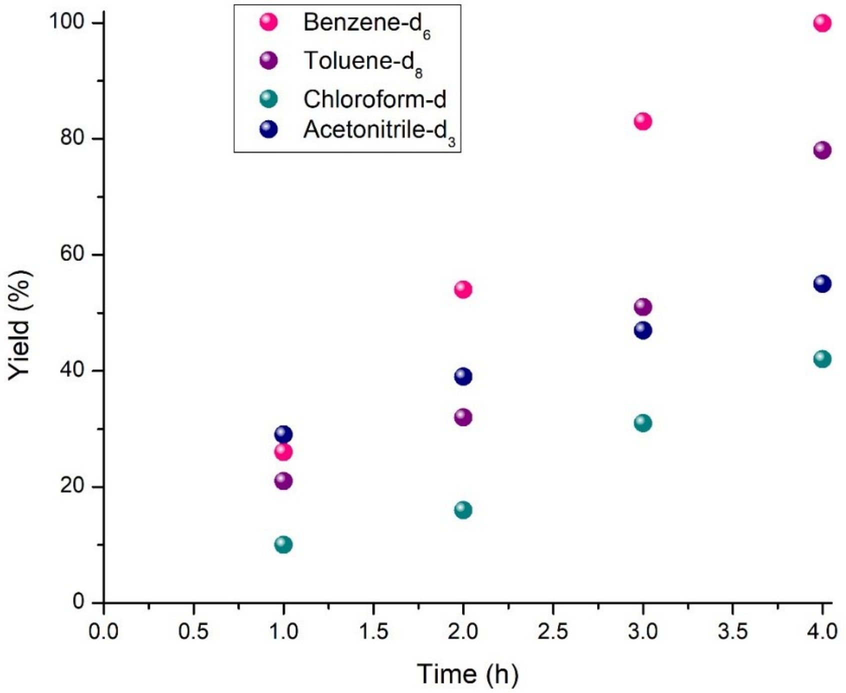

Figure S9. Product yield vs time graphs for the reaction of 4CF_3-benzaldehyde (0.2 mmol) and HBpin (0.3 mmol) catalyzed by homogenous **Ni-1** (2 mol%) in different solvents at 50°C. After 4h the product yield was as follows: benzene-d_6 (>99%), toluene-d_8 (78%), chloroform-d (42%), acetonitrile-d_3 (55%).

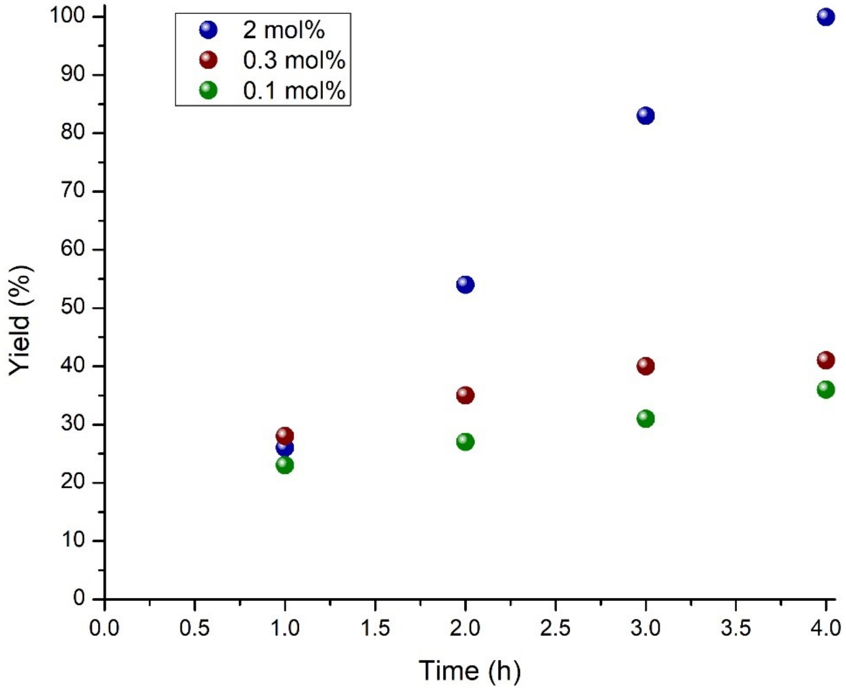

Figure S10. Product yield vs time graphs for the reaction of 4CF_3-benzaldehyde (0.2 mmol) and HBpin (0.3 mmol) catalyzed by homogenous **Ni-1** at 50°C in C_6D_6 for 4h with different catalyst concentrations: 2 mol% (>99%), 0.3 mol% (41%), 0.1 mol% (36%).

13.1.3 Homogeneous hydroboration of aldehydes: substrate scope

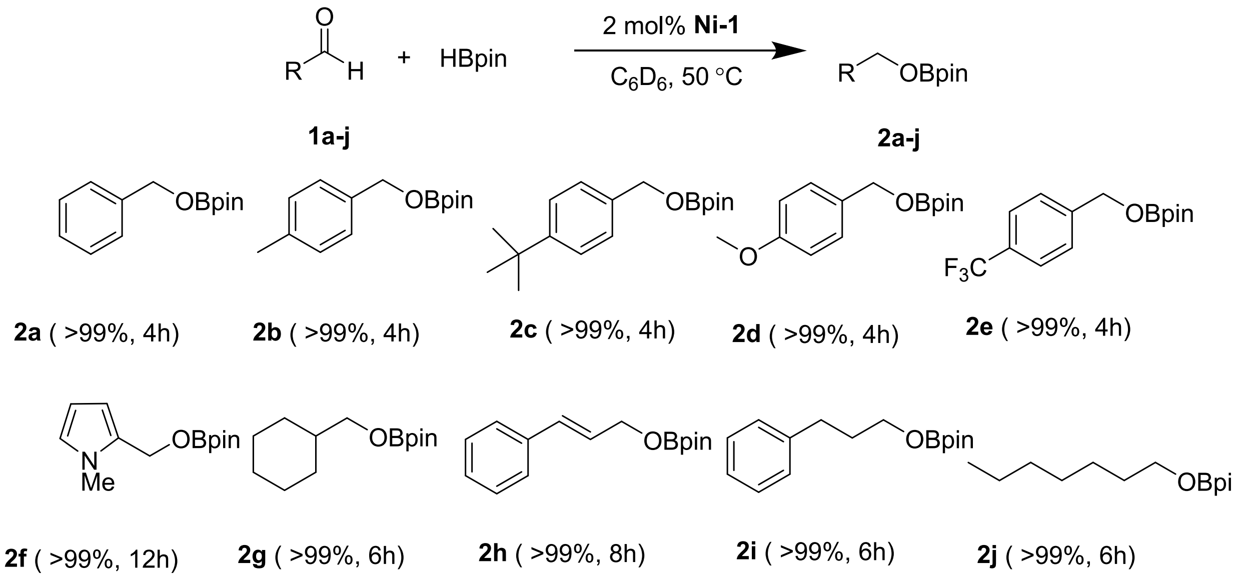

1a-j **2a-j**

2a (>99%, 4h) **2b** (>99%, 4h) **2c** (>99%, 4h) **2d** (>99%, 4h) **2e** (>99%, 4h)

2f (>99%, 12h) **2g** (>99%, 6h) **2h** (>99%, 8h) **2i** (>99%, 6h) **2j** (>99%, 6h)

Chart S2. Catalytic conditions: aldehyde (0.2 mmol), HBpin (0.3 mmol), Ni-1 (2 mol %), C_6D_6 (0.4 mL) at 50 °C, under argon. The yields were determined by NMR in the presence of 1,3,5-methoxybenzene (0.2 mmol) as the internal standard in the reaction mixture.

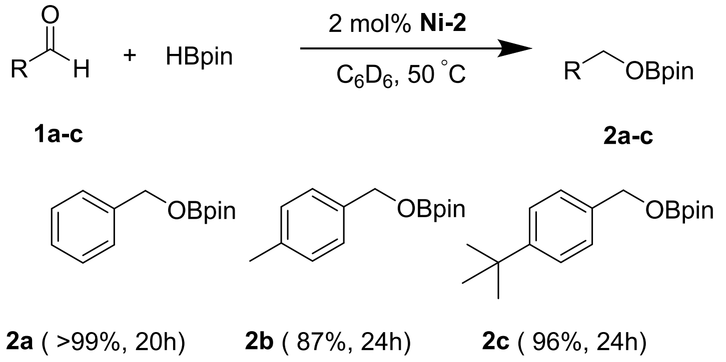

1a-c **2a-c**

2a (>99%, 20h) **2b** (87%, 24h) **2c** (96%, 24h)

Chart S3. Catalytic conditions: aldehyde (0.2 mmol), HBpin (0.3 mmol), Ni-2 (2 mol %), C_6D_6 (0.4 mL) at 50 °C, under argon. The yields were determined by NMR in the presence of 1,3,5-methoxybenzene (0.2 mmol) as the internal standard in the reaction mixture.

13.2 Heterogeneous catalysis

13.2.1 General procedure for the heterogenous catalytic hydroboration of aldehydes

In the glovebox, a 4 mL screw-capped vial equipped with a magnetic stir bar was charged with the catalyst (Ni-1@NU1000 or Ni-2@NU1000, 6.0 mg), aldehyde (0.2 mmol), and HBpin (0.3 mmol) either under an argon atmosphere or under aerobic conditions in the presence of C_6D_6 (400 µL). The reaction was stirred at room temperature and monitored periodically. 1,3,5-trimethoxybenzene (0.2mmol) was used as an internal standard to calculate the NMR yield. We verified that the use of ungrafted MOF material NU-1000 under similar conditions did not result in the formation of the product when using trifluoromethylbenzaldehyde after 4h by NMR spectroscopy.

13.2.2 Reaction conditions for the heterogeneous hydroboration of aldehydes

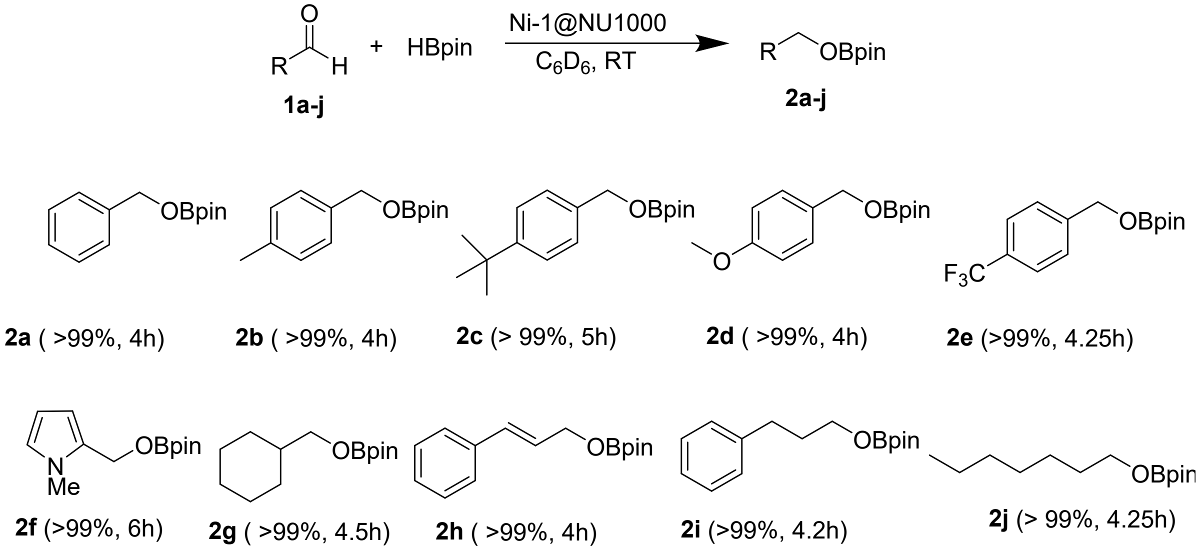

2a (>99%, 4h) **2b** (>99%, 4h) **2c** (> 99%, 5h) **2d** (>99%, 4h) **2e** (>99%, 4.25h)

2f (>99%, 6h) **2g** (>99%, 4.5h) **2h** (>99%, 4h) **2i** (>99%, 4.2h) **2j** (> 99%, 4.25h)

Chart S4. Catalytic conditions: aldehyde (0.2 mmol), HBpin (0.3 mmol), Ni-1@NU1000 (0.3 mol %), C_6D_6 (0.4 mL) at RT, under argon/air. The yields were determined by NMR in the presence of 1,3,5-methoxybenzene (0.2 mmol) as the internal standard in the reaction mixture.

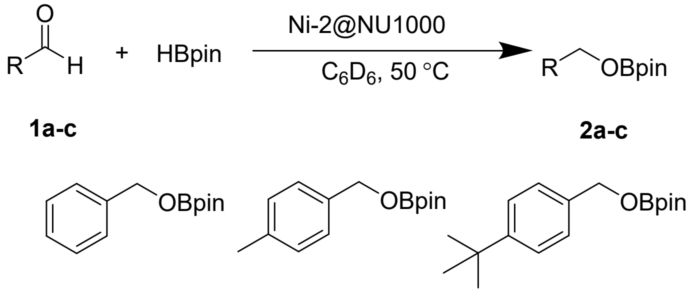

2a (>99%, 4.5h) **2b** (97%, 4.5h) **2c** (97%, 4.5h)

Chart S5. Reaction conditions: aldehyde (0.2 mmol), HBpin (0.3 mmol), Ni-2@NU1000 (0.5 mol %), C_6D_6 (0.4 mL) at 50 °C, under argon/air. The yields were determined by NMR in the presence of 1,3,5-methoxybenzene (0.2 mmol) as the internal standard in the reaction mixture.

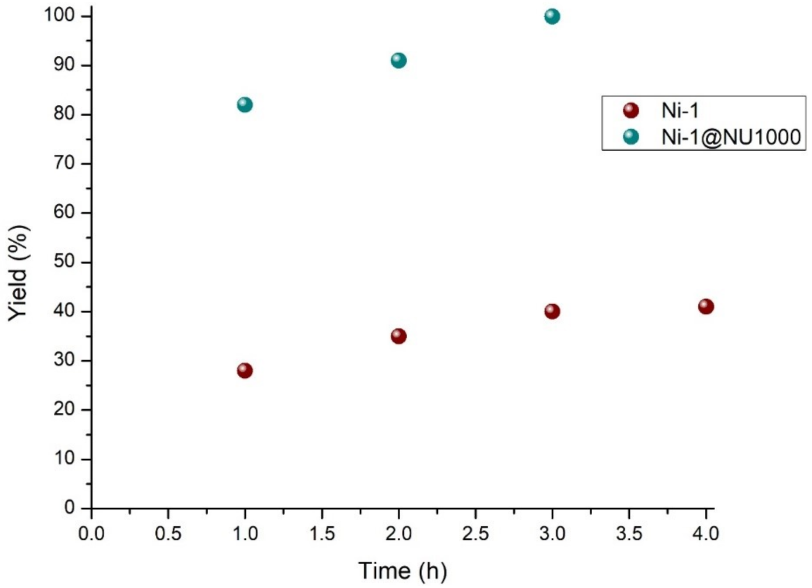

Figure S11. Product yield vs time graphs for the reaction of 4CF$_3$-benzaldehyde (0.2 mmol) and HBpin (0.3 mmol) catalyzed by Ni-1 (0.30 mol%) and Ni-1@NU1000 (0.30 mol%) at 50°C. After 4h, the catalysis by Ni-1 has occurred with 41% yield whereas that catalyzed by Ni-1@NU1000 (>99%) is completed by 3h at 50 °C .

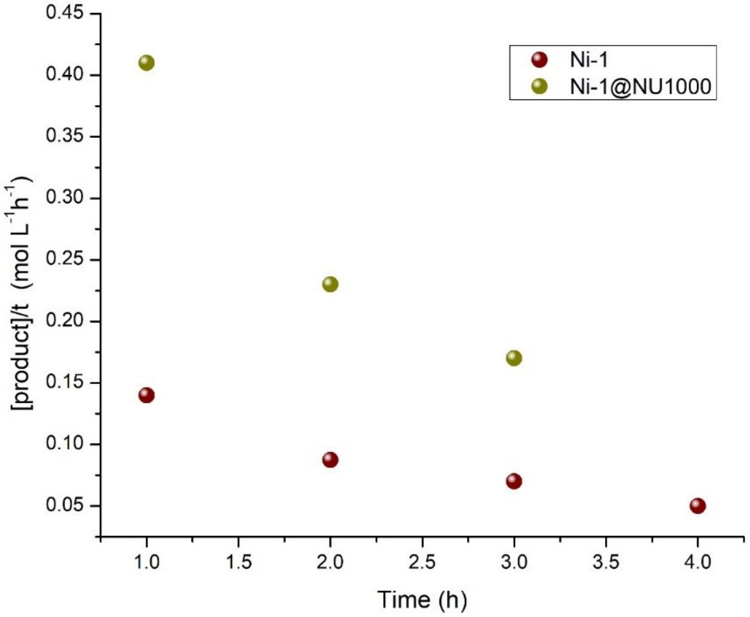

Figure S12. Rate vs time graphs for the reaction of 4CF$_3$-benzaldehyde (0.2 mmol) and HBpin (0.3 mmol) catalyzed by Ni-1 (0.30 mol%) and Ni-1@NU1000 (0.30 mol%) at 50°C. After 4h, the catalysis by Ni-1 has occurred with 41% yield whereas that catalyzed by Ni-1@NU1000 (>99%) is completed in 3h. The **x axis** is time (h) and the **y axis** is concentration of product (mol L^{-1}) divided by time.

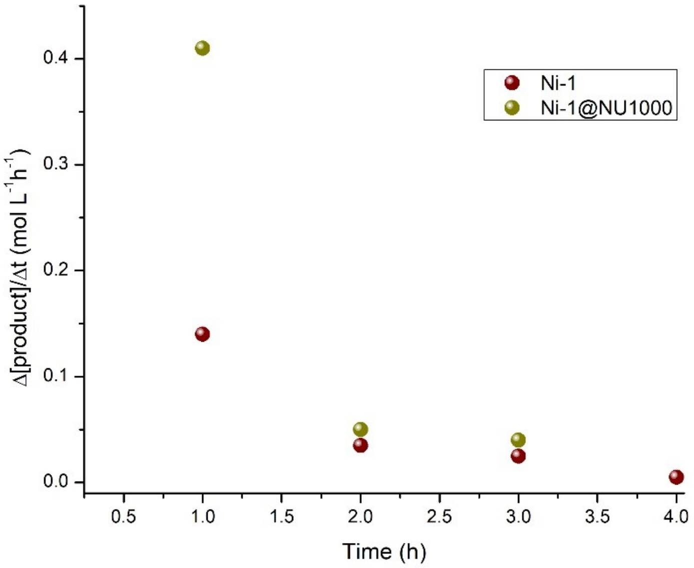

Figure S13. Rate vs time graphs for the reaction of 4CF_3-benzaldehyde (0.2 mmol) and HBpin (0.3 mmol) catalyzed by Ni-1 (0.30 mol%) and Ni-1@NU1000 (0.30 mol%) at 50°C. After 4h, the catalysis by Ni-1 has occurred with 41% yield whereas that catalyzed by Ni-1@NU-1000 (>99%) is completed in 3h. The **x axis** is time (h) and the **y axis** is change in concentration of product (mol L^{-1}) divided by change in time. Rate = ([product@t_2]-[product@t_1])/(t_2-t_1)

13.2.3 Robustness test for the heterogeneous catalyzed hydroboration of aldehydes

Ni-1@NU1000 (6mg, 0.30 mol%) was charged into a small vial and 400 µL C_6D_6. Then, 20.4 µL benzaldehyde (0.2 mmol) and 47 µL HBpin (0.3 mmol) were added to the vial, and the mixture was stirred and monitored by ^{1}H NMR each hour (1h, 2h, 3h) until completion. The catalyst Ni-1@NU1000 was subsequently recovered (centrifuged, washed and, dried), and the reaction was repeated a total of three times. In each repetition, 20.4 µL benzaldehyde (0.2 mmol), 47 µL HBpin (0.3 mmol) and 400 µL C_6D_6 were added. The recovered catalyst at the end of the three cycles was verified by SEM. There were no significant changes after catalysis.

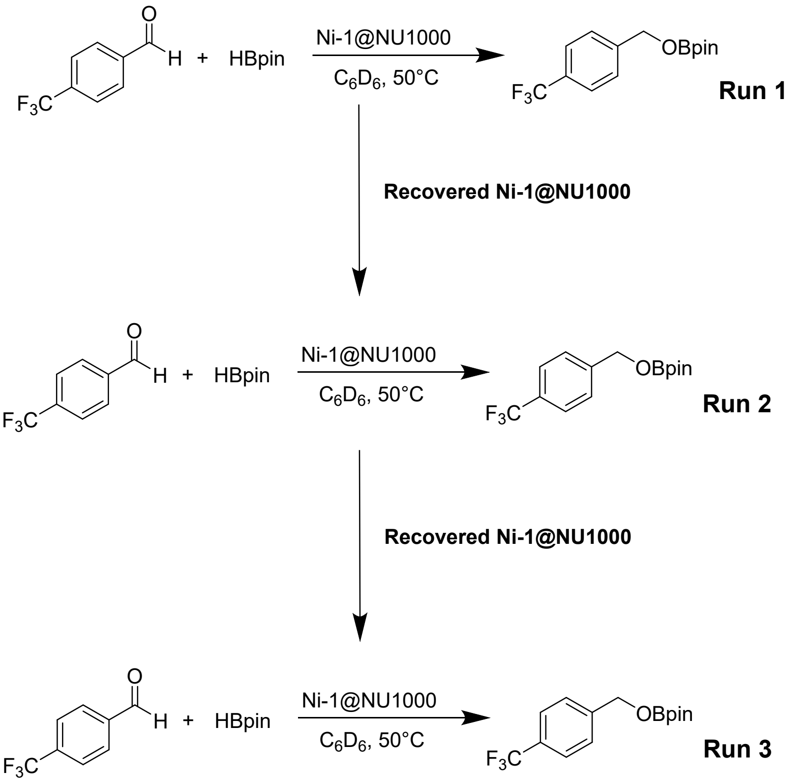

Chart S6. Description of the different runs using the recovered catalyst. for the hydroboration of p-trifluoromethylbenzaldehyde. The catalyst was recovered by centrifugation followed by filtration, washing and drying of the catalyst. Similar procedures were done with other substrates at different temperatures allowing to corroborate that there is no loss of the catalytic activity after this number of runs.

Run #	Time (h)	Product yield (%)
1	1	82
	2	91
	3	>99
2	1	82
	2	87
	3	>99
3	1	80
	2	94
	3	>99

Table S2. Product yield for the hydroboration of 4CF_3-benzaldehyde catalyzed by recovered **Ni-1@NU1000** in three different runs following the procedure described above. This series of experiments were carried out at 50 °C to mimic the conditions of the homogeneous experiments and employ harsher conditions. Similar results are obtained when this test is carried out at room temperature: the catalytic activity is not affected.

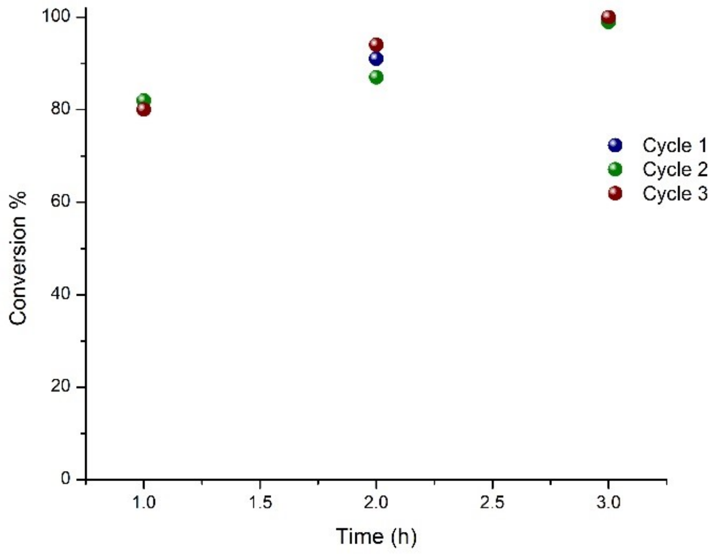

Figure S14. Robustness test for the hydroboration of 4CF$_3$-benzaldehyde catalyzed by recovered **Ni-1@NU1000** in three different runs following the procedure described above. No significant drop in the catalytic activity was observed when using the recovered catalyst.

13.2.4 General procedure for the heterogenous catalysis of ketones

A 4 mL screw-capped vial equipped with a magnetic stir bar was charged with the catalyst (Ni-1@NU-1000, 6.0 mg), ketone (0.2 mmol), and HBpin (0.3 mmol) under an argon /air atmosphere in the presence of C$_6$D$_6$ (400 μL). The reaction was stirred at 50 °C. 1,3,5-trimethoxybenzene (0.2mmol) was used as an internal standard to calculate the NMR yield.

13.2.5. Reaction conditions for hydroboration of ketones

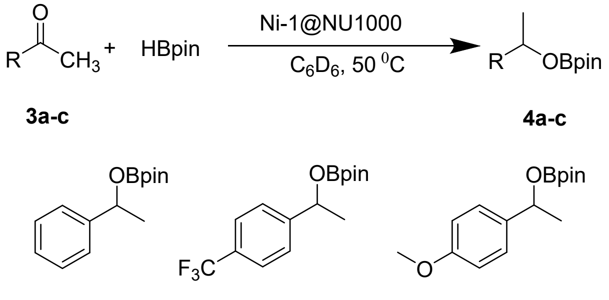

4a (95%, 8h) **4b** (>99%, 8h) **4c** (97%, 8h)

Chart S7. Reaction conditions: ketone (0.2 mmol), HBpin (0.3 mmol), Ni-1@NU1000 (0.3 mol %), C$_6$D$_6$ (0.4 mL) at 50 °C, under argon or air. The yields were determined by NMR in the presence of 1,3,5-methoxybenzene (0.2 mmol) as the internal standard in the reaction mixture.

14. Preliminary mechanistic findings

An NMR tube equipped with a J. Young valve was charged with **Ni-1** (0.037 g, 0.049 mmol) and 0.4 mL of C_6D_6. Then 10 μL (0.098 mmol) of benzaldehyde was added. The reaction mixture was heated to 50 °C. The color of the solution changed to red, and it was analyzed by NMR spectroscopy. The Ni complex shown below was isolated as a red solid (0.015 g, 36% yield). ^1H NMR (500 MHz, C_6D_6, 298 K): δ 8.38 (s, 5H, CH_{arom}), 7.55 – 7.37 (m, 6H, CH_{arom}), 7.27 (t, $^2J_{H-H}$= 7.6 Hz, 3H, CH_{arom}), 7.15 – 6.98 (m, 19H, CH_{arom}), 6.89 (td, $^2J_{H-H}$= 7.4, 1.4 Hz, 6H, CH_{arom}), 6.67 (t, $^2J_{H-H}$= 7.5 Hz, 3H, CH_{arom}), 4.82 (m, 2H, $-OCH_2$), 2.78 (s, 3H, CH_2), 2.02 (s, 3H, CH_2) ppm. $^{13}C\{^1H\}$ NMR (150.9 MHz, C_6D_6, 298 K): 142.6 (dd, J_{C-P}= 9.5, 5.6 Hz, C_{ipso}), 141.6 (s, CH_{arom}), 137.9 (s, CH_{arom}), 134.6 (dd, J_{C-P}= 20.2, 16.7 Hz, C_{ipso}), 132.3 (s, CH_{arom}), 130.8 (s, CH_{arom}), 128.7 (s, CH_{arom}), 127.4 (s, CH_{arom}), 126.6 (s, CH_{arom}), 124.4 (s, CH_{arom}), 65.2 (s, $-OCH_2$), 22.5 (m, CH_2) ppm. $^{31}P\{^1H\}$ NMR (202.46 MHz, C_6D_6, 298 K): 20.76 (s) ppm. DEPT $^{29}Si\{^1H\}$ NMR (99.36 MHz, C_6D_6, 298 K): 10.56 (s) ppm. Anal. Calc.: for $C_{64}H_{55}NiP_3SiO$: C: 75.37%, H: 5.44%; Found: C: 74.98%, H: 5.51%.

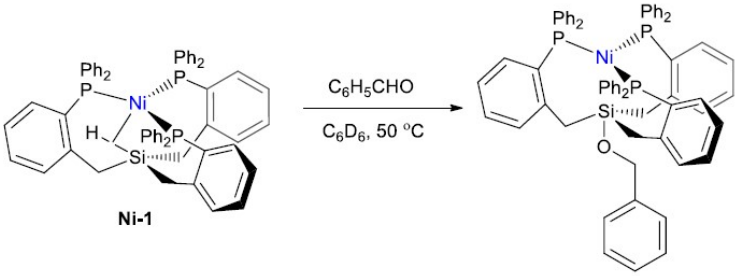

Subsequently, an NMR tube equipped with a J. Young valve was charged with the new Ni complex isolated above (20 mg, 0.019mmol) and 0.4 mL of C_6D_6. Then 4.0 μL (0.038 mmol) of benzaldehyde and 5.6 μL (0.038 mmol) HBpin were added. The reaction mixture was heated at 50 °C for 4 h. The solution was analyzed by NMR spectroscopy finding the quantitative formation of the hydroboration product **2a** while the Ni complex remain unchanged.

The above preliminary findings suggest that the catalysis takes place on the Si atom rather than on the Ni center. This is consistent with similar reaction rates in the homogeneous and heterogeneous phases and suggest that the Ni complex grafts "unmodified" into the MOF material. This is likely favored by the semirigidity of the ligand due to the presence of the methylene. The non classical sigma silane character could allow for the more facile decoordination of the σ(SiH) moiety. Herein, the preliminary proposed mechanisms for the hydroboration by **Ni-1** and **Ni-1@NU-1000** based on the above evidence. We are currently performing further experiments and DFT computations. The findings will be reported in due course.

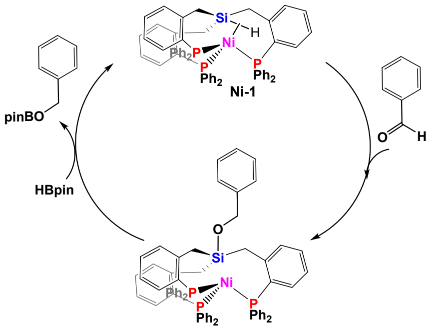

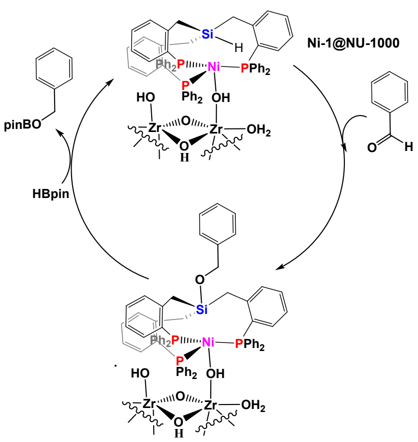

15. NMR and IR spectra of ligands **L1, L2**, metal complexes **Ni-1, Ni-2** and, boronate products

15.1 Spectra for **L1**

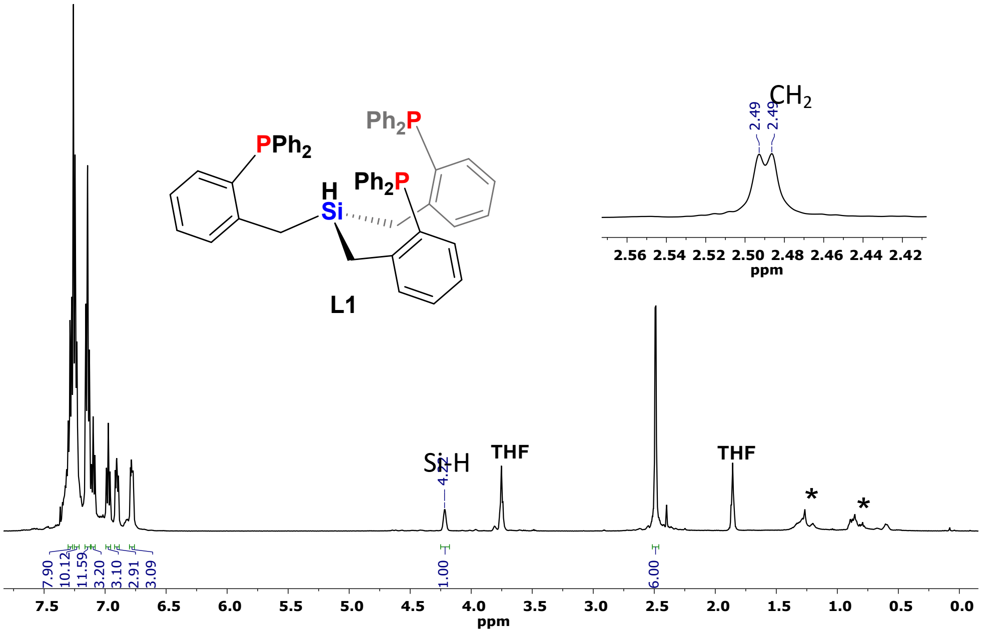

Figure S15. ^{1}H NMR spectrum (500 MHz, CDCl$_3$, 298 K) of **L1** (*=hexane)

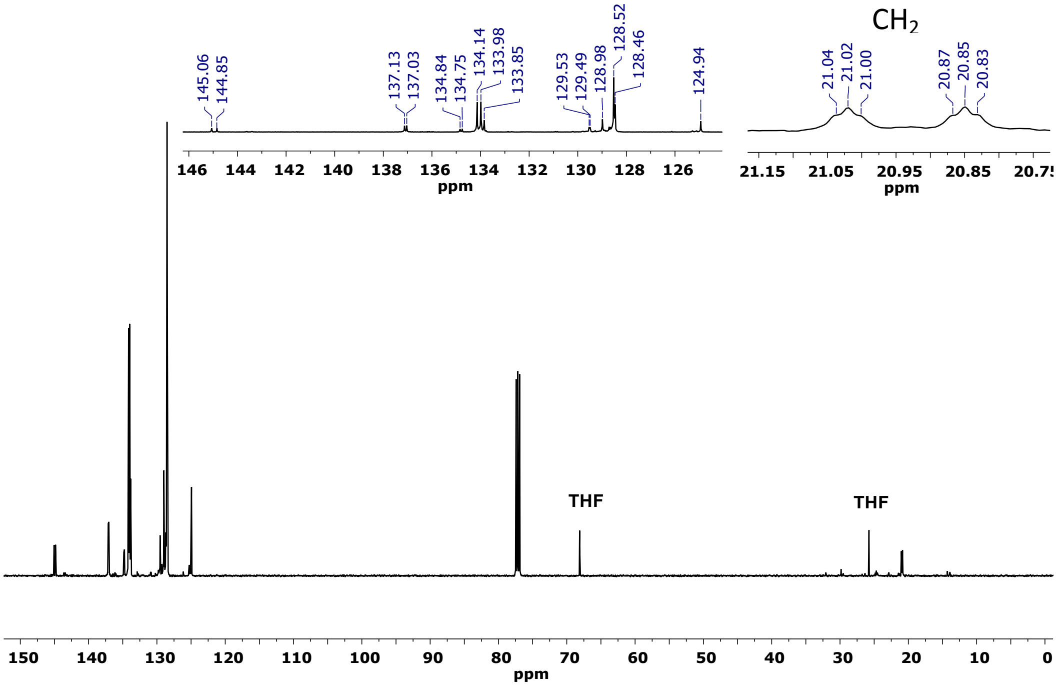

Figure S16. ^{13}C{^{1}H} NMR spectrum (125.76 MHz, CDCl$_3$, 298 K) of **L1**

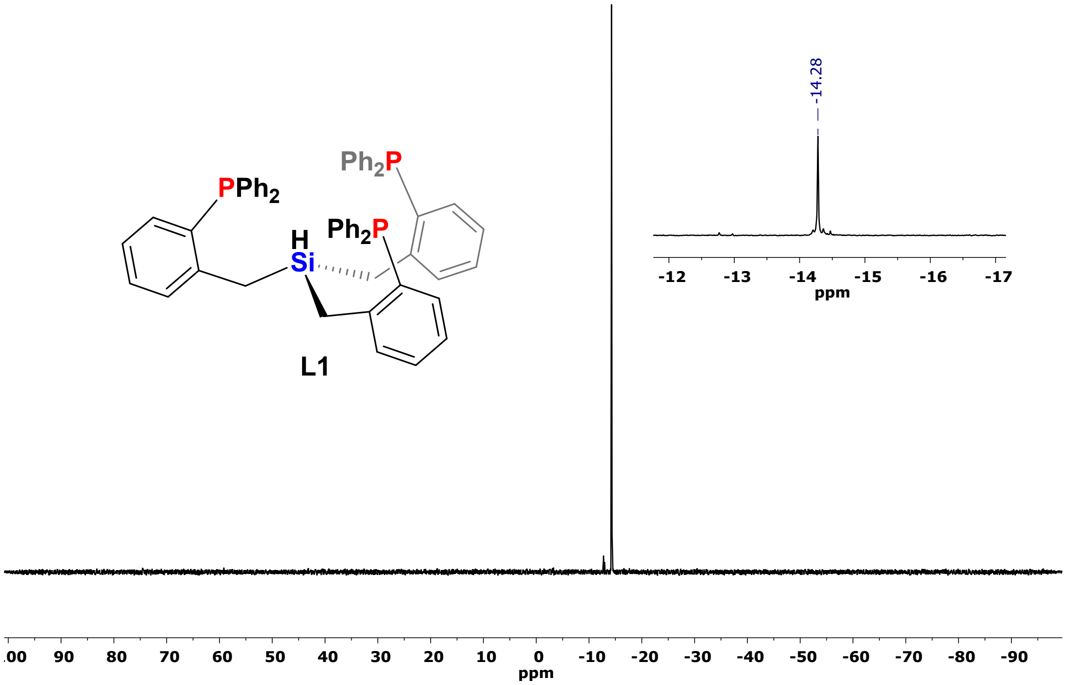

Figure S17. $^{31}P\{^1H\}$ NMR spectrum (202.46 MHz, $CDCl_3$, 298 K) of **L1**

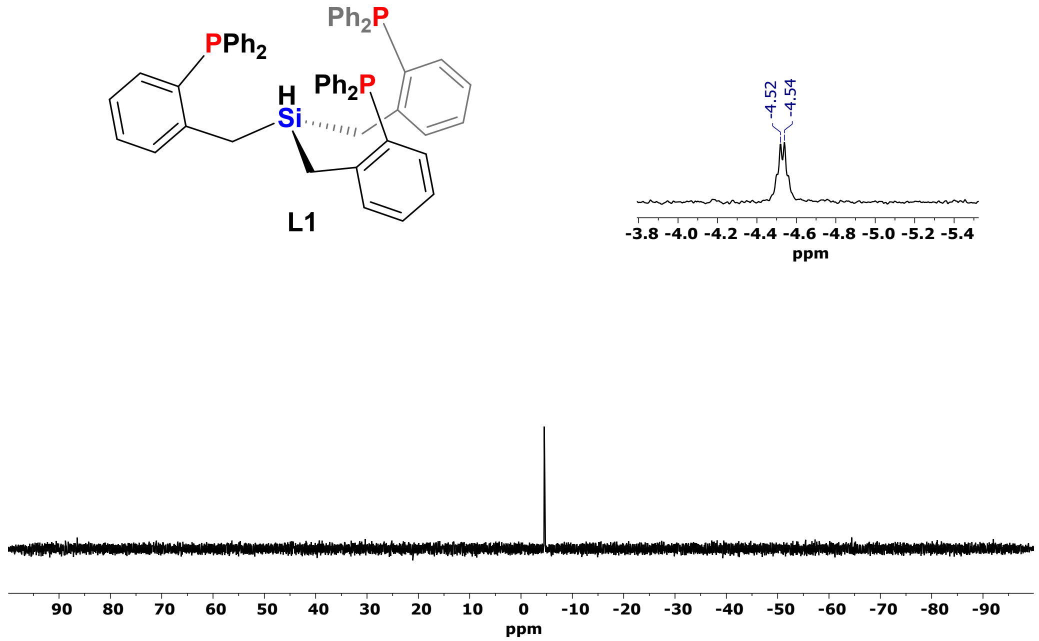

Figure S18. $^{29}Si\{^1H\}$ DEPT NMR spectrum (99.36 MHz, $CDCl_3$, 298 K) of **L1**

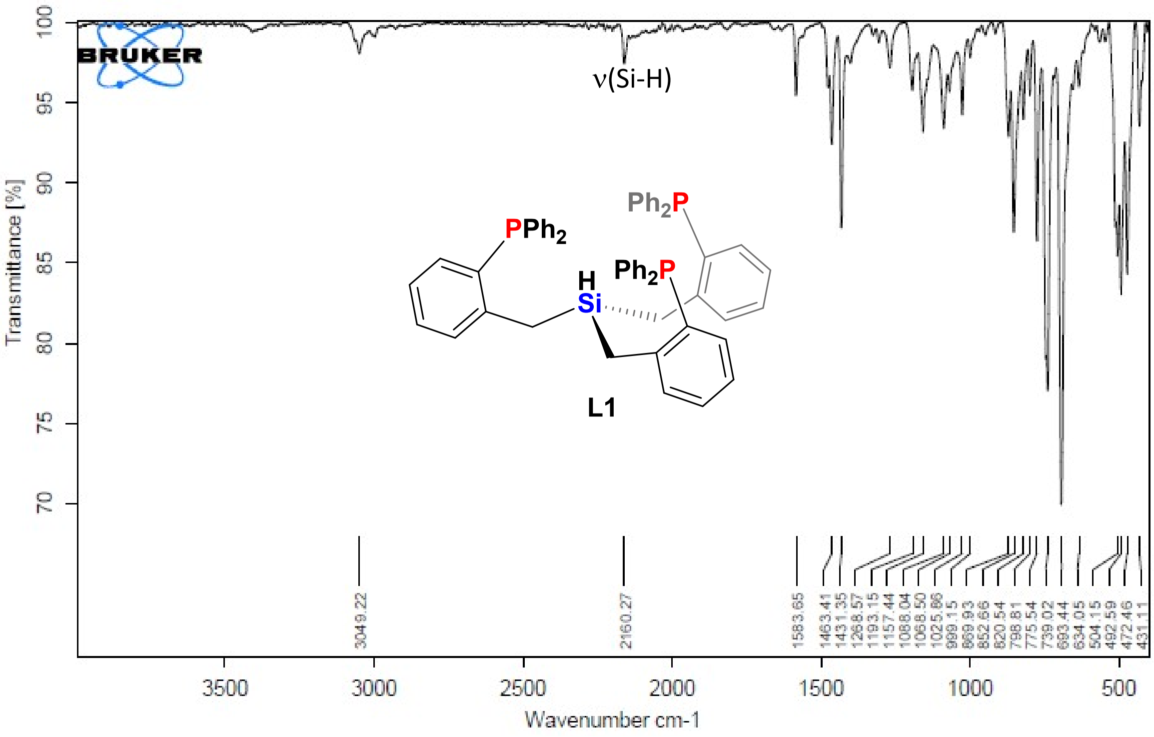

Figure S19. FT-IR (ATR) spectrum of **L1.**

15.2 Spectra for **L2**

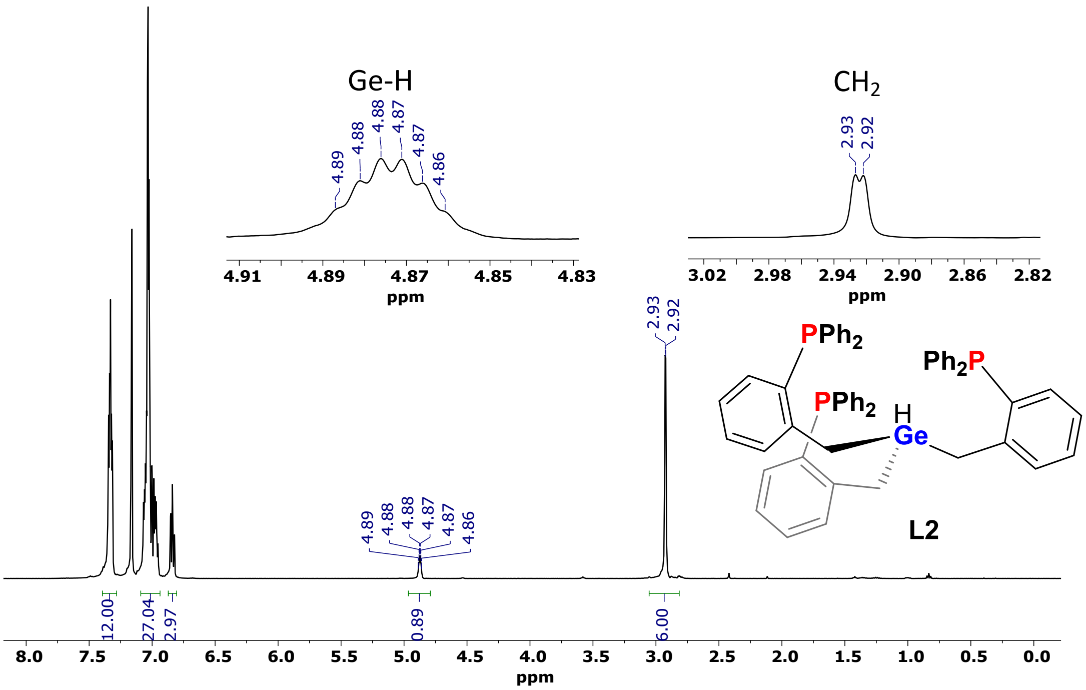

Figure S20. ^{1}H NMR spectrum (500 MHz, C_6D_6, 298 K) of **L2**

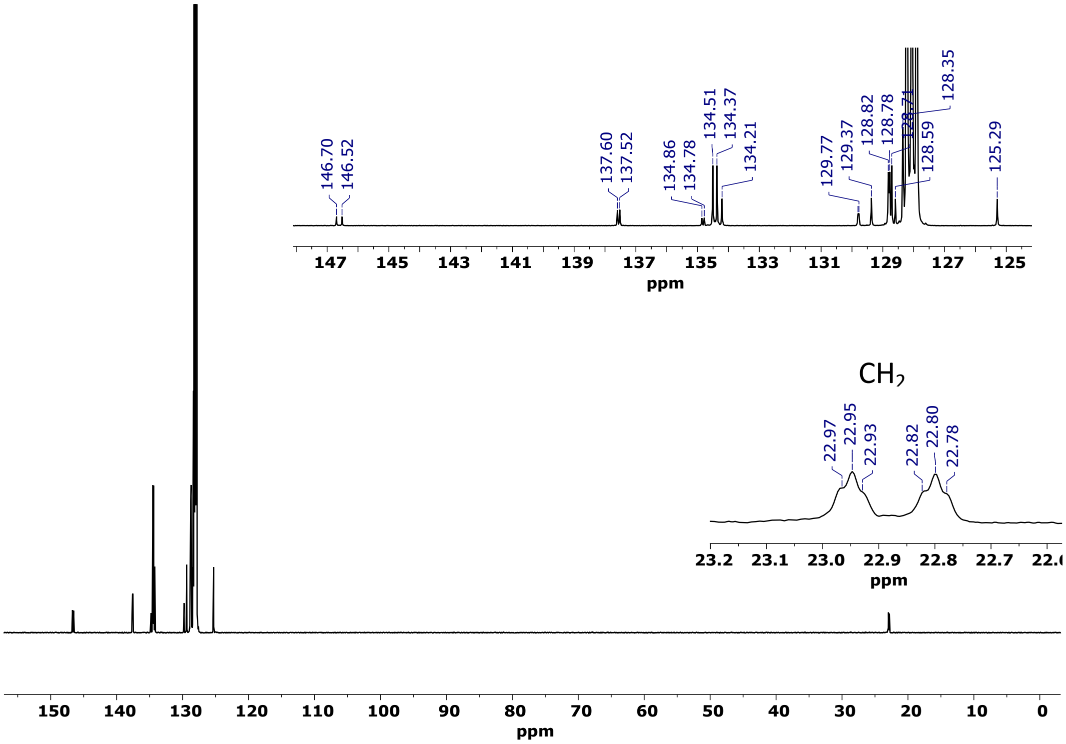

Figure S21. $^{13}C\{^{1}H\}$ NMR spectrum (150.92 MHz, C_6D_6, 298 K) of **L2**

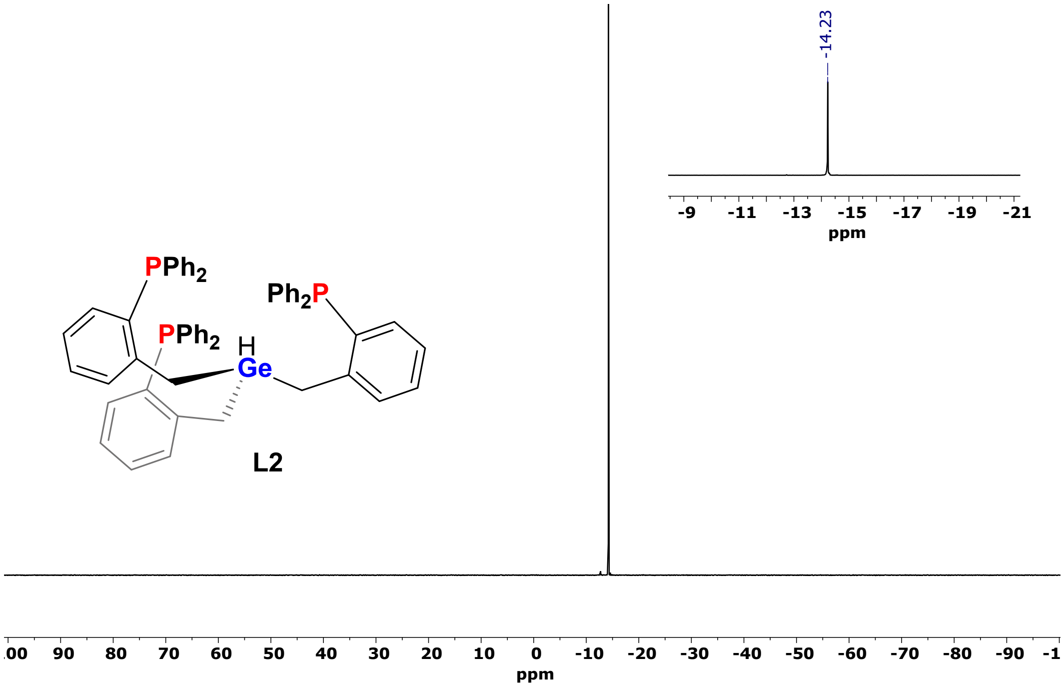

Figure S22. $^{31}P\{^{1}H\}$ NMR spectrum (202.46 MHz, C_6D_6, 298 K) of **L2**

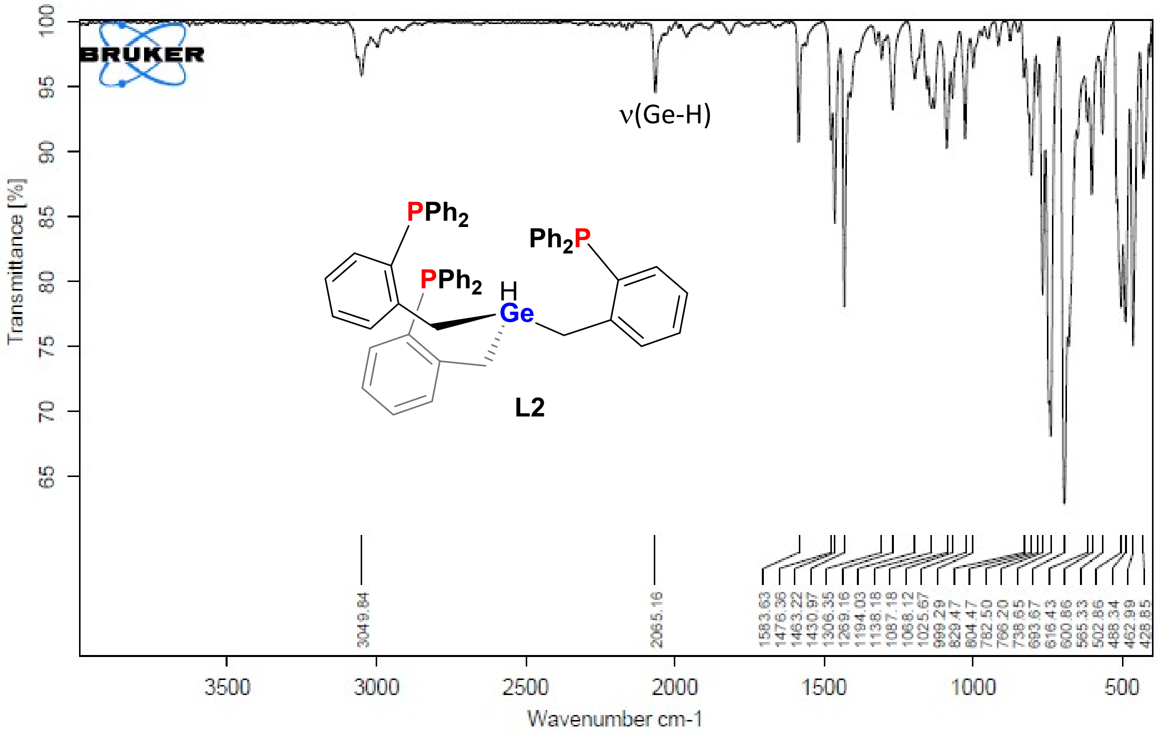

Figure S23. FT-IR (ATR) spectrum of **L2**

15.3 Spectra for **Ni-1**

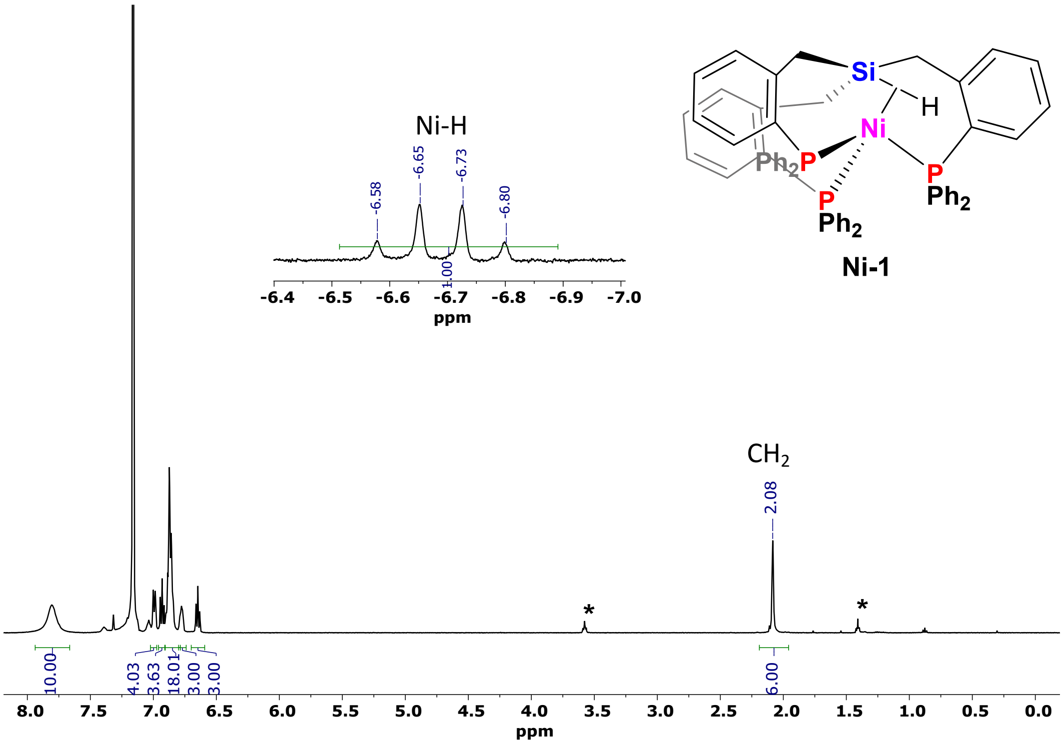

Figure S24. ^{1}H NMR spectrum (500 MHz, C_6D_6, 298 K) of **Ni-1** (*= THF)

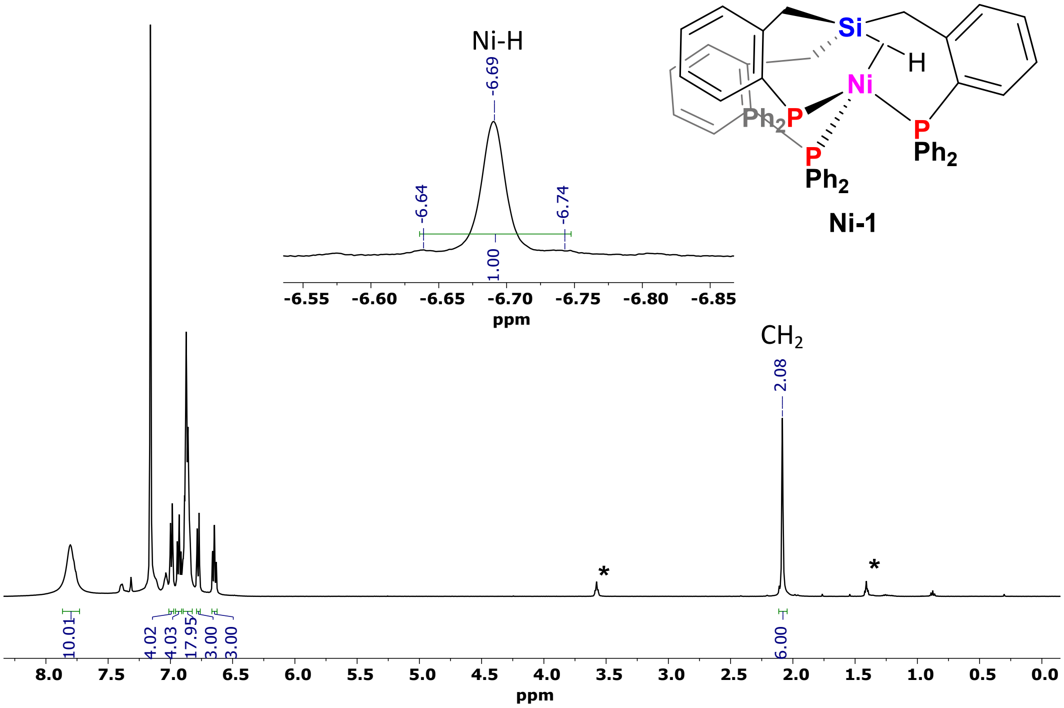

Figure S25. $^1H\{^{31}P\}$ NMR spectrum (500 MHz, C_6D_6, 298 K) of **Ni-1** (*= THF). The inset shows the satellites due to coupling of the hydride signal with ^{29}Si from which the $J_{H\text{-}Si}$ = 52.2 Hz is measured.

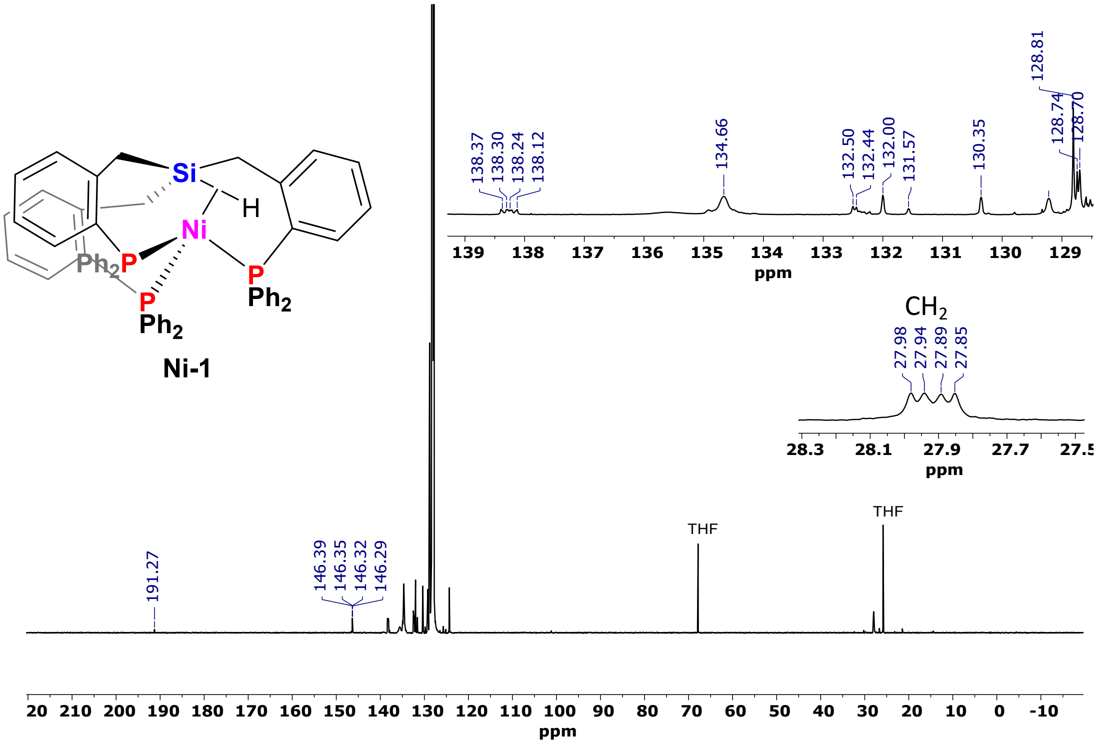

Figure S26. $^{13}C\{^1H\}$ NMR spectrum (150.9 MHz, C_6D_6, 298 K) of **Ni-1**

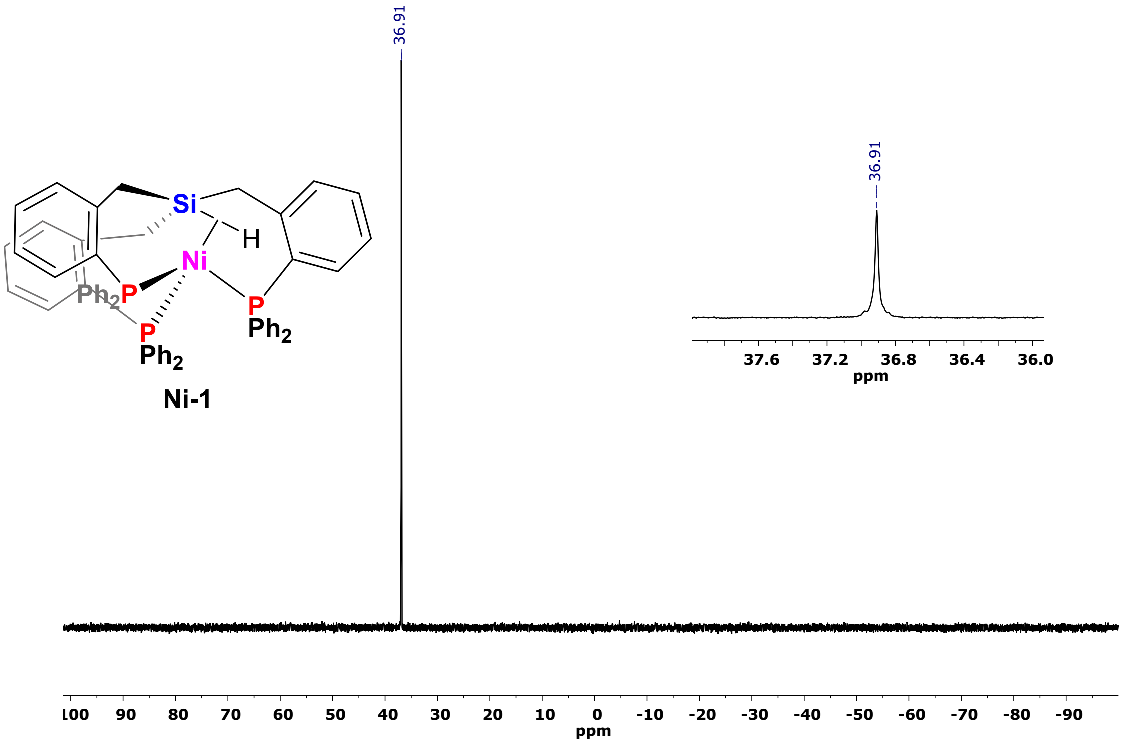

Figure S27. $^{31}P\{^{1}H\}$ NMR spectrum (202.46 MHz, C_6D_6, 298 K) of **Ni-1**

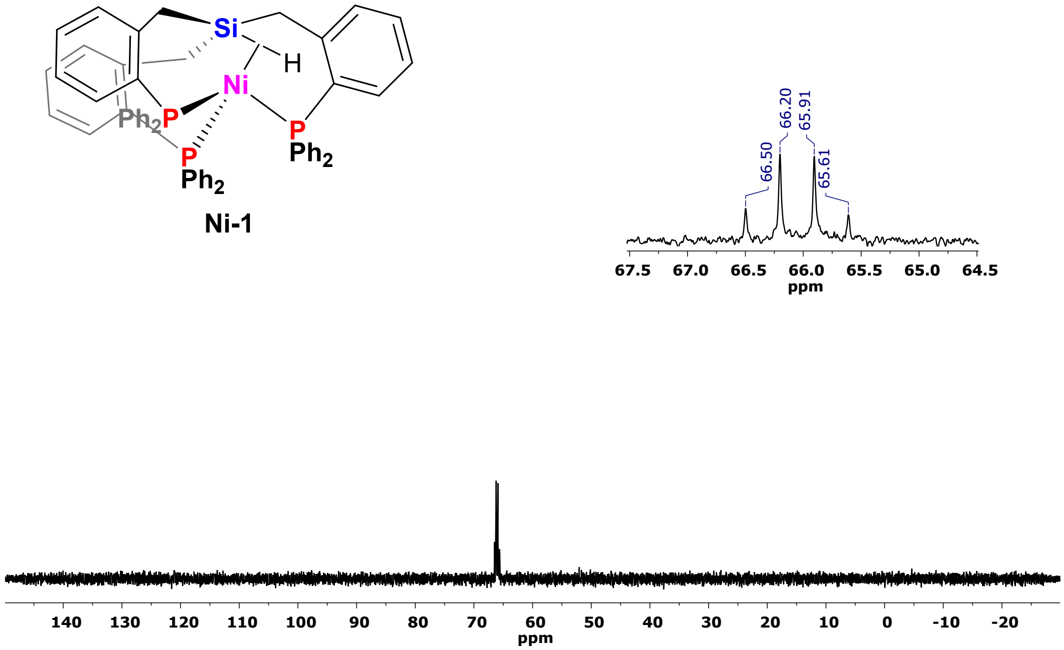

Figure S28. $^{29}Si\{^{1}H\}$ DEPT NMR spectrum (99.36 MHz, C_6D_6, 298 K) of **Ni-1**

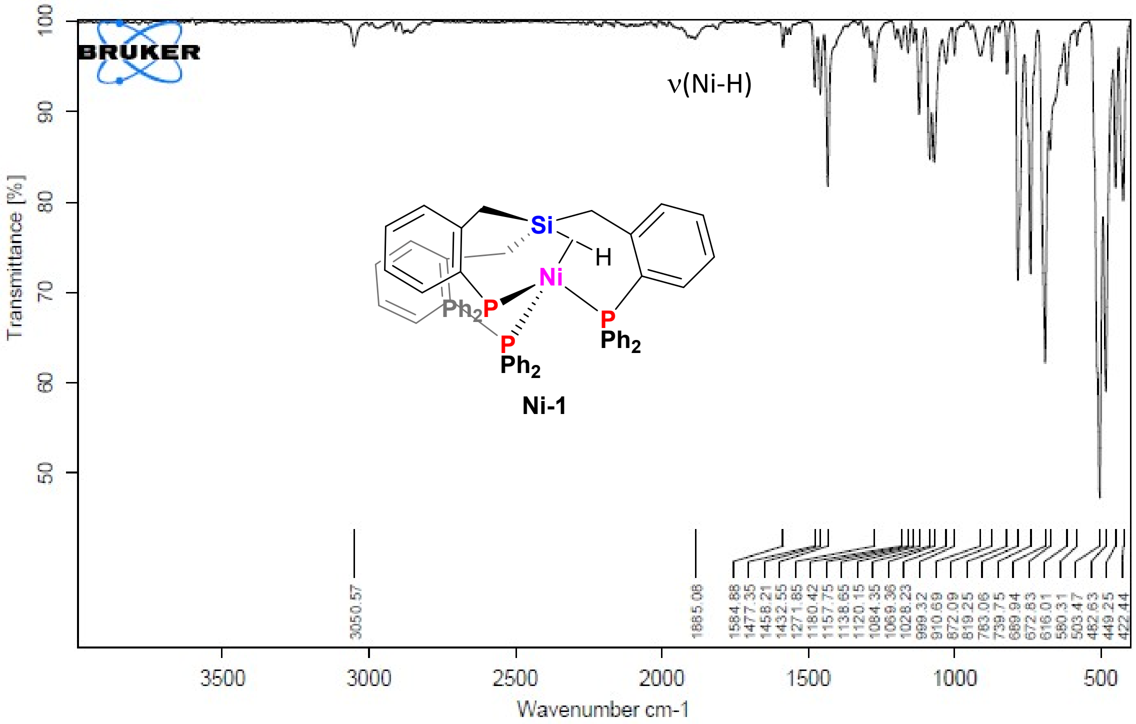

Figure S29. FT-IR (ATR) spectrum of **Ni-1**

15.4 Spectra for **Ni-2**

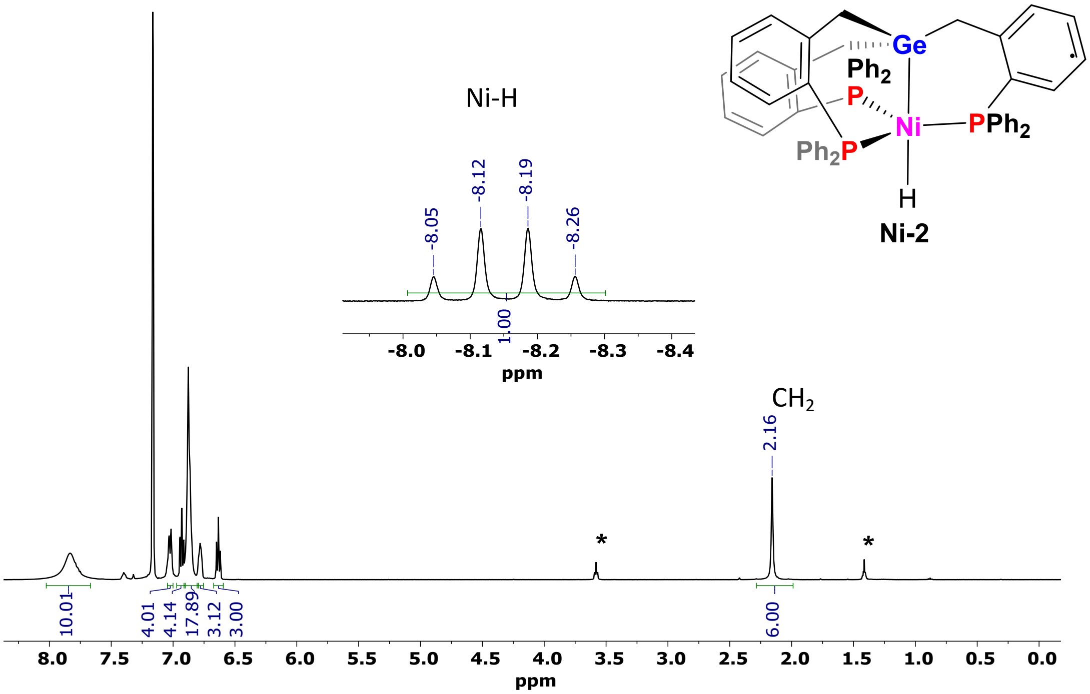

Figure S30. ^{1}H NMR spectrum (500 MHz, C_6D_6, 298 K) of **Ni-2** (*= THF)

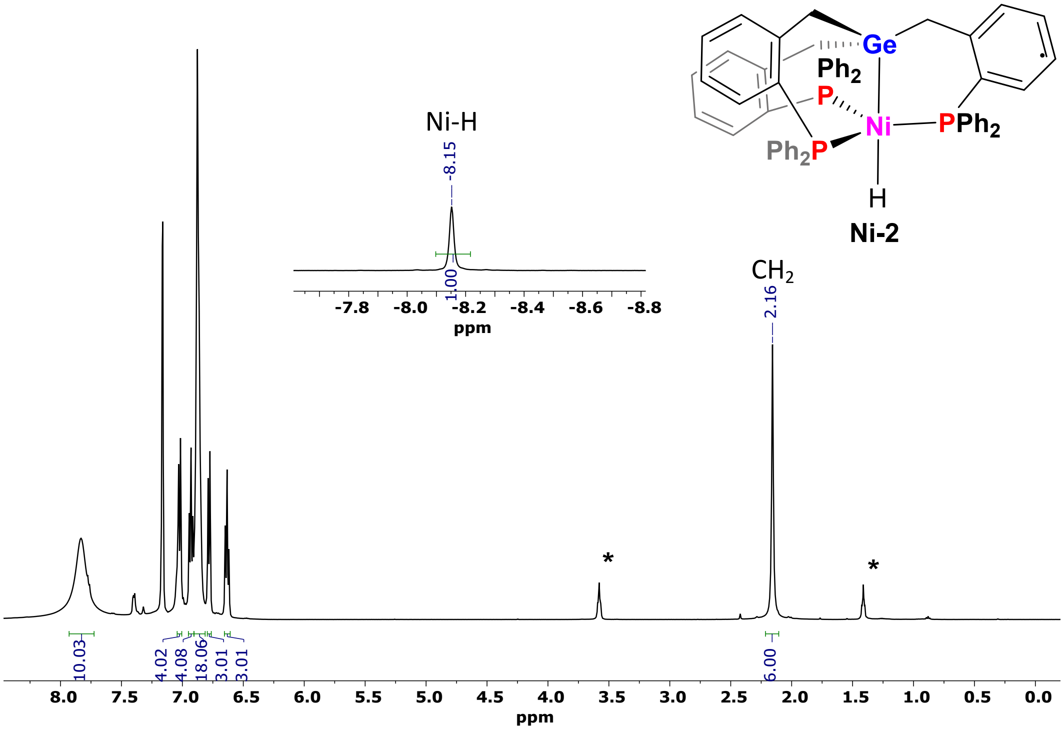

Figure S31. $^{1}H\{^{31}P\}$ NMR spectrum (500 MHz, C_6D_6, 298 K) of **Ni-2** (*= THF)

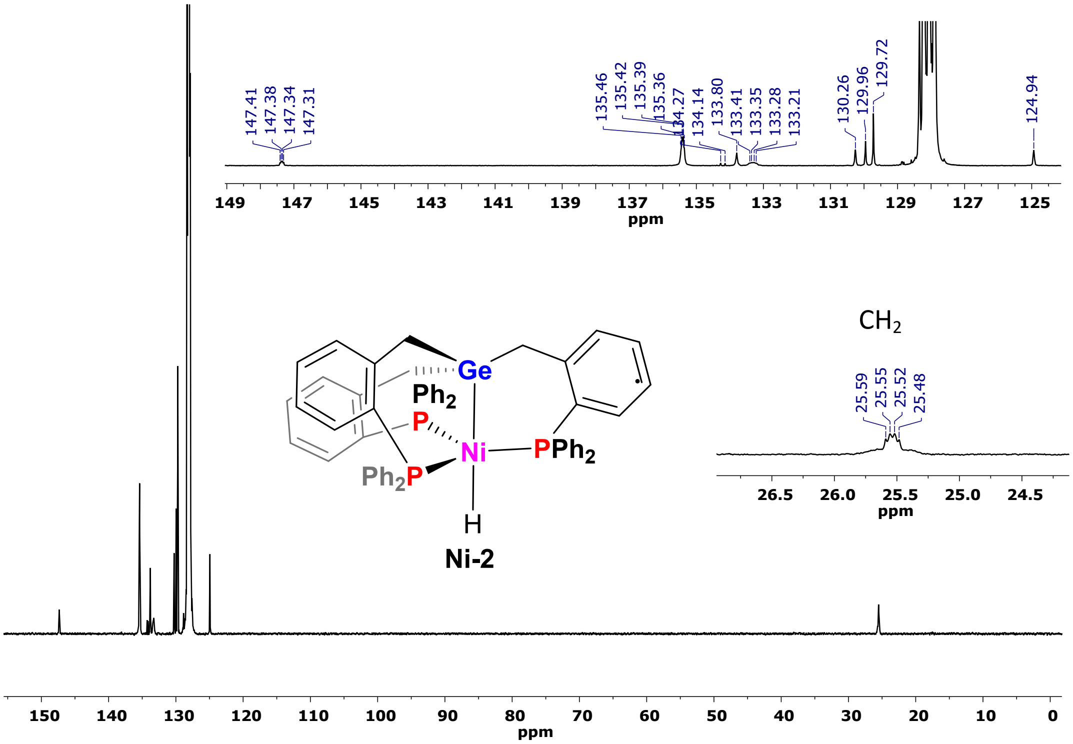

Figure S32. $^{13}C\{^{1}H\}$ NMR spectrum (150.9MHz, C_6D_6, 298 K) of **Ni-2.**

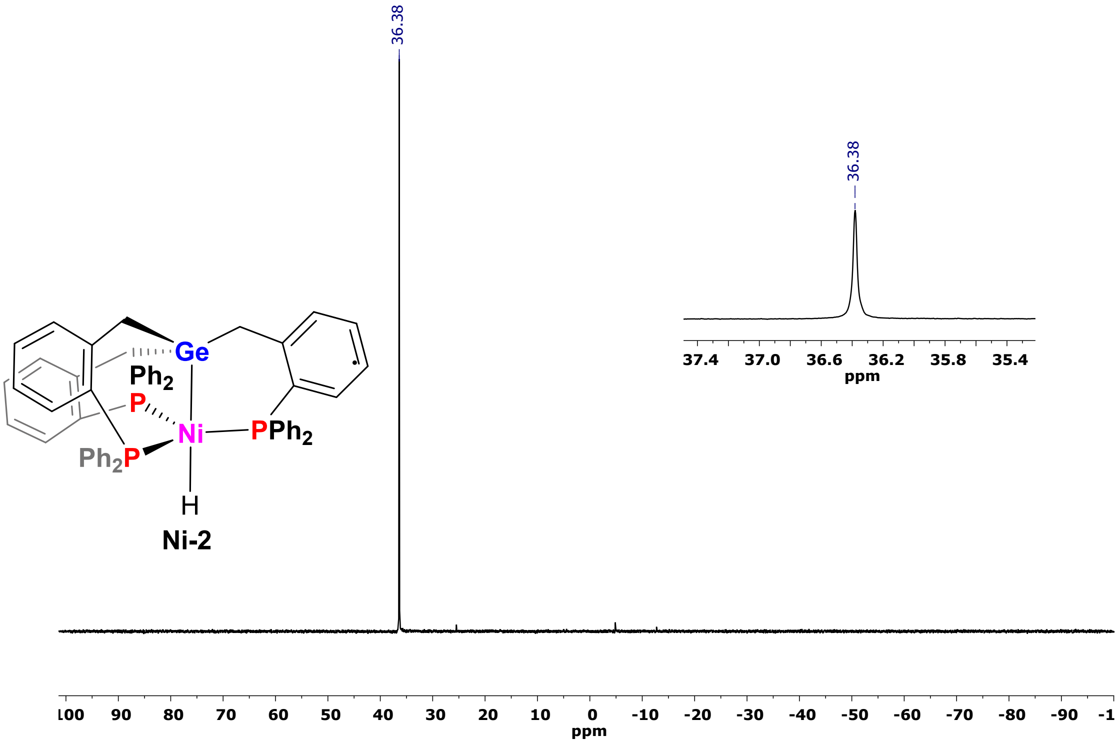

Figure S33. $^{31}P\{^{1}H\}$ NMR spectrum (202.46 MHz, C_6D_6, 298 K) of **Ni-2**

15.5 NMR spectra of aldehyde hydroboration products

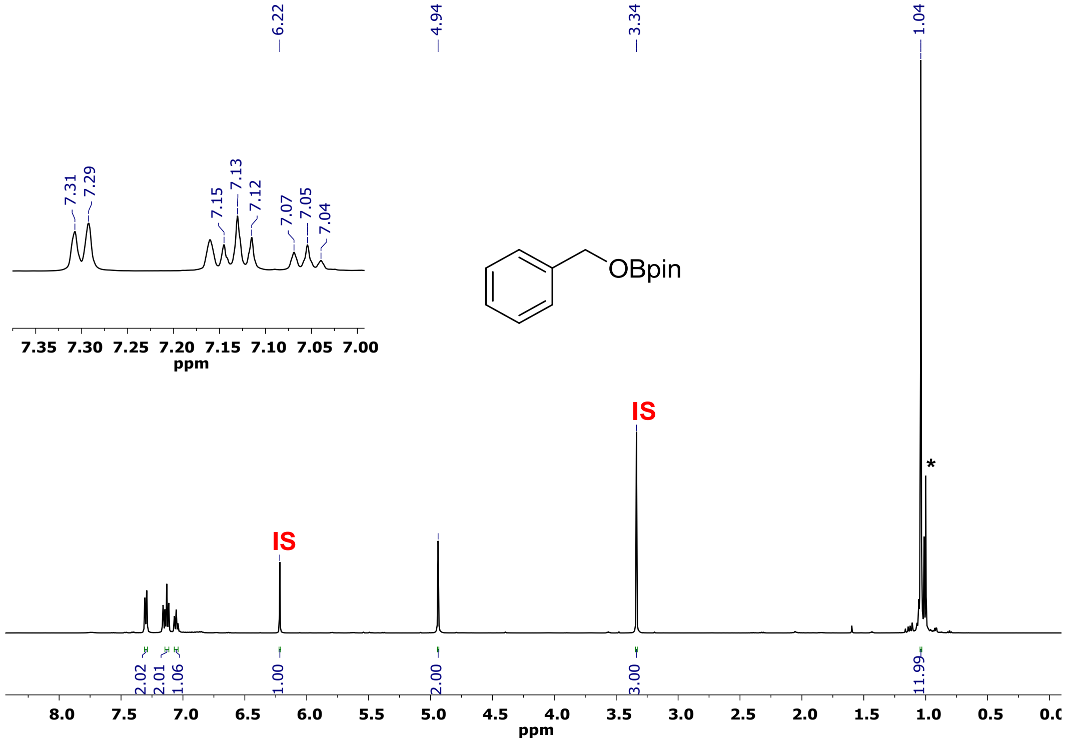

Figure S34. ^{1}H NMR spectrum of **2a** (500 MHz, C_6D_6, 298 K) (*=excess HBpin). IS= internal standard.

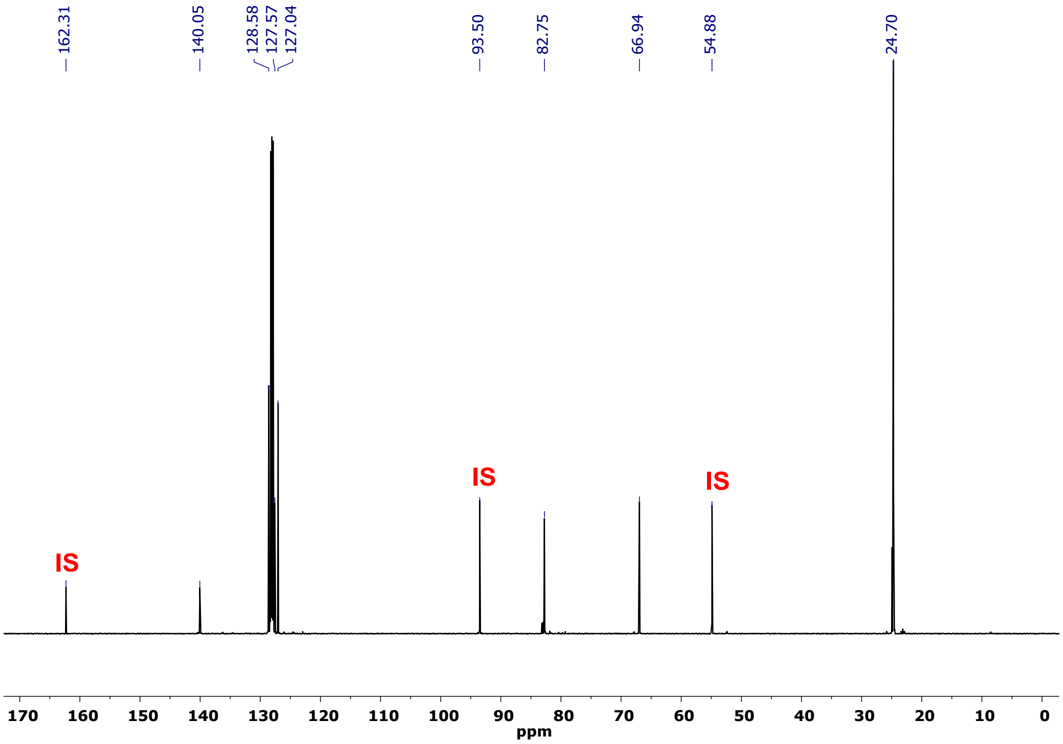

Figure S35. ^{13}C{^{1}H} NMR spectrum of **2a** (125.76 MHz, C_6D_6, 298 K). IS= internal standard.

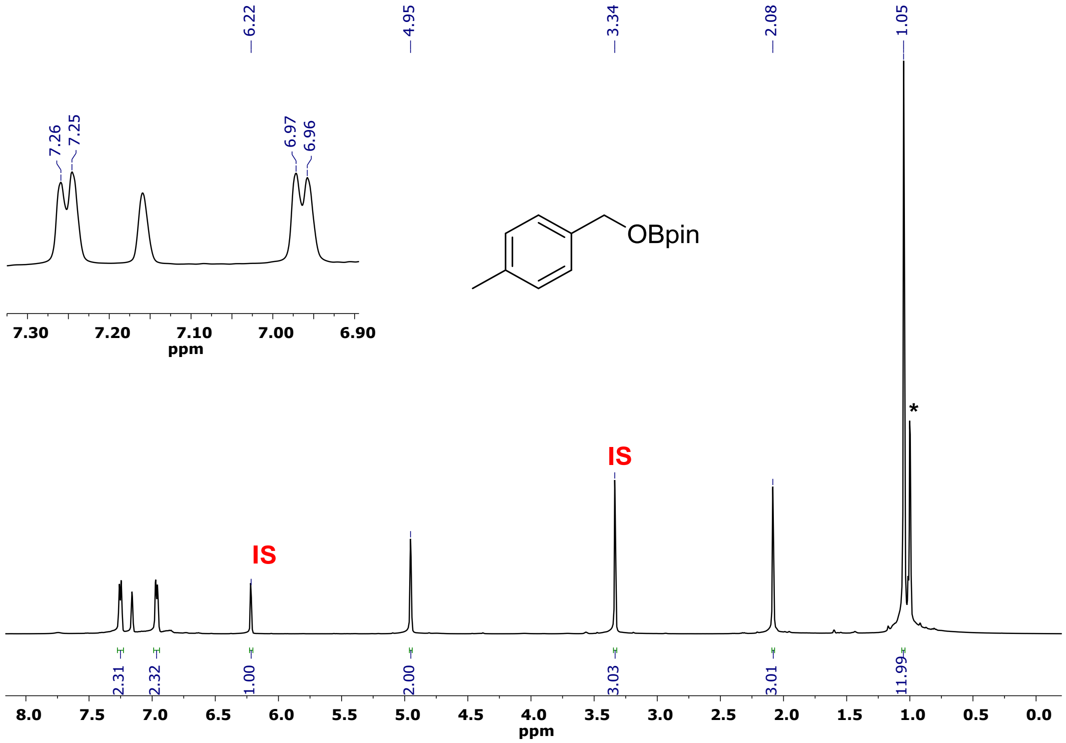

Figure S36. ^{1}H NMR spectrum of **2b** (500 MHz, C_6D_6, 298 K) (*=excess HBpin). IS= internal standard.

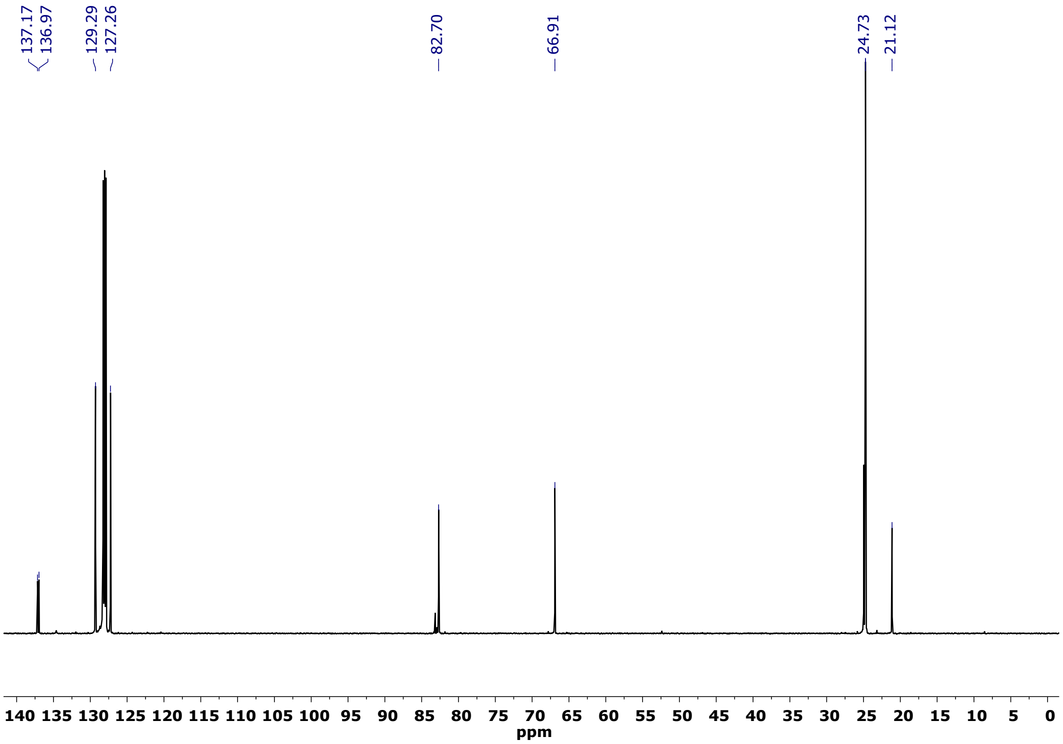

Figure S37. $^{13}C\{^{1}H\}$ NMR spectrum of **2b** (125.76 MHz, C_6D_6, 298 K)

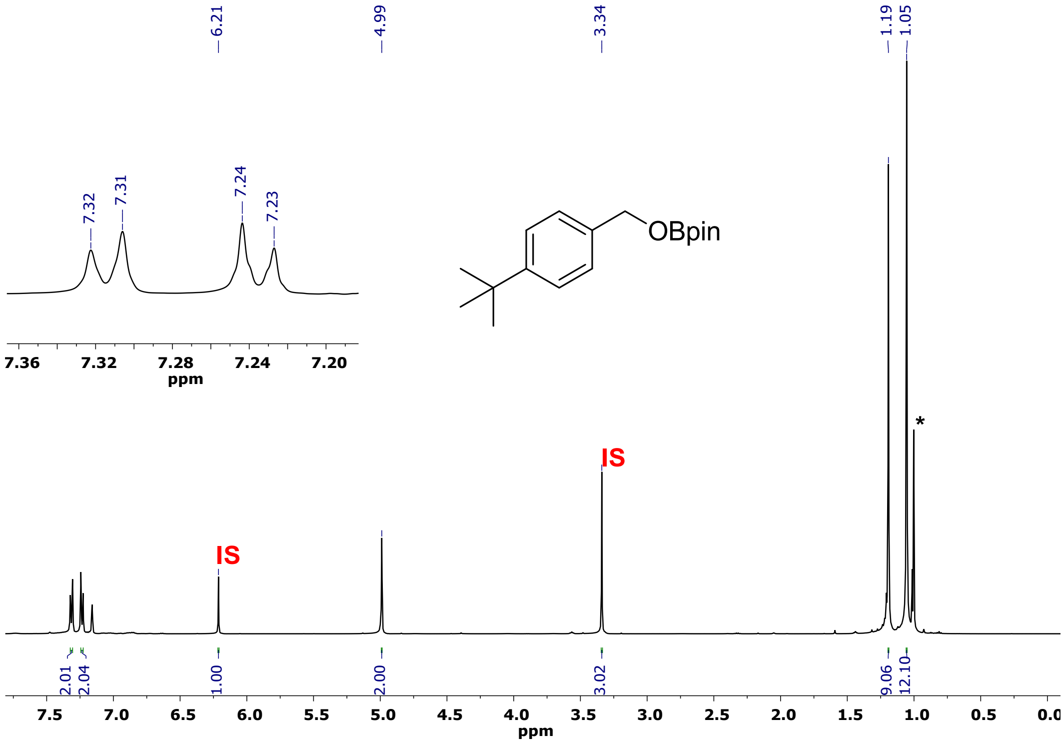

Figure S38. ^{1}H NMR spectrum of **2c** (500 MHz, C_6D_6, 298 K) (*=excess HBpin). IS= internal standard.

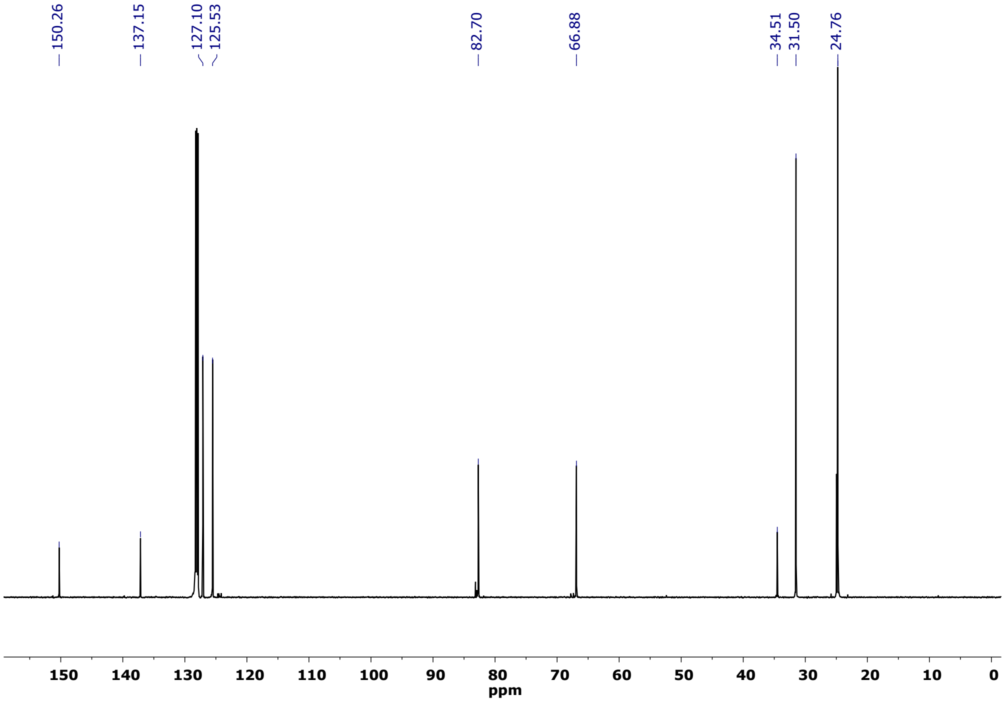

Figure S39. $^{13}C\{^1H\}$ NMR spectrum of **2c** (125.76 MHz, C_6D_6, 298 K)

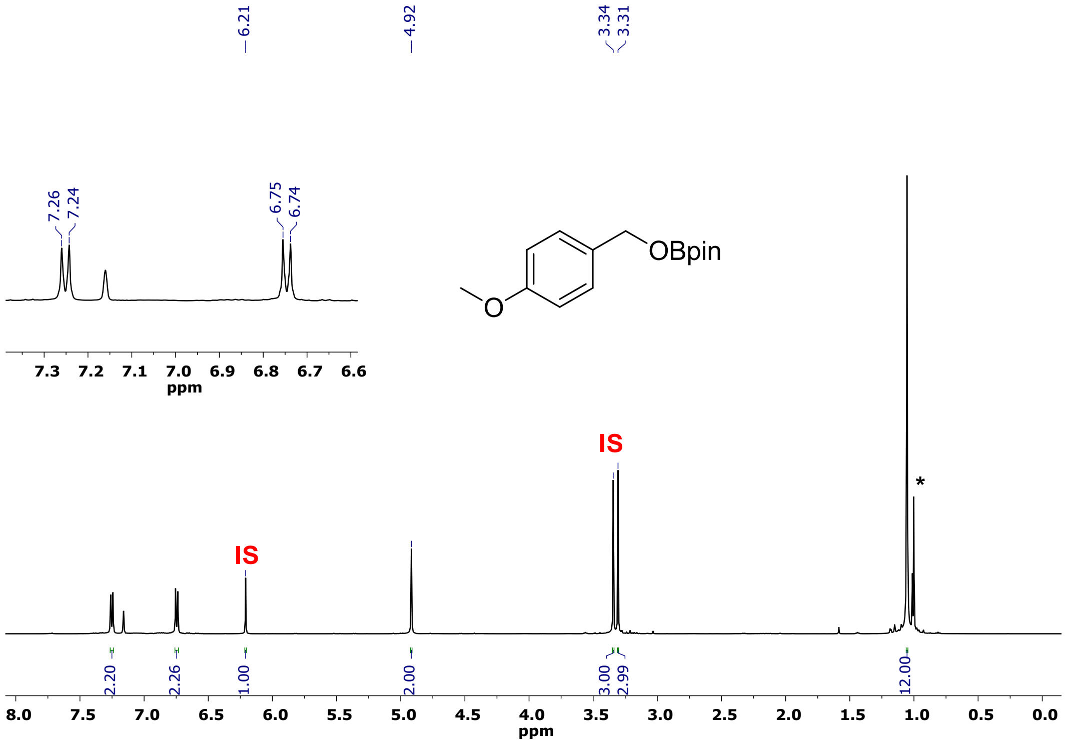

Figure S40. ^{1}H NMR spectrum of **2d** (500 MHz, C_6D_6, 298 K) (*=excess HBpin). IS= internal standard.

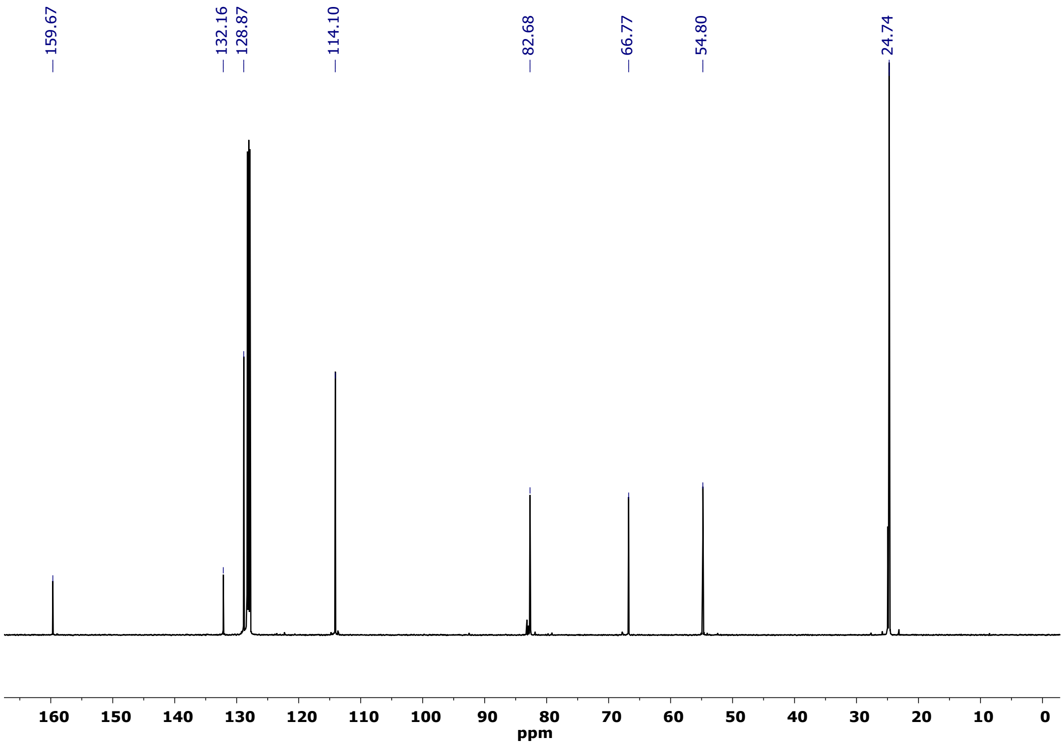

Figure S41. $^{13}C\{^1H\}$ NMR spectrum of **2d** (125.76 MHz, C_6D_6, 298 K)

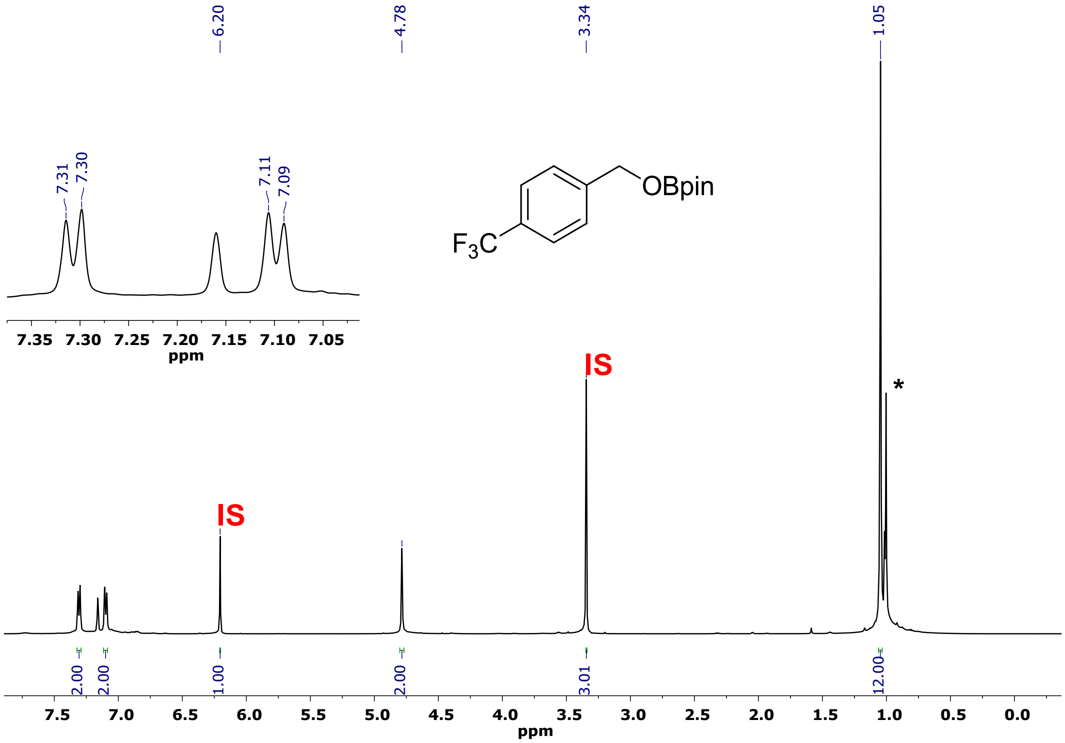

Figure S42. ^{1}H NMR spectrum of **2e** (500 MHz, C_6D_6, 298 K) (*=excess HBpin). IS= internal standard.

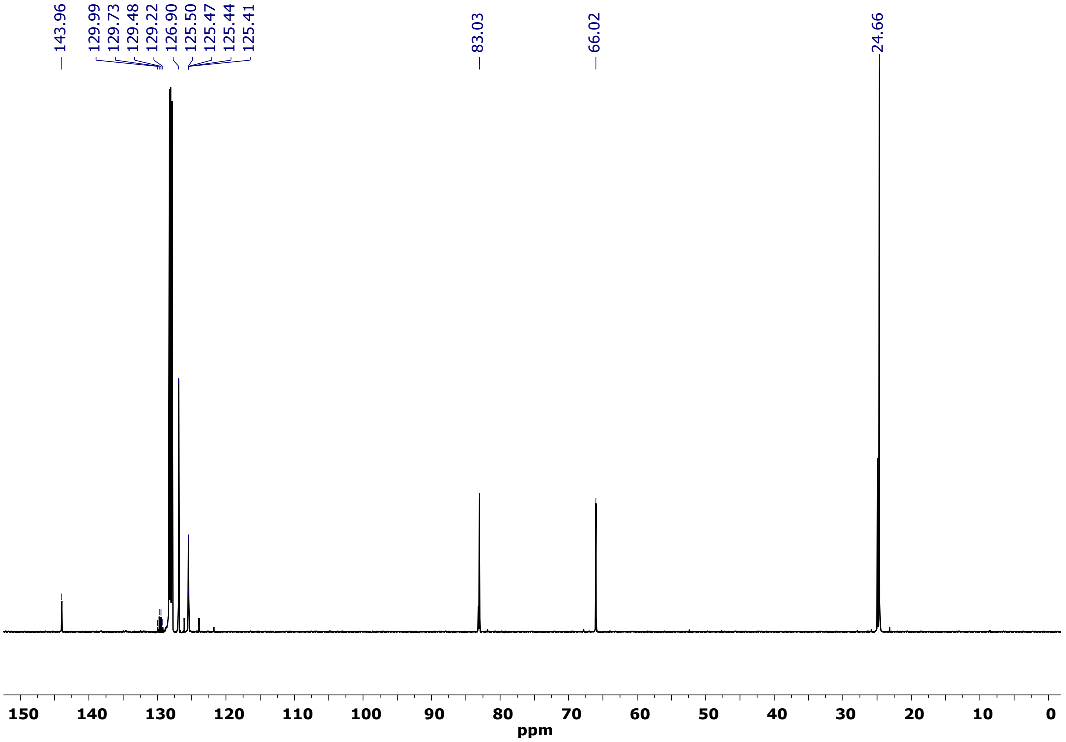

Figure S43. $^{13}C\{^1H\}$ NMR spectrum of **2e** (125.76 MHz, C_6D_6, 298 K)

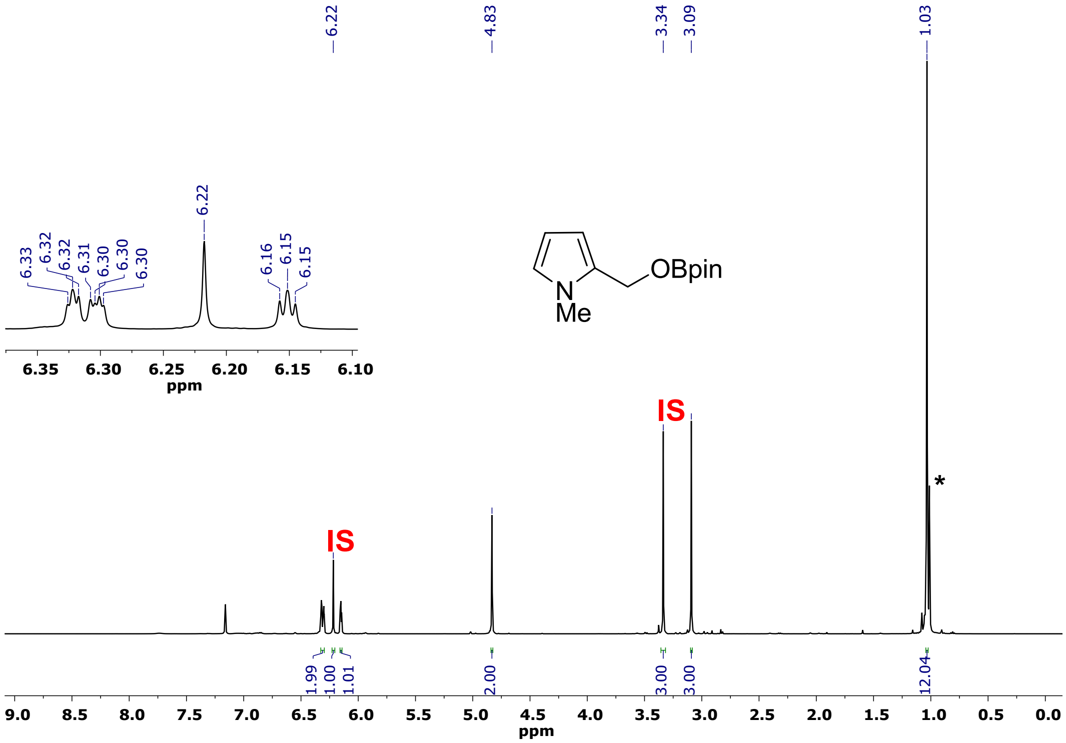

Figure S44. ^{1}H NMR spectrum of **2f** (500 MHz, C_6D_6, 298 K) (*=excess HBpin). IS= internal standard.

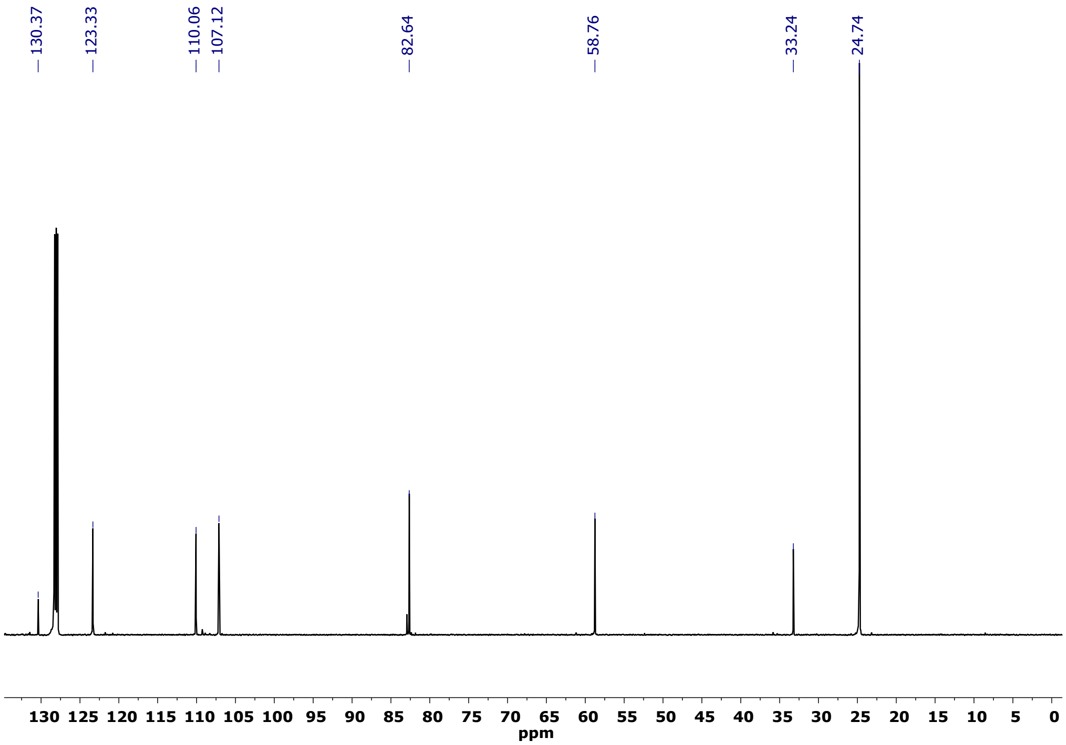

Figure S45. $^{13}C\{^1H\}$ NMR spectrum of **2f** (125.76 MHz, C_6D_6, 298 K)

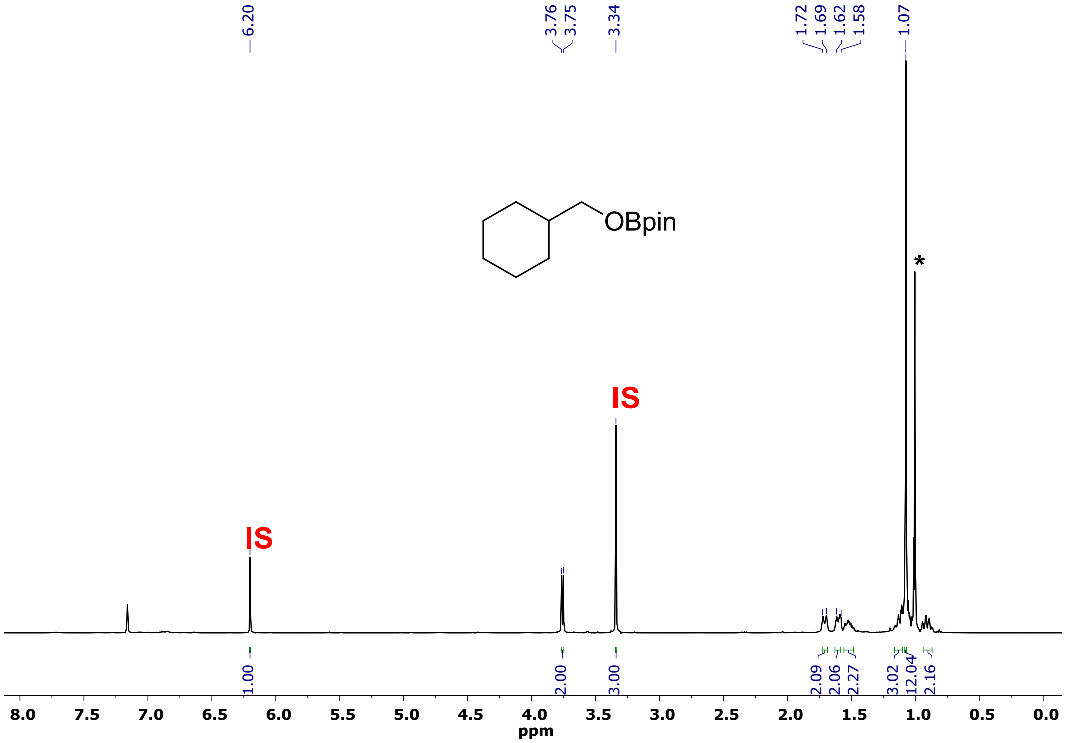

Figure S46. ^{1}H NMR spectrum of **2g** (500 MHz, C_6D_6, 298 K) (*=excess HBpin). IS= internal standard.

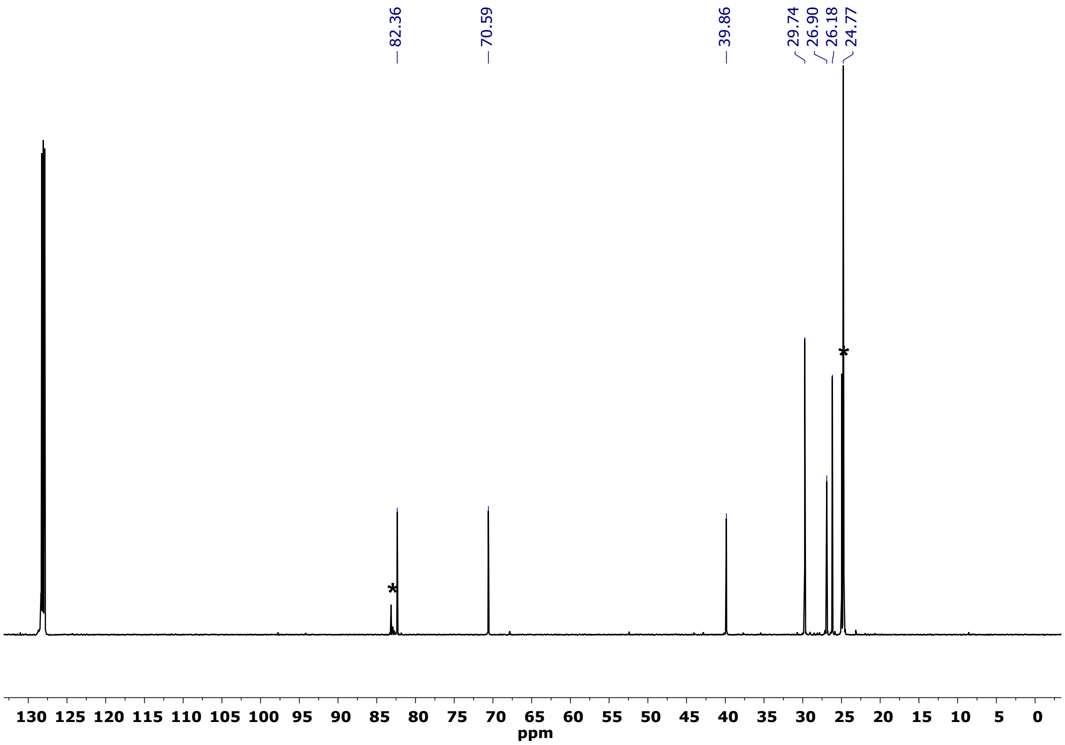

Figure S47. ^{13}C{^{1}H} NMR spectrum of **2g** (125.76 MHz, C_6D_6, 298 K) (*=excess HBpin)

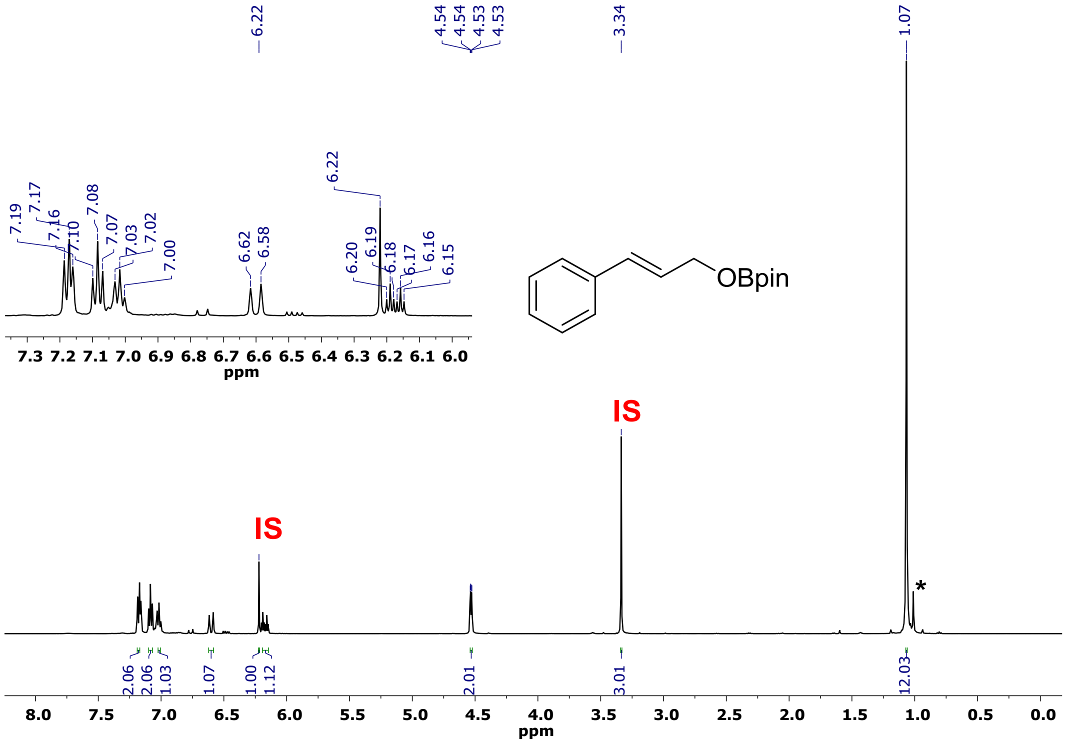

Figure S48. ^{1}H NMR spectrum of **2h** (500 MHz, C_6D_6, 298 K) (*=excess HBpin). IS= internal standard.

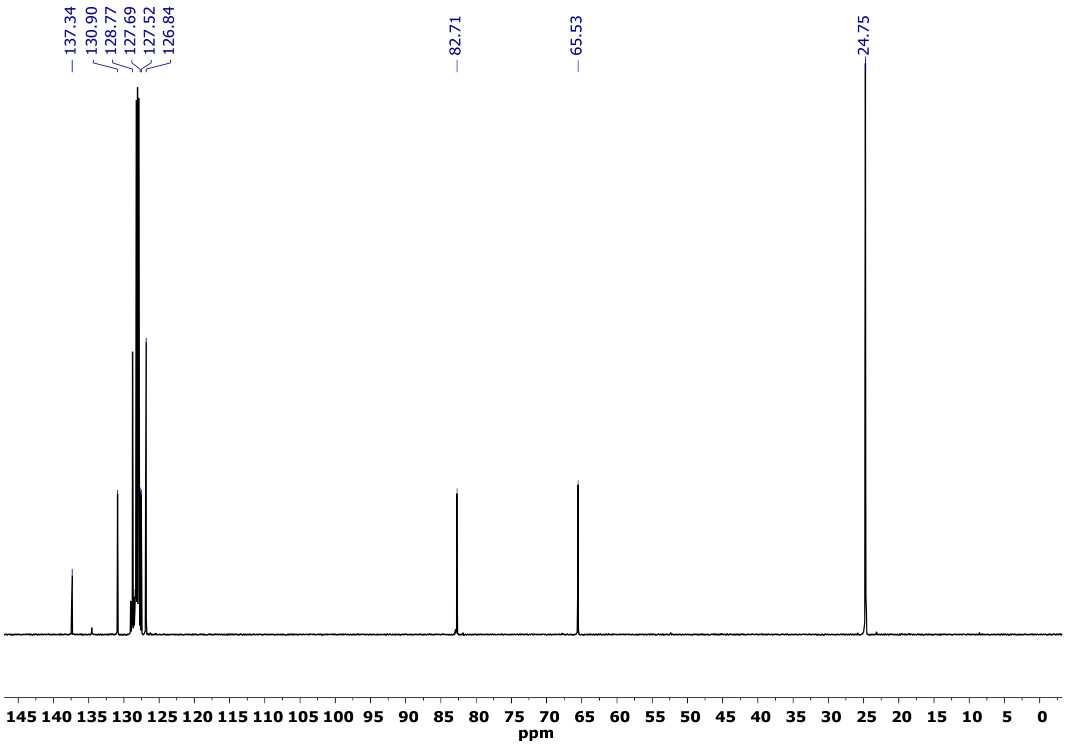

Figure S49. ^{13}C{^{1}H} NMR spectrum of **2h** (125.76 MHz, C_6D_6, 298 K)

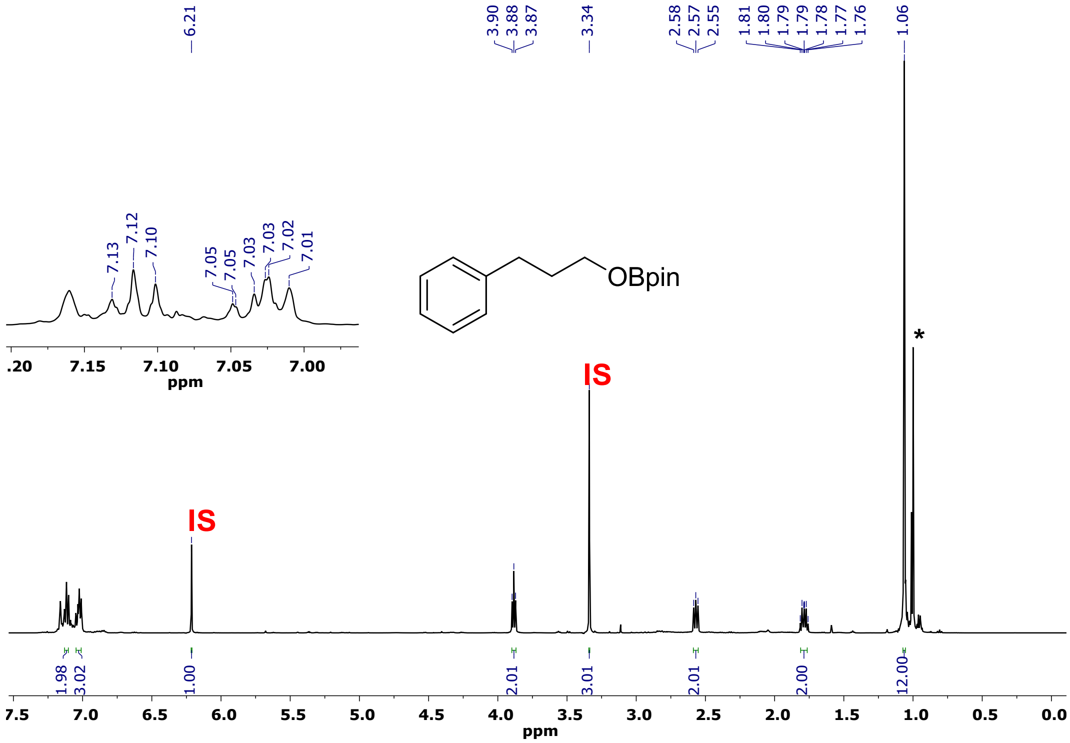

Figure S50. ^{1}H NMR spectrum of **2i** (500 MHz, C_6D_6, 298 K) (*=excess HBpin). IS= internal standard.

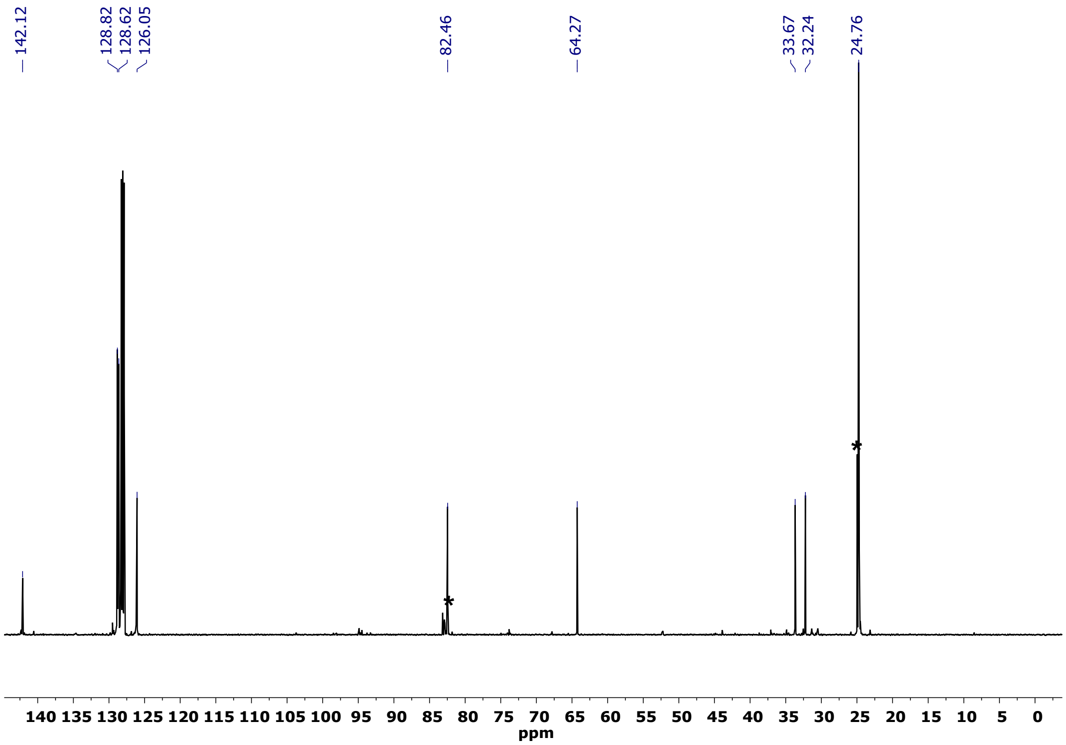

Figure S51. $^{13}C\{^1H\}$ NMR spectrum of **2i** (125.76 MHz, C_6D_6, 298 K) (*=excess HBpin)

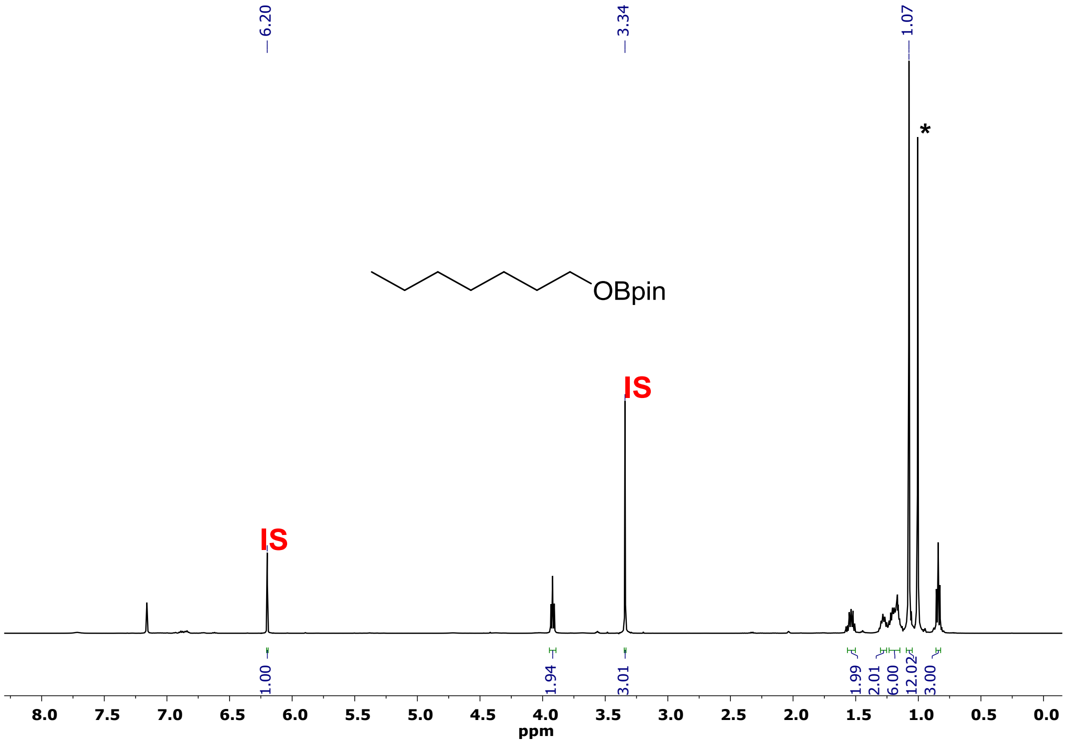

Figure S52. ^{1}H NMR spectrum of **2j** (500 MHz, C_6D_6, 298 K) (*=excess HBpin). IS= internal standard.

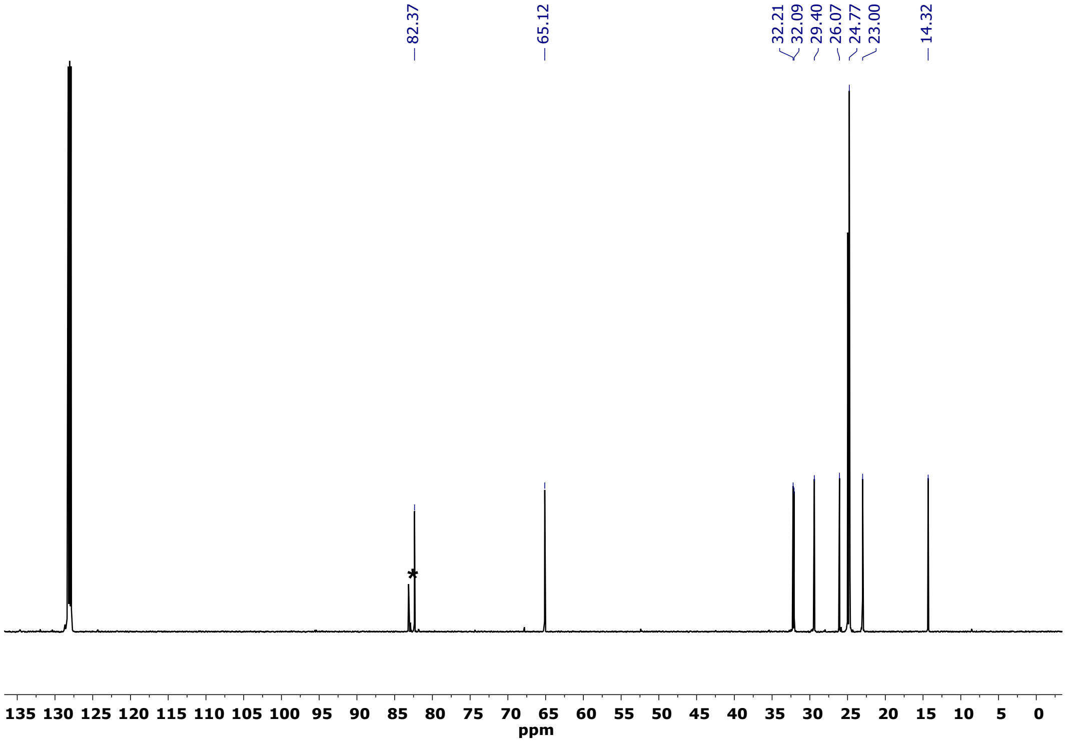

Figure S53. ^{13}C{^{1}H} NMR spectrum of **2j** (125.76 MHz, C_6D_6, 298 K) (*=excess HBpin)

15.6 NMR spectra of ketone hydroboration products

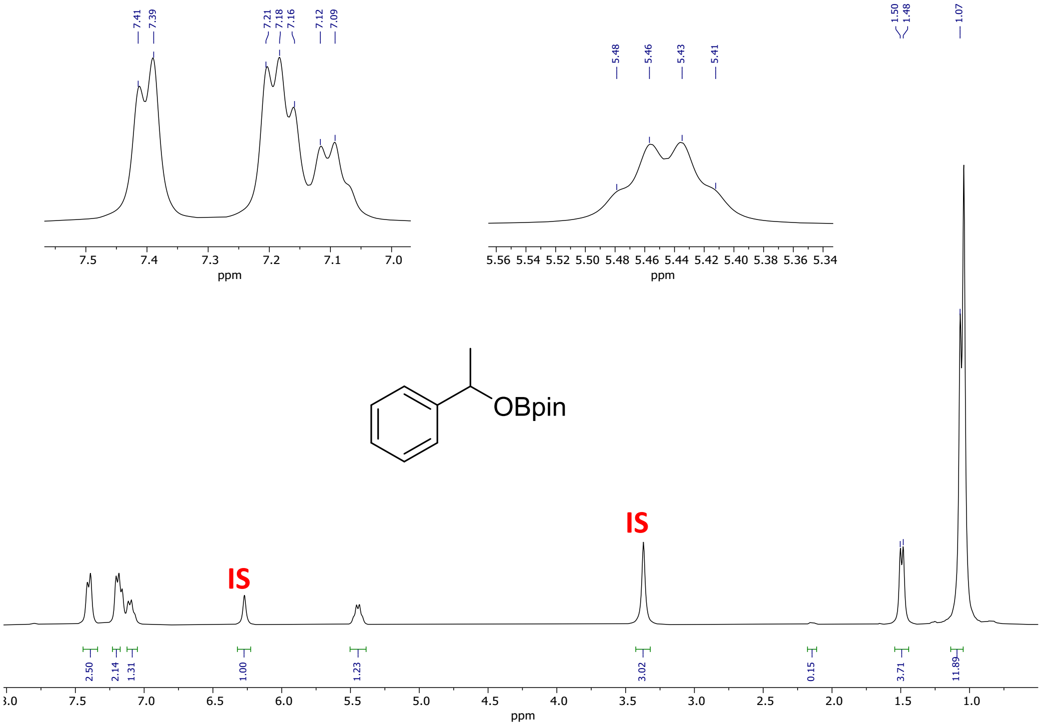

Figure S54. ^{1}H NMR spectrum of **4a** (300 MHz, C_6D_6, 298 K) (*=excess HBpin). IS= internal standard.

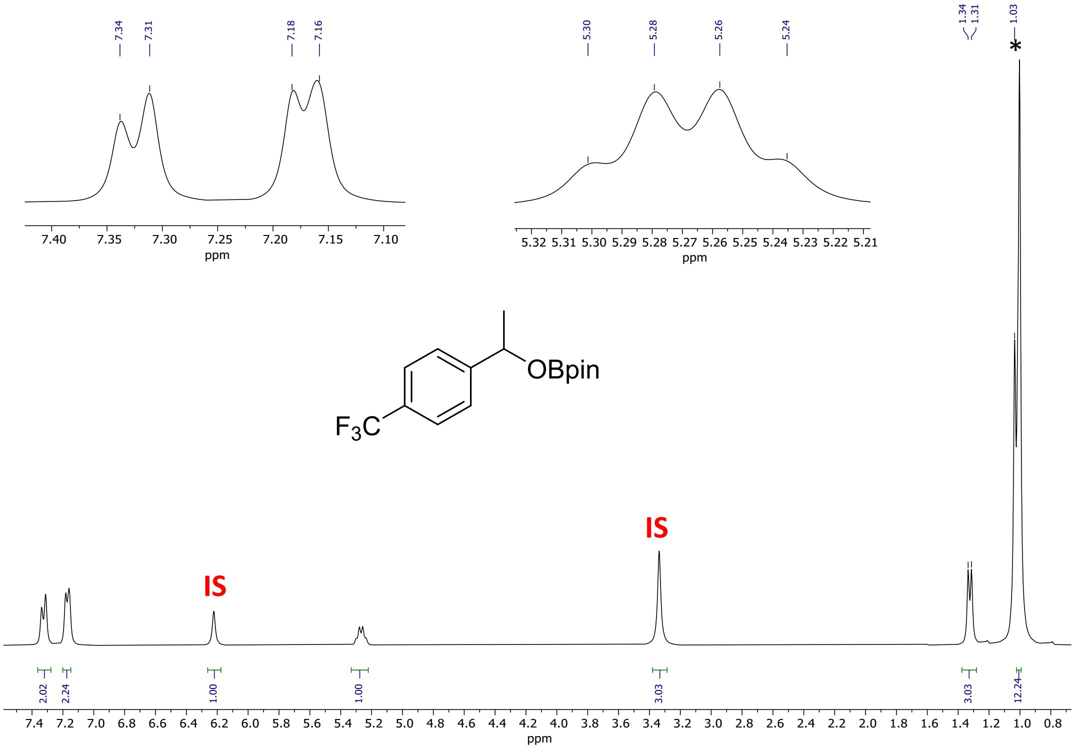

Figure S55. ^{1}H NMR spectrum of **4b** (300 MHz, C_6D_6, 298 K) (*=excess HBpin). IS= internal standard.

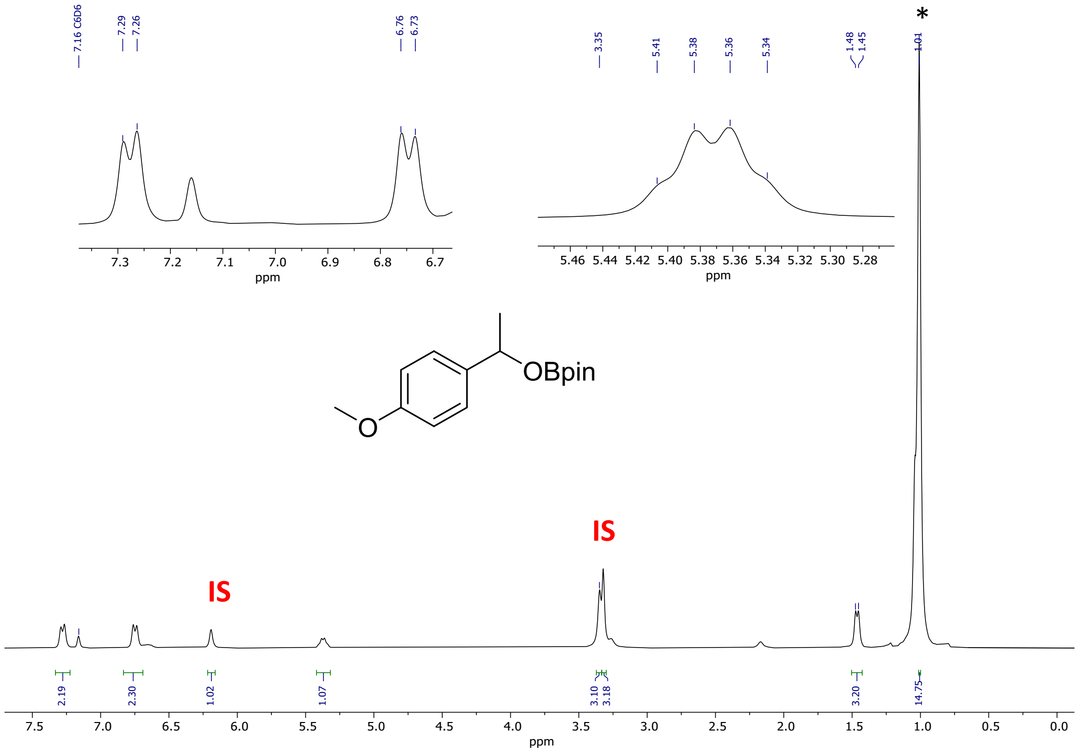

Figure S56. ^{1}H NMR spectrum of **4c** (300 MHz, C_6D_6, 298 K) (*=excess HBpin). IS= internal standard.

15.7 Summarized spectroscopic data of the boron-containing products

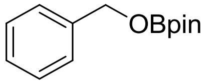

2a: ^{1}H NMR (500 MHz, C_6D_6): δ 7.30 (d, *J*= 7.5 Hz, 2H, CH_{arom}), 7.13 (t, *J*= 7.5 Hz, 2H, CH_{arom}), 7.05 (t, *J*= 7.3 Hz, 1H, CH_{arom}), 4.94 (s, 2H, CH_2), 1.04 (s, 12H, Bpin-CH_3) ppm.**^{13}C{^{1}H} NMR (125.76 MHz, C_6D_6):** 140.05, 128.58, 127.57, 127.04, 82.75, 66.94, 24.70 ppm. This compound has been previously characterized and the above data agree with the reported values.[18]

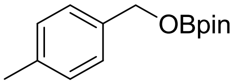

2b: ^{1}H NMR (500 MHz, C_6D_6): δ 7.25 (d, *J*= 6.7 Hz, 2H, CH_{arom}), 6.96 (d, *J*= 6.9 Hz, 2H, CH_{arom}), 4.95 (s, 2H, CH_2), 2.08 (s, 3H, CH_3), 1.05 (s, 12H, Bpin-CH_3) ppm.**^{13}C{^{1}H} NMR (125.76 MHz, C_6D_6):** 137.15, 136.97, 129.29, 127.26, 82.70, 66.91, 24.73, 21.12 ppm. This compound has been previously characterized, and the above data agree with the reported values.[18]

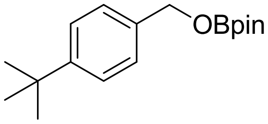

2c: ^{1}H NMR (500 MHz, C_6D_6): δ 7.31 (d, *J*= 8.2 Hz, 2H, CH_{arom}), 7.24 (t, *J*= 8.3 Hz, 2H, CH_{arom}), 4.99 (s, 2H, CH_2), 1.19 (s, 9H, CH_3), 1.05 (s, 12H, Bpin-CH_3) ppm.**^{13}C{^{1}H} NMR (125.76 MHz, C_6D_6):** 150.26, 137.15, 127.10, 125.53, 82.70, 66.88, 34.51, 31.50, 24.76 ppm. This compound has been previously characterized, and the above data agree with the reported values.[19]

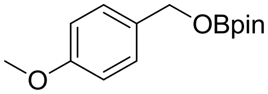

2d: ^{1}H NMR (500 MHz, C_6D_6): δ 7.25 (d, *J*= 8.5 Hz, 2H, CH_{arom}), 6.75 (d, *J*= 8.6 Hz, 2H, CH_{arom}), 4.92 (s, 2H, CH_2), 3.31 (s, 3H, -OCH_3), 1.05 (s, 12H, Bpin-CH_3) ppm.**^{13}C{^{1}H} NMR (125.76 MHz, C_6D_6):** 159.67, 132.16, 128.87, 114.10, 82.68, 66.77, 54.80, 24.74 ppm. This compound has been previously characterized and the above data agree with the reported values.[18]

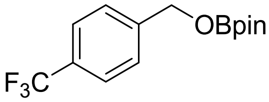

2e: ^{1}H NMR (500 MHz, C_6D_6): δ 7.31 (d, *J*= 8.0 Hz, 2H, CH_{arom}), 7.10 (t, *J*= 7.9 Hz, 2H, CH_{arom}), 4.78 (s, 2H, CH_2), 1.05 (s, 12H, Bpin-CH_3) ppm.**^{13}C{^{1}H} NMR (125.76 MHz, C_6D_6):** 140.05, 129.61 (q, $^3J_{CF}$= 32.2 Hz), 126.90, 125.46 (q, $^4J_{CF}$= 3.7 Hz,), 83.03, 66.02, 24.66 ppm. This compound has been previously characterized and the above data agree with the reported values.[20]

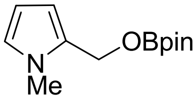

2f: ^{1}H NMR (500 MHz, C_6D_6): δ 6.33-6.31 (m, 1H, CH_{arom}), 6.30 (dd, *J*= 3.4, 1.7 Hz, 1H, CH_{arom}), 6.17-6.14 (m, 1H, CH_{arom}), 4.83 (s, 2H, CH_2), 3.09 (s, 3H, CH_3), 1.03 (s, 12H, Bpin-CH_3) ppm.**^{13}C{^{1}H} NMR (125.76 MHz, C_6D_6):** 130.37, 123.33, 110.06, 107.12, 82.64, 58.76, 33.24, 24.74 ppm. HRMS (ESI) Calcd. for $C_{12}H_{20}BNO_3$ [M+Na]$^+$ 260.1428; found 260.1442

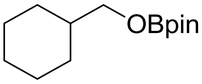

2g: ^{1}H NMR (500 MHz, C_6D_6): δ 3.76 (d, *J*= 6.4 Hz, 2H, CH_2), 1.71 (d, *J*= 15.3 Hz, 2H, CH_2), 1.60 (d, *J*= 17.8 Hz, 2H, CH_2), 1.55-1.45 (m, 2H, Bpin-CH_3), 1.17-1.10 (m, 3H, (CH_3 +CH)), 1.07 (s, 12H, Bpin-CH_3), 0.95-0.87 (m, 2H, CH_2) ppm.**^{13}C{^{1}H} NMR (125.76 MHz, C_6D_6):** 82.36, 70.59, 39.86, 29.74, 26.90, 26.18, 24.77 ppm. This compound has been previously characterized and the above data agree with the reported values.[18]

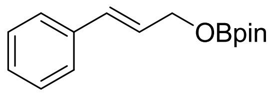

2h: ^{1}H NMR (500 MHz, C_6D_6): δ 7.21-715 (m, 2H, CH_{arom}), 7.08 (t, *J*= 7.5 Hz, 2H, CH_{arom}), 7.02 (t, *J*= 7.3 Hz, 1H, CH_{arom}), 6.60 (d, *J*= 15.9 Hz, 1H, CH), 6.17 (dt, *J*= 15.9, 5.3 Hz, 1H, CH), 4.53 (dd, *J*= 5.3, 1.4 Hz, 2H, CH_2), 1.04 (s, 12H, Bpin-CH_3) ppm.**^{13}C{^{1}H} NMR (125.76 MHz, C_6D_6):** 137.34, 130.90, 128.77 , 127.69, 127.52, 126.84, 82.71, 65.53, 24.75 ppm. This compound has been previously characterized and the above data agree with the reported values.[21]

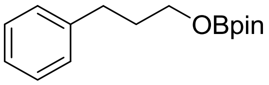

2i: ^{1}H NMR (500 MHz, C_6D_6): δ 7.12 (t, *J*= 7.4 Hz, 2H, CH_{arom}), 7.05-7.00 (m, 3H, CH_{arom}), 3.88 (t, *J*= 6.3Hz, 2H, CH_2), 2.67-2.49 (m, 2H, CH_2), 1.87-1.72 (m, 2H, CH_2), 1.06 (s, 12H, Bpin-CH_3) ppm.**^{13}C{^{1}H} NMR (125.76 MHz, C_6D_6):** 142.12, 128.82 128.62, 126.05, 82.46, 64.27, 32.67, 32.24, 24.76 ppm. This compound has been previously characterized, and the above data agree with the reported values.[19]

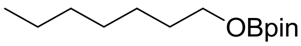

2j: ^{1}H NMR (500 MHz, C_6D_6): δ 3.92 (t, *J*= 6.6 Hz, 2H, CH_2), 1.59-1.45 (m, 2H, CH_2), 1.34-1.25 (m, 2H, CH_2), 1.22-1.11 (m, 6H, CH_2), 1.07 (s, 12H, Bpin-CH_3), 0.84 (t, *J*= 7.0 Hz, 3H, CH_3) ppm.**^{13}C{^{1}H} NMR (125.76 MHz, C_6D_6):** 82.37, 65.12, 32.21 (d, *J*= 16.1 Hz), 32.09, 26.07, 24.77 ppm. This compound has been previously characterized and the above data agree with the reported values.[21]

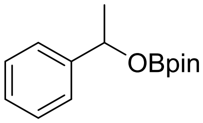

4a: ^{1}H NMR (300 MHz, C_6D_6): δ 7.40 (d, *J*= 7.3 Hz, 2H, CH_{arom}), 7.24-7.15 (m, 2H, CH_{arom}), 7.10 (d, J= 7.3 Hz, 1H, C_{arom}), 5.45 (q, *J*= 7.3 Hz, 1H, CH), 1.49 (d, *J*= 6.5 Hz, 3H, CH_3), 1.05 (s, 12H, Bpin-CH_3) ppm. This compound has been previously characterized and the above data agree with the reported values.[21]

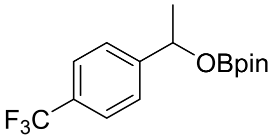

4b: ^{1}H NMR (300 MHz, C_6D_6): δ 7.32 (d, *J*= 7.8 Hz, 2H, CH_{arom}), 7.17 (d, *J*= 6.8 Hz, 2H, CH_{arom}), 5.27 (q, *J*= 6.6 Hz, 1H, CH), 1.32 (d, *J*= 6.6 Hz, 3H, CH_3), 1.00 (s, 12H, Bpin-CH_3) ppm. This compound has been previously characterized, and the above data agree with the reported values.[21]

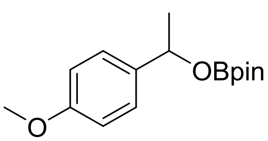

4c: ^{1}H NMR (300 MHz, C_6D_6): δ 7.28 (d, *J*= 8.0 Hz, 2H, CH_{arom}), 6.75 (d, *J*= 8.0 Hz, 2H, CH_{arom}), 5.37 (q, *J*= 6.7 Hz, 1H, CH), 3.35 (s, 3H, -OCH_3), 1.46 (d, *J*= 6.5 Hz, 3H, CH_3), 1.01 (s, 12H, Bpin-CH_3) ppm. This compound has been previously characterized, and the above data agree with the reported values.[21]

16. X-ray diffraction analysis data for the complexes

16.1 Crystal Structure of **Ni-1** (CCDC deposition 2247469)

Crystal Structure Report for (Ni-1).

A yellow prism single crystal of $C_{20.5}H_{17.5}Si_{0.33}Ni_{0.33}P$, approximate dimensions (0.079 x 0.095 x 0.160) mm^3, was selected for the X-ray crystallographic analysis and mounted on a cryoloop using an oil cryoprotectant. The X-ray intensity data was measured at low temperature (T = 100K), using a three circles goniometer geometry with a fixed Chie angle at = 54.74 deg Bruker AXS D8 Venture, equipped with a Photon 100 CMOS active pixel sensor detector. A monochromatized Copper X-ray radiation (λ = 1.54178 Å) was selected for the measurement. All frames were integrated with the aid of the Bruker SAINT software[22,23] using a narrow-frame algorithm. The integration of the data using a cubic unit cell yielded a total of 239227 reflections to a maximum θ angle of 74.78° (0.80 Å resolution), of which 3542 were independent (average redundancy 67.540, completeness = 99.6%, R_{int} =20.16%, R_{sig} = 2.47%) and 3087 (87.15%) were greater than 2σ (F^2). The final cell constants of a = 21.7616(2) Å, b = 21.7616(2) Å, c = 21.7616(2) Å, volume = 10305.6(3) Å^3, are based upon the refinement of the XYZ-centroids of 1181 reflections above 20 σ(I). The calculated minimum and maximum transmission coefficients (based on crystal size) are 0.7470 and 0.8620. The structure was solved in a cubic unit cell; non-centrosymmetric Space group: P -4 3 n, with Z = 24 for the formula unit, $C_{20.5}H_{17.5}Si_{0.33}Ni_{0.33}P$. The asymmetric unit was built on 1/3 of the molecule. Using the Bruker SHELXT Software Package[24], refinement of the structure was carried out by least squares procedures on weighted F^2 values using the SHELXTL-2018/3[25] included in the APEX4 v2022, 10-0, AXS Bruker program.[26] Hydrogen atoms were localized on difference Fourier maps but then introduced in the refinement as fixed contributors in idealized geometry with an isotropic thermal parameters fixed at 20 % higher than those carbons atoms they were connected. A molecule of solvent: Benzene C_6H_6 was found in the unit-cell statistically distributed around two-fold axes and was anisotropically refined with an occupancy factor fixed at 0.25. Restraints were used on interatomic lengths, angles, and constraints on ADP's parameters. The Flack's parameter value was found to be 0.08(6) and refined as a racemic twin.[27] Finally, during the structure analysis voids: 149 Å^3 were found in the crystal structure, which could not be related to any solvent molecules. The final anisotropic full-matrix least-squares refinement on F^2 with 208 variables converged at R1 = 5.19%, for the observed data and wR2 = 14.32% for all data. The goodness-of-fit: GOF was 1.113. The largest peak in the final difference electron density synthesis was 0.559 e$^-$/Å^3 and the largest hole was -0.272 e$^-$/Å^3 with an RMS deviation of 0.051 e$^-$/Å^3. Based on the final model, the calculated density was 1.252 g/cm^3 and F (000), 4068 e$^-$. Graphics were performed using softwares: Mercury V.4.2.0: (https://www.ccdc.cam.ac.uk/) and POV-Ray v 3.7: (The Persistence of Vision Raytracer, high quality, Free Software tool).

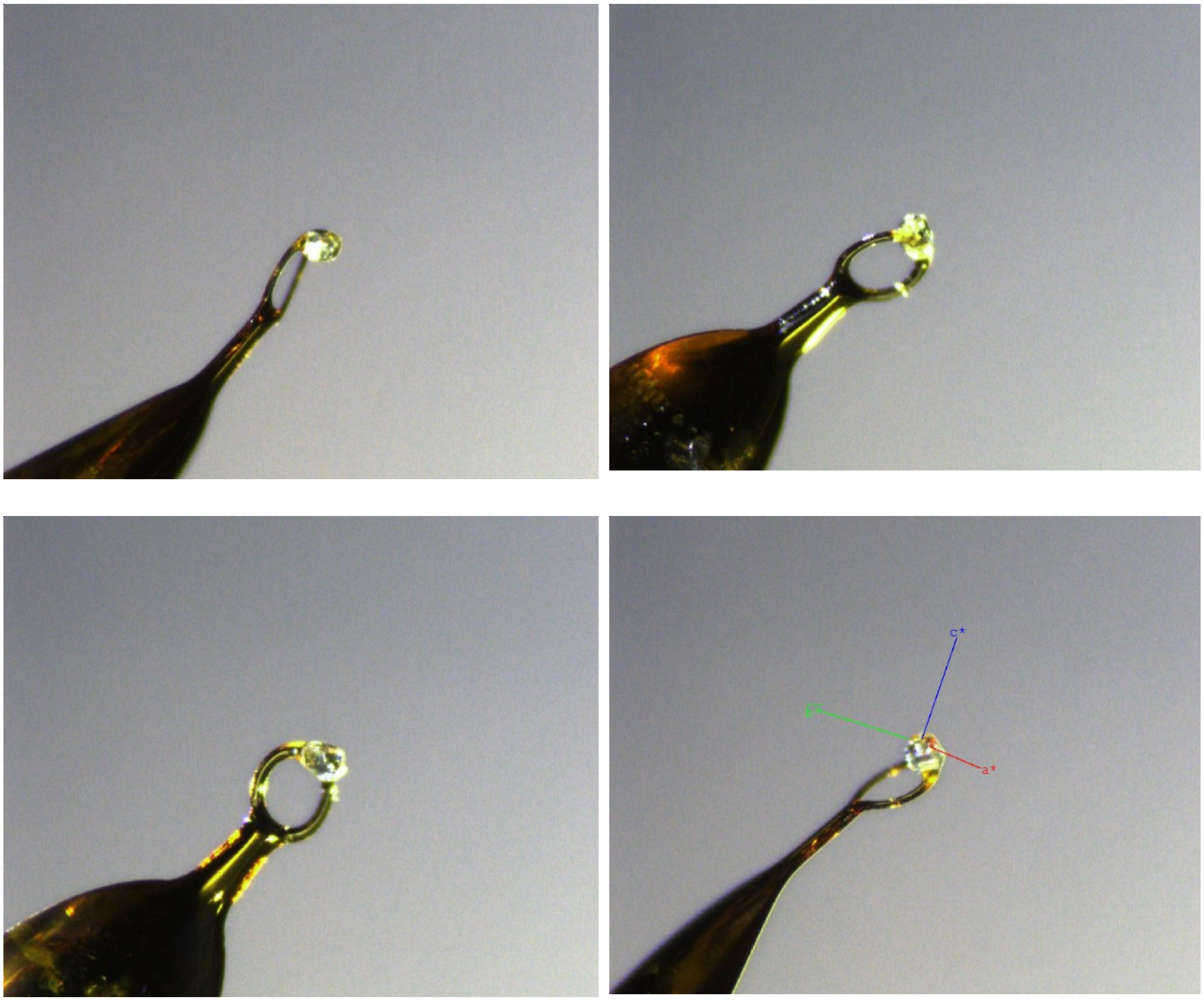

Crystal views:

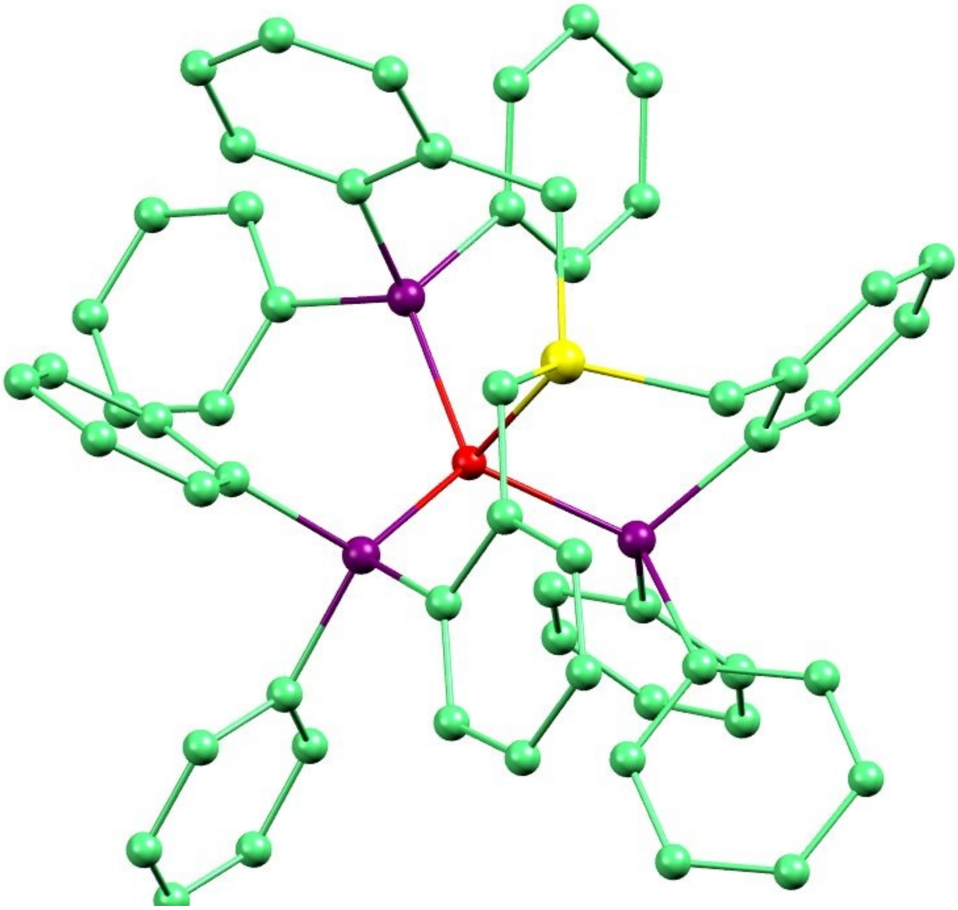

View of the complex: Ni-1.

Table S3. Sample and crystal data for (Ni1).

Identification code	C_VM003 (Ni1)	
Chemical formula	$C_{20.5}H_{17.5}Ni_{0.33}PSi_{0.33}$	
Formula weight	323.75 g/mol	
Temperature	100(2) K	
Wavelength	1.54178 Å	
Crystal size	(0.079 x 0.095 x 0.160) mm^3	
Crystal system	cubic	
Space group	P -4 3 n	
Unit cell dimensions	a = 21.7616(2) Å	α = 90°
	b = 21.7616(2) Å	β = 90°

	c = 21.7616(2) Å	γ = 90°
Volume	10305.6(3) $Å^3$	
Z	24	
Density (calculated)	1.252 g/cm^3	
Absorption coefficient	1.936 mm^{-1}	
F(000)	4068	

Table S4. Data collection and structure refinement for (Ni1).

Theta range for data collection	4.06 to 74.78°	
Index ranges	-27<=h<=27, -27<=k<=25, -27<=l<=27	
Reflections collected	239227	
Independent reflections	3542 [R(int) = 0.2016]	
Max. and min. transmission	0.8620 and 0.7470	
Structure solution technique	direct methods	
Structure solution program	SHELXT	
Refinement method	Full-matrix least-squares on F^2	
Refinement program	SHELXTL-2018/3	
Function minimized	$\Sigma\ w(F_o^2 - F_c^2)^2$	
Data / restraints / parameters	3542 / 15 / 208	
Goodness-of-fit on F^2	1.113	
Final R indices	3087 data; $I>2\sigma(I)$	R1 = 0.0519, wR2 = 0.1353
	all data	R1 = 0.0619, wR2 = 0.1432
Weighting scheme	$w=1/[\sigma^2(F_o^2)+(0.0887P)^2+1.1679P]$ where $P=(F_o^2+2F_c^2)/3$	
Absolute structure parameter	0.08(6)	
Extinction coefficient	0.0002(1)	
Largest diff. peak and hole	0.559 and -0.272 $eÅ^{-3}$	
R.M.S. deviation from mean	0.051 $eÅ^{-3}$	

Table S5. Atomic coordinates and equivalent isotropic atomic displacement parameters ($Å^2$) for (Ni1).

U(eq) is defined as one third of the trace of the orthogonalized U_{ij} tensor.

	x/a	**y/b**	**z/c**	**U(eq)**
Ni1	0.68285(3)	0.31715(3)	0.31715(3)	0.0423(3)
P1	0.65516(6)	0.37129(6)	0.23756(6)	0.0430(3)
Si1	0.74244(6)	0.25756(6)	0.25756(6)	0.0573(6)
C1	0.7357(3)	0.2744(3)	0.1722(3)	0.0739(19)
C2	0.7515(3)	0.3396(3)	0.1590(3)	0.0716(16)
C3	0.8022(4)	0.3542(5)	0.1220(4)	0.108(3)
C4	0.8195(5)	0.4128(6)	0.1104(5)	0.142(4)
C5	0.7866(5)	0.4614(5)	0.1334(4)	0.114(3)
C6	0.7353(3)	0.4494(3)	0.1708(3)	0.0760(18)
C7	0.7182(2)	0.3890(3)	0.1837(3)	0.0551(12)
C8	0.5953(2)	0.3412(2)	0.1854(2)	0.0517(11)
C9	0.5985(4)	0.3475(4)	0.1214(3)	0.086(2)
C10	0.5504(5)	0.3289(5)	0.0849(4)	0.110(3)
C11	0.4975(4)	0.3058(4)	0.1109(4)	0.098(3)
C12	0.4939(3)	0.2992(3)	0.1729(4)	0.088(2)
C13	0.5428(3)	0.3172(3)	0.2102(3)	0.0659(15)
C14	0.6208(2)	0.4486(2)	0.2513(2)	0.0462(11)
C15	0.5934(3)	0.4814(3)	0.2052(3)	0.0615(14)
C16	0.5679(3)	0.5382(3)	0.2156(3)	0.0690(16)
C17	0.5700(3)	0.5630(3)	0.2724(4)	0.081(2)
C18	0.5969(4)	0.5314(3)	0.3176(4)	0.097(3)
C19	0.6216(3)	0.4740(3)	0.3089(3)	0.0678(16)
C1S	0.5146(14)	0.4668(10)	0.0579(12)	0.107(5)
C2S	0.5627(13)	0.4842(11)	0.0186(14)	0.107(5)
C3S	0.5525(15)	0.5072(12)	0.9617(13)	0.107(5)
C4S	0.4941(16)	0.5145(12)	0.9394(11)	0.107(5)
C5S	0.4443(14)	0.4977(14)	0.9768(13)	0.107(5)

	x/a	y/b	z/c	U(eq)
C6S	0.4547(13)	0.4741(12)	0.0356(13)	0.107(5)

Table S6. Bond lengths (Å) for (Ni1).

Ni1-P1	2.1796(13)	Ni1-P1#2	2.1797(13)
Ni1-P1#1	2.1797(13)	Ni1-Si1	2.246(2)
P1-C7	1.845(5)	P1-C8	1.847(5)
P1-C14	1.864(5)	Si1-C1#2	1.899(7)
Si1-C1#1	1.899(7)	Si1-C1	1.899(7)
C1-C2	1.487(10)	C1-H1A	0.990000
C1-H1B	0.990000	C2-C7	1.403(8)
C2-C3	1.404(9)	C3-C4	1.353(14)
C3-H3	0.950000	C4-C5	1.371(15)
C4-H4	0.950000	C5-C6	1.405(10)
C5-H5	0.950000	C6-C7	1.396(9)
C6-H6	0.950000	C8-C13	1.368(8)
C8-C9	1.401(8)	C9-C10	1.377(10)
C9-H9	0.950000	C10-C11	1.378(13)
C10-H10	0.950000	C11-C12	1.359(12)
C11-H11	0.950000	C12-C13	1.393(9)
C12-H12	0.950000	C13-H13	0.950000
C14-C15	1.368(8)	C14-C19	1.371(7)
C15-C16	1.374(9)	C15-H15	0.950000
C16-C17	1.350(10)	C16-H16	0.950000
C17-C18	1.335(10)	C17-H17	0.950000
C18-C19	1.371(8)	C18-H18	0.950000
C19-H19	0.950000	C1S-C6S	1.400(11)
C1S-C2S	1.403(11)	C1S-H1S	0.950000
C2S-C3S	1.354(15)	C2S-H2S	0.950000
C3S-C4S	1.370(17)	C3S-H3S	0.950000
C4S-C5S	1.405(12)	C4S-H4S	0.950000

C5S-C6S	1.397(11)	C5S-H5S	0.950000
C6S-H6S	0.950000		

Symmetry transformations used to generate equivalent atoms:

#1 -y+1, z, -x+1

#2 -z+1, -x+1, y

Table S7. Bond angles (°) for C_VM003 (Ni1).

P1-Ni1-P1#2	119.985(2)	P1-Ni1-P1#1	119.982(2)
P1#2-Ni1-P1#1	119.983(2)	P1-Ni1-Si1	90.74(4)
P1#2-Ni1-Si1	90.74(4)	P1#1-Ni1-Si1	90.74(4)
C7-P1-C8	102.0(2)	C7-P1-C14	102.2(2)
C8-P1-C14	97.8(2)	C7-P1-Ni1	114.4(2)
C8-P1-Ni1	119.42(18)	C14-P1-Ni1	118.11(16)
C1#2-Si1-C1#1	104.5(2)	C1#2-Si1-C1	104.5(2)
C1#1-Si1-C1	104.5(2)	C1#2-Si1-Ni1	114.1(2)
C1#1-Si1-Ni1	114.1(2)	C1-Si1-Ni1	114.1(2)
C2-C1-Si1	110.8(5)	C2-C1-H1A	109.500000
Si1-C1-H1A	109.500000	C2-C1-H1B	109.500000
Si1-C1-H1B	109.500000	H1A-C1-H1B	108.100000
C7-C2-C3	116.9(7)	C7-C2-C1	122.5(5)
C3-C2-C1	120.6(7)	C4-C3-C2	122.6(8)
C4-C3-H3	118.700000	C2-C3-H3	118.700000
C3-C4-C5	120.9(8)	C3-C4-H4	119.600000
C5-C4-H4	119.600000	C4-C5-C6	118.9(9)
C4-C5-H5	120.500000	C6-C5-H5	120.500000
C7-C6-C5	120.1(7)	C7-C6-H6	119.900000
C5-C6-H6	119.900000	C6-C7-C2	120.5(5)
C6-C7-P1	121.5(5)	C2-C7-P1	117.8(5)
C13-C8-C9	118.0(6)	C13-C8-P1	118.9(4)
C9-C8-P1	122.7(5)	C10-C9-C8	120.5(8)
C10-C9-H9	119.700000	C8-C9-H9	119.700000

C9-C10-C11	120.3(8)	C9-C10-H10	119.900000
C11-C10-H10	119.900000	C12-C11-C10	119.7(7)
C12-C11-H11	120.200000	C10-C11-H11	120.200000
C11-C12-C13	120.3(8)	C11-C12-H12	119.900000
C13-C12-H12	119.900000	C8-C13-C12	121.1(7)
C8-C13-H13	119.400000	C12-C13-H13	119.400000
C15-C14-C19	117.7(5)	C15-C14-P1	121.9(4)
C19-C14-P1	120.4(4)	C14-C15-C16	121.7(6)
C14-C15-H15	119.200000	C16-C15-H15	119.200000
C17-C16-C15	119.9(6)	C17-C16-H16	120.100000
C15-C16-H16	120.100000	C18-C17-C16	118.8(6)
C18-C17-H17	120.600000	C16-C17-H17	120.600000
C17-C18-C19	122.7(7)	C17-C18-H18	118.700000
C19-C18-H18	118.700000	C14-C19-C18	119.3(6)
C14-C19-H19	120.400000	C18-C19-H19	120.400000
C6S-C1S-C2S	116.9(11)	C6S-C1S-H1S	121.600000
C2S-C1S-H1S	121.600000	C3S-C2S-C1S	122.4(12)
C3S-C2S-H2S	118.800000	C1S-C2S-H2S	118.800000
C2S-C3S-C4S	121.1(12)	C2S-C3S-H3S	119.400000
C4S-C3S-H3S	119.400000	C3S-C4S-C5S	118.8(12)
C3S-C4S-H4S	120.600000	C5S-C4S-H4S	120.600000
C6S-C5S-C4S	120.0(11)	C6S-C5S-H5S	120.000000
C4S-C5S-H5S	120.000000	C5S-C6S-C1S	120.7(10)
C5S-C6S-H6S	119.600000	C1S-C6S-H6S	119.600000

Symmetry transformations used to generate equivalent atoms:

#1 -y+1, z, -x+1

#2 -z+1, -x+1, y

Table S8. Anisotropic atomic displacement parameters (Å^2) for (Ni1).

The anisotropic atomic displacement factor exponent takes the form: -2π^2[h^2 a^{*2} U$_{11}$ + ... + 2 h k a* b* U$_{12}$]

	U_{11}	U_{22}	U_{33}	U_{23}	U_{13}	U_{12}
Ni1	0.0423(3)	0.0423(3)	0.0423(3)	-0.0068(3)	0.0068(3)	0.0068(3)
P1	0.0441(6)	0.0454(6)	0.0394(6)	-0.0049(5)	0.0048(5)	0.0005(5)
Si1	0.0573(6)	0.0573(6)	0.0573(6)	-0.0147(5)	0.0147(5)	0.0147(5)
C1	0.082(4)	0.085(5)	0.055(3)	-0.021(3)	0.011(3)	0.025(3)
C2	0.069(4)	0.096(5)	0.050(3)	-0.006(3)	0.022(3)	0.012(3)
C3	0.095(6)	0.139(8)	0.089(5)	0.000(5)	0.051(5)	0.011(6)
C4	0.111(7)	0.188(12)	0.125(9)	0.019(8)	0.077(7)	-0.010(8)
C5	0.104(6)	0.128(8)	0.111(7)	0.022(6)	0.046(6)	-0.029(6)
C6	0.072(4)	0.088(4)	0.068(4)	0.003(3)	0.021(3)	-0.021(3)
C7	0.053(3)	0.070(3)	0.043(3)	0.000(2)	0.008(2)	-0.005(2)
C8	0.058(3)	0.047(3)	0.050(3)	-0.009(2)	-0.001(2)	0.003(2)
C9	0.089(5)	0.119(6)	0.049(3)	-0.017(4)	-0.009(3)	-0.018(5)
C10	0.124(8)	0.136(8)	0.071(5)	-0.036(5)	-0.026(5)	-0.013(6)
C11	0.098(6)	0.090(5)	0.107(6)	-0.021(5)	-0.052(5)	-0.010(4)
C12	0.064(4)	0.084(5)	0.116(6)	0.008(4)	-0.021(4)	-0.011(3)
C13	0.052(3)	0.068(4)	0.077(4)	0.006(3)	-0.009(3)	-0.001(3)
C14	0.045(2)	0.046(2)	0.048(3)	-0.001(2)	0.001(2)	0.001(2)
C15	0.068(3)	0.052(3)	0.065(3)	0.005(3)	-0.015(3)	-0.006(3)
C16	0.061(4)	0.060(4)	0.085(4)	0.019(3)	-0.015(3)	0.002(3)
C17	0.085(5)	0.057(4)	0.102(6)	-0.016(4)	-0.020(4)	0.024(3)
C18	0.135(7)	0.076(4)	0.081(4)	-0.030(4)	-0.036(5)	0.051(5)
C19	0.084(4)	0.057(3)	0.062(3)	-0.017(3)	-0.015(3)	0.026(3)

Table S9. Hydrogen atomic coordinates and isotropic atomic displacement parameters ($Å^2$) for (Ni1).

	x/a	y/b	z/c	U(eq)
H1A	0.7637	0.2470	0.1491	0.089000
H1B	0.6931	0.2660	0.1584	0.089000
H3	0.8253	0.3216	0.1043	0.129000

	x/a	**y/b**	**z/c**	**U(eq)**
H4	0.8549	0.4204	0.0860	0.170000
H5	0.7982	0.5024	0.1241	0.137000
H6	0.7123	0.4826	0.1875	0.091000
H9	0.6342	0.3647	0.1031	0.103000
H10	0.5536	0.3320	0.0414	0.132000
H11	0.4637	0.2945	0.0857	0.118000
H12	0.4580	0.2822	0.1909	0.105000
H13	0.5395	0.3127	0.2535	0.079000
H15	0.5919	0.4644	0.1650	0.074000
H16	0.5489	0.5599	0.1829	0.083000
H17	0.5526	0.6023	0.2801	0.097000
H18	0.5991	0.5493	0.3573	0.117000
H19	0.6390	0.4522	0.3424	0.081000
H1S	0.5224	0.4507	1.0977	0.129000
H2S	0.6038	0.4798	1.0325	0.129000
H3S	0.5866	0.5184	0.9367	0.129000
H4S	0.4874	0.5307	0.8994	0.129000
H5S	0.4034	0.5025	0.9622	0.129000
H6S	0.4208	0.4629	1.0607	0.129000

16.2 Crystal Structure of **Ni-2** (CCDC deposition 2247468)

Crystal Structure Report for (Ni-2).

An orange prism single crystal of $C_{20.5}H_{17.5}Ge_{0.33}Ni_{0.33}P$, approximate dimensions (0.083 x 0.105 x 0.157) mm^3, was selected for the X-ray crystallographic analysis and mounted on a cryoloop using an oil cryoprotectant. The X-ray intensity data was measured at low temperature (T = 273K), using a three circles goniometer geometry with a fixed Chie angle at = 54.74 deg Bruker AXS D8 Venture, and equipped with a Photon 100 CMOS active pixel sensor detector. A monochromatized Copper X-ray radiation (λ = 1.54178 Å) was selected for the measurement. All frames were integrated with the aid of the Bruker SAINT software [22,23]using a narrow-frame algorithm. The integration of the data using a cubic unit cell yielded a total of 189068 reflections to a maximum θ angle of 74.54° (0.80 Å resolution), of which 3547 were independent (average redundancy 53.304, completeness = 99.8%, R_{int} =18.07%, R_{sig} = 2.38%) and 3163 (89.17%) were greater than 2σ (F^2). The final cell constants of <u>a</u> = 21.7872(3) Å, <u>b</u> = 21.7872(3) Å, <u>c</u> = 21.7872(3) Å, volume = 10342.0(4) Å^3, are based upon the refinement of the XYZ-centroids of 2807 reflections above 20 σ (I). The calculated minimum and maximum transmission coefficients (based on crystal size) are 0.7110 and 0.8300. The structure was solved in a cubic unit cell; non-centrosymmetric Space group: P -4 3 n, with Z = 24 for the formula unit, $C_{20.5}H_{17.5}Ge_{0.33}Ni_{0.33}P$. The asymmetric unit was built on 1/3 of the molecule. Using the Bruker SHELXT Software Package,[24] refinement of the structure was carried out by least squares procedures on weighted F^2 values using the SHELXTL-2018/3 included in the APEX4 v2022, 10-0, AXS Bruker program.[25] Hydrogen atoms were localized on difference Fourier maps but then introduced in the refinement as fixed contributors in idealized geometry with an isotropic thermal parameters fixed at 20 % higher than those carbons atoms they were connected. A molecule of solvent: Benzene C_6H_6 was found in the unit-cell statistically disordered around two-fold axes and was anisotropically refined with an occupancy factor fixed at 0.25. Restraints were used on interatomic lengths, angles, and constraints on ADP's parameters. The Flack's parameter value was found to be 0.07(6) and refined as a racemic twin.[26] Finally, during the structure analysis voids: 159 Å^3 were found in the crystal structure, which could not be related to resolved solvent molecules. The final anisotropic full-matrix least-squares refinement on F^2 with 242 variables converged at R1 = 5.20%, for the observed data and wR2 = 12.50% for all data. The goodness-of-fit: GOF was 1.180. The largest peak in the final difference electron density synthesis was 0.751 $e^-/Å^3$ and the largest hole was -0.320 $e^-/Å^3$ with an RMS deviation of 0.068 $e^-/Å^3$. On the basis of the final model, the calculated density was 1.305 g/cm^3 and F (000), 4212 e^-. Graphics were performed using softwares: Mercury V.4.2.0: (https://www.ccdc.cam.ac.uk/) and POV-Ray v 3.7: (The Persistence of Vision Raytracer, high quality, Free Software tool).

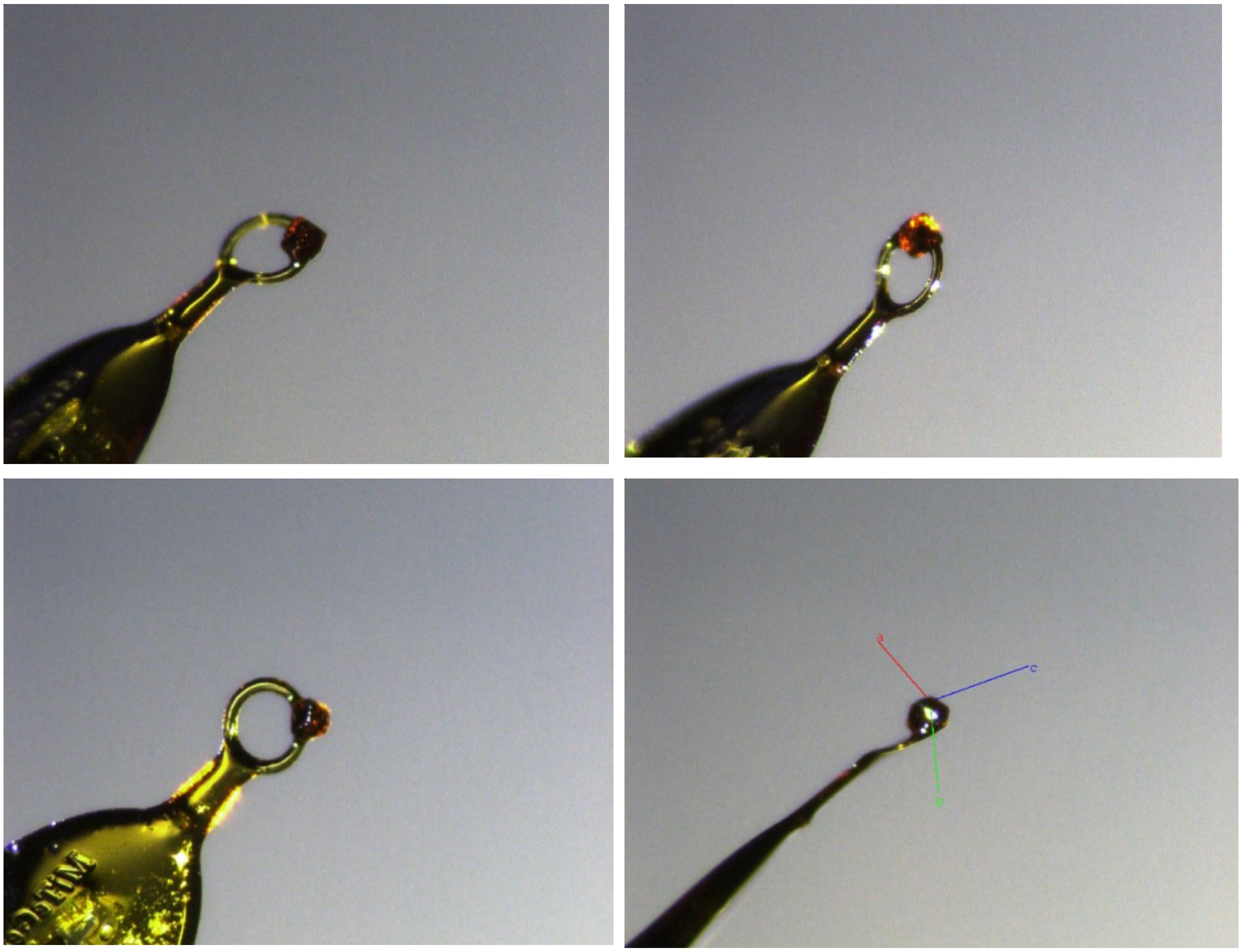

Crystal’s views:

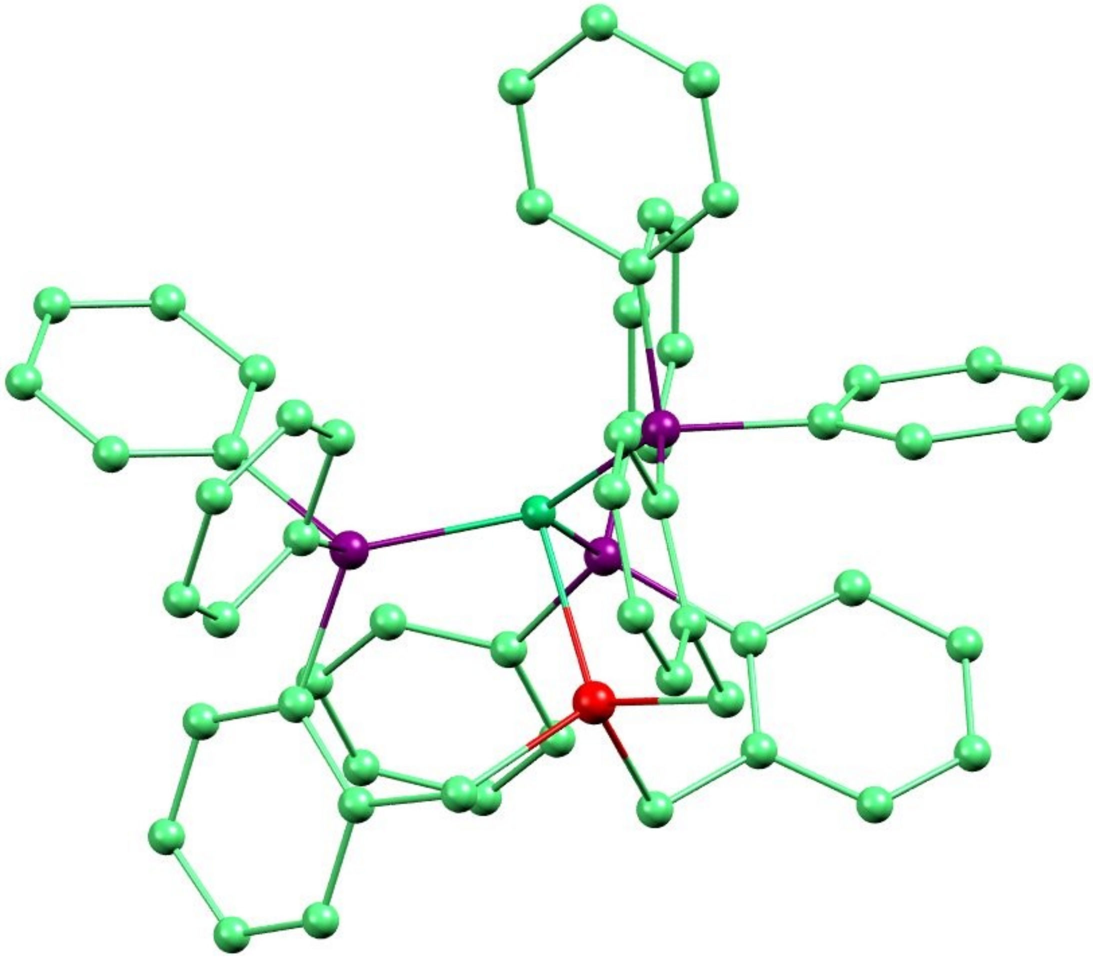

View of the complex: Ni-2.

Table S10. Sample and crystal data for (Ni2).

Identification code	C_VM003 (Ni2)
Chemical formula	$C_{20.5}H_{17.5}Ge_{0.33}Ni_{0.33}P$
Formula weight	338.58 g/mol
Temperature	273(2) K
Wavelength	1.54178 Å
Crystal size	0.083 x 0.105 x 0.157 mm
Crystal system	cubic

Space group	P -4 3 n	
Unit cell dimensions	a = 21.7872(3) Å	α = 90°
	b = 21.7872(3) Å	β = 90°
	c = 21.7872(3) Å	γ = 90°
Volume	10342.0(4) Å^3	
Z	24	
Density (calculated)	1.305 g/cm^3	
Absorption coefficient	2.332 mm^{-1}	
F(000)	4212	

Table S11. Data collection and structure refinement for (Ni2).

Theta range for data collection	4.06 to 74.54°	
Index ranges	-27<=h<=27, -27<=k<=27, -26<=l<=27	
Reflections collected	189068	
Independent reflections	3547 [R(int) = 0.1807]	
Max. and min. transmission	0.8300 and 0.7110	
Structure solution technique	direct methods	
Structure solution program	SHELXT	
Refinement method	Full-matrix least-squares on F^2	
Refinement program	SHELXTL-2018/3	
Function minimized	Σ w(F$_o^2$ - F$_c^2$)^2	
Data / restraints / parameters	3547 / 63 / 242	
Goodness-of-fit on F^2	1.180	
Final R indices	3163 data; I>2σ(I)	R1 = 0.0520, wR2 = 0.1191
	all data	R1 = 0.0607, wR2 = 0.1250
Weighting scheme	w=1/[σ^2(F$_o^2$)+(0.0586P)^2+4.9914P] where P=(F$_o^2$+2F$_c^2$)/3	
Absolute structure parameter	0.07(6)	
Largest diff. peak and hole	0.751 and -0.320 eÅ^{-3}	
R.M.S. deviation from mean	0.068 eÅ^{-3}	

Table S12. Atomic coordinates and equivalent isotropic atomic displacement parameters (Å^2) for (Ni2).

U(eq) is defined as one third of the trace of the orthogonalized U_{ij} tensor.

	x/a	**y/b**	**z/c**	**U(eq)**
Ge1	0.25678(3)	0.74322(3)	0.74322(3)	0.0571(3)
Ni1	0.31765(3)	0.68235(3)	0.68235(3)	0.0394(3)
P1	0.23737(6)	0.62821(6)	0.65545(6)	0.0399(3)
C1	0.1681(3)	0.7239(4)	0.7360(4)	0.076(2)
C2	0.1577(3)	0.6586(4)	0.7515(3)	0.0722(19)
C3	0.1223(4)	0.6435(6)	0.8037(5)	0.106(3)
C4	0.1127(5)	0.5859(8)	0.8212(5)	0.141(5)
C5	0.1361(5)	0.5367(6)	0.7868(5)	0.119(4)
C6	0.1730(3)	0.5495(4)	0.7362(4)	0.076(2)
C7	0.1838(3)	0.6109(3)	0.7183(3)	0.0552(15)
C8	0.1849(3)	0.6582(3)	0.5960(3)	0.0476(12)
C9	0.1213(3)	0.6519(4)	0.5997(4)	0.080(2)
C10	0.0850(4)	0.6699(5)	0.5513(5)	0.100(3)
C11	0.1095(4)	0.6927(4)	0.4980(5)	0.092(3)
C12	0.1723(5)	0.6997(4)	0.4951(3)	0.087(3)
C13	0.2090(3)	0.6821(3)	0.5432(3)	0.0610(16)
C14	0.2513(2)	0.5514(2)	0.6210(2)	0.0423(11)
C15	0.2049(3)	0.5182(3)	0.5937(3)	0.0590(16)
C16	0.2158(4)	0.4613(3)	0.5689(3)	0.0676(18)
C17	0.2729(4)	0.4366(3)	0.5702(4)	0.081(2)
C18	0.3182(4)	0.4685(4)	0.5975(5)	0.095(3)
C19	0.3086(3)	0.5255(3)	0.6222(3)	0.0654(18)
C1S	0.5189(15)	0.4549(15)	0.0409(13)	0.105(6)
C2S	0.5287(12)	0.5150(16)	0.0599(13)	0.105(6)
C3S	0.5134(16)	0.5629(15)	0.0218(15)	0.104(5)

	x/a	y/b	z/c	U(eq)
C4S	0.4885(17)	0.5534(14)	0.9648(15)	0.104(6)
C5S	0.4790(15)	0.4938(15)	0.9464(13)	0.104(6)
C6S	0.4940(18)	0.4456(14)	0.9841(14)	0.104(6)

Table S13. Bond lengths (Å) for (Ni2).

Ge1-C1#1	1.984(7)	Ge1-C1#2	1.984(7)
Ge1-C1	1.984(7)	Ge1-Ni1	2.2972(16)
Ni1-P1	2.1896(14)	Ni1-P1#1	2.1896(14)
Ni1-P1#2	2.1896(14)	P1-C7	1.839(6)
P1-C8	1.848(6)	P1-C14	1.858(5)
C1-C2	1.478(11)	C2-C7	1.388(10)
C2-C3	1.415(10)	C3-C4	1.327(15)
C4-C5	1.404(17)	C5-C6	1.394(11)
C6-C7	1.411(10)	C8-C13	1.367(9)
C8-C9	1.393(8)	C9-C10	1.375(11)
C10-C11	1.372(13)	C11-C12	1.379(13)
C12-C13	1.374(10)	C14-C19	1.373(8)
C14-C15	1.377(8)	C15-C16	1.374(10)
C16-C17	1.355(11)	C17-C18	1.345(11)
C18-C19	1.369(9)	C1S-C6S	1.366(11)
C1S-C2S	1.390(11)	C2S-C3S	1.374(13)
C3S-C4S	1.371(14)	C4S-C5S	1.377(14)
C5S-C6S	1.372(12)		

Symmetry transformations used to generate equivalent atoms:

#1	-y+1, z, -x+1
#2	-z+1, -x+1, y

Table S14. Bond angles (°) for C_VM003 (Ni2).

C1#1-Ge1-C1#2	105.5(2)	C1#1-Ge1-C1	105.5(2)

C1#2-Ge1-C1	105.5(2)	C1#1-Ge1-Ni1	113.2(2)
C1#2-Ge1-Ni1	113.2(2)	C1-Ge1-Ni1	113.2(2)
P1-Ni1-P1#1	119.9990(10)	P1-Ni1-P1#2	119.9980(10)
P1#1-Ni1-P1#2	119.9980(10)	P1-Ni1-Ge1	90.25(5)
P1#1-Ni1-Ge1	90.25(5)	P1#2-Ni1-Ge1	90.25(5)
C7-P1-C8	101.7(3)	C7-P1-C14	102.7(3)
C8-P1-C14	97.8(2)	C7-P1-Ni1	114.7(2)
C8-P1-Ni1	119.48(19)	C14-P1-Ni1	117.58(18)
C2-C1-Ge1	109.6(5)	C7-C2-C3	117.9(8)
C7-C2-C1	122.7(6)	C3-C2-C1	119.4(8)
C4-C3-C2	122.4(9)	C3-C4-C5	120.9(8)
C6-C5-C4	118.5(10)	C5-C6-C7	120.3(9)
C2-C7-C6	119.9(6)	C2-C7-P1	119.6(5)
C6-C7-P1	120.4(5)	C13-C8-C9	118.0(6)
C13-C8-P1	119.1(5)	C9-C8-P1	122.7(5)
C10-C9-C8	120.0(8)	C11-C10-C9	121.9(8)
C10-C11-C12	117.7(7)	C13-C12-C11	120.8(8)
C8-C13-C12	121.6(7)	C19-C14-C15	117.3(5)
C19-C14-P1	120.8(4)	C15-C14-P1	121.9(4)
C16-C15-C14	121.2(7)	C17-C16-C15	120.6(7)
C18-C17-C16	118.5(7)	C17-C18-C19	122.1(8)
C18-C19-C14	120.3(7)	C6S-C1S-C2S	118.1(10)
C3S-C2S-C1S	120.0(11)	C4S-C3S-C2S	121.9(12)
C3S-C4S-C5S	117.8(11)	C6S-C5S-C4S	120.8(11)
C1S-C6S-C5S	121.5(11)		

Symmetry transformations used to generate equivalent atoms:

#1 -y+1, z, -x+1

#2 -z+1, -x+1, y

Table S15. Anisotropic atomic displacement parameters (Å^2) for (Ni2).

The anisotropic atomic displacement factor exponent takes the form: -2π²[h² a*² U₁₁ + ... + 2 h k a* b* U₁₂]

	U_{11}	**U_{22}**	**U_{33}**	**U_{23}**	**U_{13}**	**U_{12}**
Ge1	0.0571(3)	0.0571(3)	0.0571(3)	-0.0158(3)	0.0158(3)	0.0158(3)
Ni1	0.0394(3)	0.0394(3)	0.0394(3)	-0.0073(3)	0.0073(3)	0.0073(3)
P1	0.0356(6)	0.0431(7)	0.0411(6)	0.0005(5)	0.0056(5)	0.0048(5)
C1	0.048(3)	0.092(5)	0.086(5)	-0.019(4)	0.015(3)	0.028(3)
C2	0.047(3)	0.100(5)	0.070(4)	-0.009(4)	0.021(3)	0.005(4)
C3	0.087(6)	0.137(9)	0.095(7)	-0.003(6)	0.053(5)	-0.005(6)
C4	0.118(9)	0.200(14)	0.107(8)	0.012(9)	0.079(7)	-0.013(9)
C5	0.120(8)	0.127(8)	0.110(8)	0.047(7)	0.056(7)	-0.016(7)
C6	0.070(4)	0.087(5)	0.071(5)	0.021(4)	0.015(4)	-0.007(4)
C7	0.042(3)	0.077(4)	0.047(3)	0.004(3)	0.014(2)	0.002(3)
C8	0.045(3)	0.047(3)	0.051(3)	-0.002(2)	0.000(2)	0.006(3)
C9	0.047(4)	0.107(6)	0.087(5)	0.019(5)	0.001(3)	0.018(4)
C10	0.060(5)	0.121(8)	0.119(8)	0.016(7)	-0.022(5)	0.026(5)
C11	0.097(6)	0.080(5)	0.100(7)	0.010(5)	-0.047(5)	0.019(5)
C12	0.128(8)	0.078(5)	0.055(4)	0.015(4)	-0.022(5)	-0.014(5)
C13	0.065(4)	0.069(4)	0.049(3)	-0.002(3)	-0.007(3)	-0.009(3)
C14	0.046(3)	0.040(3)	0.041(3)	-0.001(2)	0.004(2)	0.001(2)
C15	0.057(4)	0.052(4)	0.067(4)	0.007(3)	-0.016(3)	-0.004(3)
C16	0.088(5)	0.053(4)	0.061(4)	-0.003(3)	-0.019(4)	-0.017(4)
C17	0.100(6)	0.057(4)	0.086(5)	-0.025(4)	-0.017(5)	0.013(4)
C18	0.073(5)	0.077(5)	0.134(8)	-0.054(5)	-0.029(5)	0.025(4)
C19	0.053(4)	0.065(4)	0.078(4)	-0.028(4)	-0.014(3)	0.013(3)
C1S	0.130(14)	0.113(11)	0.072(11)	-0.014(8)	-0.029(9)	0.022(12)
C2S	0.130(14)	0.112(12)	0.072(10)	-0.014(8)	-0.029(8)	0.022(12)
C3S	0.129(14)	0.112(11)	0.070(11)	-0.015(8)	-0.027(8)	0.022(13)
C4S	0.128(14)	0.112(11)	0.070(11)	-0.014(9)	-0.028(8)	0.021(12)
C5S	0.128(14)	0.111(12)	0.072(10)	-0.013(8)	-0.030(8)	0.021(12)
C6S	0.128(14)	0.112(11)	0.072(11)	-0.014(8)	-0.031(9)	0.022(12)

Table S16. Hydrogen atomic coordinates and isotropic

atomic displacement parameters (Å^2) for (Ni2).

	x/a	**y/b**	**z/c**	**U(eq)**
H1A	0.1447	0.7498	0.7637	0.091000
H1B	0.1542	0.7319	0.6945	0.091000
H3	0.1050	0.6751	0.8267	0.127000
H4	0.0902	0.5781	0.8566	0.170000
H5	0.1271	0.4964	0.7976	0.143000
H6	0.1906	0.5176	0.7140	0.091000
H9	0.1035	0.6356	0.6349	0.096000
H10	0.0426	0.6665	0.5549	0.120000
H11	0.0846	0.7031	0.4649	0.111000
H12	0.1901	0.7166	0.4602	0.105000
H13	0.2514	0.6865	0.5399	0.073000
H15	0.1656	0.5347	0.5920	0.071000
H16	0.1838	0.4395	0.5509	0.081000
H17	0.2806	0.3984	0.5527	0.097000
H18	0.3572	0.4513	0.5996	0.113000
H19	0.3412	0.5467	0.6399	0.078000
H1S	0.5289	0.4220	0.0662	0.126000
H2S	0.5455	0.5228	0.0983	0.126000
H3S	0.5202	0.6029	0.0351	0.125000
H4S	0.4784	0.5862	-0.0606	0.124000
H5S	0.4621	0.4860	-0.0920	0.124000
H6S	0.4872	0.4057	-0.0294	0.125000

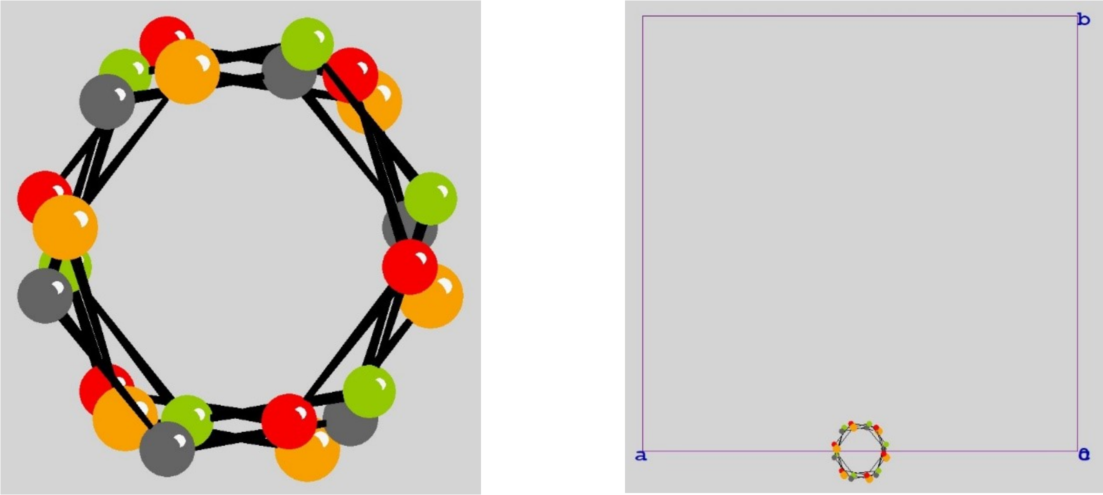

Views of disordered toluene for (Ni1) and (Ni2).

17. References

1. R. A. Gossage, G. D. McLennan and S. R. Stobart, "(Phosphinoalkyl)silanes. 3.1 Poly(o-(diphenylphosphino)benzyl)silanes: Synthesis, Spectroscopic Properties, and Complexation at Platinum or Iridium," *Inorganic Chemistry*, 1996, **35**, 1729-1732.

2. J. Takaya and N. Iwasawa, "Reaction of bis(o-phosphinophenyl)silane with M(PPh3)4 (M = Ni, Pd, Pt): synthesis and structural analysis of [small eta]2-(Si-H) metal(0) and pentacoordinate silyl metal(ii) hydride complexes of the Ni triad bearing a PSiP-pincer ligand," *Dalton Transactions*, 2011, **40**, 8814-8821.

3. H.-W. Suh, L. M. Guard and N. Hazari, "Synthesis and reactivity of a masked PSiP pincer supported nickel hydride," *Polyhedron*, 2014, **84**, 37-43.

4. M. T. Whited, N. P. Mankad, Y. Lee, P. F. Oblad and J. C. Peters, "Dinitrogen Complexes Supported by Tris(phosphino)silyl Ligands," *Inorg. Chem.*, 2009, **48**, 2507-2517.

5. C. Tsay and J. C. Peters, "Thermally stable N2 and H2 adducts of cationic nickel(II)," *Chem. Sci.*, 2012, **3**, 1313-1318.

6. D. J. Charboneau, D. Balcells, N. Hazari, H. M. C. Lant, J. M. Mayer, P. R. Melvin, B. Q. Mercado, W. D. Morris, M. Repisky and H.-W. Suh, "Dinitrogen-Facilitated Reversible Formation of a Si–H Bond in a Pincer-Supported Ni Complex," *Organometallics*, 2016, **35**, 3154-3162.

7. M. J. Frisch, G. W. Trucks, H. B. Schlegel, G. E. Scuseria, M. A. Robb, J. R. Cheeseman, G. Scalmani, V. Barone, B. Mennucci, G. A. Petersson, H. Nakatsuji, M. Caricato, X. Li, H. P. Hratchian, A. F. Izmaylov, J. Bloino, G. Zheng, J. L. Sonnenberg, M. Hada, M. Ehara, K. Toyota, R. Fukuda, J. Hasegawa, M. Ishida, T. Nakajima, Y. Honda, O. Kitao, H. Nakai, T. Vreven, J. A. Montgomery Jr., J. E. Peralta, F. Ogliaro, M. J. Bearpark, J. Heyd, E. N. Brothers, K. N. Kudin, V. N. Staroverov, R. Kobayashi, J. Normand, K. Raghavachari, A. P. Rendell, J. C. Burant, S. S. Iyengar, J. Tomasi, M. Cossi, N. Rega, N. J. Millam, M. Klene, J. E. Knox, J. B. Cross, V. Bakken, C. Adamo, J. Jaramillo, R. Gomperts, R. E. Stratmann, O. Yazyev, A. J. Austin, R. Cammi, C. Pomelli, J. W. Ochterski, R. L. Martin, K. Morokuma, V. G. Zakrzewski, G. A. Voth, P. Salvador, J. J. Dannenberg, S. Dapprich, A. D. Daniels, Ö. Farkas, J. B. Foresman, J. V. Ortiz, J. Cioslowski and D. J. Fox, *Gaussian*, 2009.

8. W. J. Hehre, R. Ditchfield and J. A. Pople, "Self—Consistent Molecular Orbital Methods. XII. Further Extensions of Gaussian—Type Basis Sets for Use in Molecular Orbital Studies of Organic Molecules," *The Journal of Chemical Physics*, 1972, **56**, 2257-2261.

9. P. C. Hariharan and J. A. Pople, "The influence of polarization functions on molecular orbital hydrogenation energies," *Theoretica chimica acta*, 1973, **28**, 213-222.

10. G. A. Petersson and M. A. Al-Laham, "A complete basis set model chemistry. II. Open-shell systems and the total energies of the first-row atoms," *The Journal of Chemical Physics*, 1991, **94**, 6081-6090.

11. P. J. Hay and W. R. Wadt, "Ab initio effective core potentials for molecular calculations. Potentials for K to Au including the outermost core orbitals," *The Journal of Chemical Physics*, 1985, **82**, 299-310.

12. P. J. Hay and W. R. Wadt, "Ab initio effective core potentials for molecular calculations. Potentials for the transition metal atoms Sc to Hg," *The Journal of Chemical Physics*, 1985, **82**, 270-283.

13. M. Couty and M. B. Hall, "Basis sets for transition metals: Optimized outer p functions," *Journal of Computational Chemistry*, 1996, **17**, 1359-1370.

14. R. Ditchfield, "Self-consistent perturbation theory of diamagnetism," *Molecular Physics*, 1974, **27**, 789-807.

15. R. Krishnan, J. S. Binkley, R. Seeger and J. A. Pople, "Self-consistent molecular orbital methods. XX. A basis set for correlated wave functions," *The Journal of Chemical Physics*, 1980, **72**, 650-654.

16. A. D. McLean and G. S. Chandler, "Contracted Gaussian basis sets for molecular calculations. I. Second row atoms, Z=11–18," *The Journal of Chemical Physics*, 1980, **72**, 5639-5648.

17. A. V. Marenich, C. J. Cramer and D. G. Truhlar, "Universal Solvation Model Based on Solute Electron Density and on a Continuum Model of the Solvent Defined by the Bulk Dielectric Constant and Atomic Surface Tensions," *The Journal of Physical Chemistry B*, 2009, **113**, 6378-6396.

18. N. Eedugurala, Z. Wang, U. Chaudhary, N. Nelson, K. Kandel, T. Kobayashi, I. I. Slowing, M. Pruski and A. D. Sadow, "Mesoporous Silica-Supported Amidozirconium-Catalyzed Carbonyl Hydroboration," *ACS Catalysis*, 2015, **5**, 7399-7414.

19. S. Kisan, V. Krishnakumar and C. Gunanathan, "Ruthenium-Catalyzed Deoxygenative Hydroboration of Carboxylic Acids," *ACS Catalysis*, 2018, **8**, 4772-4776.

20. C.-C. Chia, Y.-C. Teo, N. Cham, S. Y.-F. Ho, Z.-H. Ng, H.-M. Toh, N. Mézailles and C.-W. So, "Aluminum-Hydride-Catalyzed Hydroboration of Carbon Dioxide," *Inorganic Chemistry*, 2021, **60**, 4569-4577.

21. S. Lau, C. B. Provis-Evans, A. P. James and R. L. Webster, "Hydroboration of aldehydes, ketones and CO2 under mild conditions mediated by iron(iii) salen complexes," *Dalton Transactions*, 2021, **50**, 10696-10700.

22. Saint Program included in the package software: APEX4 v2021.4-0
23. Bruker (2001). Bruker AXS Inc., Madison, Wisconsin, USA.
24. SHELXT-Integrated space group and crystal -structure determination Sheldrick, G. M. Acta Crystallogr., Sect. A 2015, A71, 3-8.
25. SHELXT Sheldrick, G. M. Ver. 2018/3. Acta Crystallogr. Sect. C Structural Chemistry 71, 3-8.
26. APEX4 v2021, 4-0, AXS Bruker program.
27. Flack, H. D. Acta Crystallogr., Sect. A 1983, 39, 876-881.